UNIVERSITAT DE BARCELONA

Analysis of the *in vivo* effect of carnitine palmitoyltransferase 1A deletion in AgRP neurons

Sebastián Zagmutt Caroca

UNIVERSITAT DE BARCELONA

FACULTAT DE FARMÀCIA I CIÈNCIES DE L'ALIMENTACIÓ

Sebastián Zagmutt Caroca

Analysis of the *in vivo* effect of carnitine palmitoyltransferase 1A deletion in AgRP neurons

Sebastián Zagmutt Caroca

2020

UNIVERSITAT DE BARCELONA

FACULTAT DE FARMÀCIA I CIÈNCIES DE L'ALIMENTACIÓ

Programa de doctorat en Biotecnologia

Analysis of the *in vivo* effect of carnitine palmitoyltransferase 1A deletion in AgRP neurons

Memòria presentada per Sebastián Zagmutt Caroca per optar al títol de doctor per la Universitat de Barcelona

Dra. Dolors Serra Cucurull

Dra. Laura Herrero Rodríguez

Sebastián Zagmutt Caroca

Barcelona, 2020

- “Te podrías dedicar al arte me dijeron mil veces”-. Y aquí está mi obra les contesté,
porque para hacer ciencia hay que ser un poco artista.
Cristian, Carmen y Josefa, habéis estado presente en cada pincelada…

AGRADECIMIENTOS

La música es ciencia y la ciencia también es arte

Bien podría ser esta una de esas presentaciones reliquias que rondan por la línea de tiempo y engrosan el pomposo currículum de gestas, pero no, no tengo condecoraciones de esa índole (todavía), por eso mi sitio es el violín segundo.

Miré la cúpula del teatro para controlar el unísono de instrumentos antes de que el director se asomara y volví a mi infancia. Porque siento yo niño, recuerdo con detalle cuando mi madre decía que tenía que llegar a lo más alto. –"Pues aún me tocará pasar las partituras madre, pero que sepas que se requiere mucha valentía para estrenar una pieza de Tchaikovski así de buenas a primeras"-.

En primera fila estaba mi familia. Podía notar el agobio de mi hermana sentada en aquella butaca roja y aunque se mueva con el sigilo de un reptil, este ejercito de violines le abruma. Los latidos de mi madre me llegaban como el retumbar de los timbales, ha dado tantos discursos en su vida profesional que me sigue sorprendiendo que esté más nerviosa que yo. Y mi padre, mi padre es indemne a estos eventos, solo le importa que noten muy claramente lo orgulloso que se siente de mí.

A breves minutos de empezar la presentación pensé: - "Han pasado cuatro años desde que los abrazos tenían que cruzar todo el atlántico para que llegasen. Cuatro años en que sus ojos ilusionados pusieron toda la confianza en lo que me tocaba vivir, porque nunca hubo un impedimento para embarcarme en esta epopeya, nunca hubo peros. Madre; ¿recuerdas nuestra primera llamada telefónica a once mil kilómetros de distancia?, seguramente escuchabas mi llanto y morías por brindarme tu cobijo, no obstante, tus palabras fueron; Sebastián, tú estás allí porque esto es algo que tú buscaste con ilusión, nadie te ha obligado y seca esas lágrimas hombre!!, que nosotros ya te hemos dado alas para volar.

-"He crecido madre, pero parte de este crecimiento fue porque tus consejos tienen esa mítica magia de alquimista que cura todos los males.

Cristian, Carmen y Josefa, daros las gracias compensa muy poco todo lo que habéis hecho por mí y dedicaros este manojo de partituras no es la manera que más me gusta de amortizar la deuda, solo espero que os sintáis orgullosos de la manera que he llevado nuestro emblema porque vuestra felicidad es mi energía"-.

De súbito y trepidante volví al teatro como resurgido de un trance, cuando el ensordecedor mar de aplausos acusaba la entrada de la directora. La mujer tenía elegancia para aparecer entre la multitud porque su aura imponía. Hizo una reverencia

muy fría, tal como hacen todos los directores y rápidamente dio la espalda al público para situarse sobre la peana en lo alto de esta hueste, desde aquí, veía que su mano le temblaba porque la batuta vibraba en medio del vacío.

Como era de rutina, coordinó las cuerdas, los vientos y la percusión en un solo tono y el silencio volvía a inundar el teatro. Ojalá pudierais sentir lo excitante que es comenzar una obra y en especial la obertura 1812 de Tchaikovski.

El inicio era de violas y cellos, muy solemne y sedante, me gustaba este inicio porque podía ver a mis compañeros como un espectador más siendo yo parte de esta orquesta. Los arpegios nacían de sus cuerdas como pétalos en primavera que alimentan el hipnótico placer del público.

Divisaba a Maricarmen que tocaba el cello con irrefutable usanza, no hay ninguna tormenta que irrumpa su rostro de concentración porque quiere que todo salga a la perfección. ¿Recuerdas nuestros inicios Maricarmen? Y me remonto al *initium* porque nunca imaginé que llegarías a ser tan importante en mi vida. Me siento orgulloso de ver como desplazas el arco sobre las cuerdas y aunque te lo he dicho tantas veces, la que más ha crecido has sido tú. Benditas son todas las horas que me dedicaste inundados de cerveza y de café y todo el cariño que me has brindado, porque no hay nadie que tenga un corazón tan noble como el tuyo. Afortunado soy de llegar a recorrer la raíz de tu estirpe y el cobijo de tu familia han sido de mis mejores regalos.

Carlos, Carlos estaba sentado al piano y aunque aún no era su entrada, nuestras miradas cómplices se cruzaron en medio de los primeros compases de la 1812. Me quedé mirándolo hipnotizadamente porque él y su vida aparecieron en la mía como eso que sabes que necesitas, pero no estás seguro si llegará. Lo necesitaba Carlos, necesitaba sentarme en tu balcón y perderme en el lábil horizonte manteniendo conversaciones que nadie, absolutamente nadie me daría. Nuestro estado demencial para algunos, incomprendido para otros es una pletórica abstracción que me hace resucitar. ¿Entender el algoritmo de cómo nuestras líneas conectaron? Da igual, ya estamos juntos dentro de esta película y es muy placentera de observar.

Faltaba muy poco para los violines, lo sabía, aún estaban los vientos acompañado el melódico trance de las violas y cellos. Todavía el flujo es lento y las notas musicales reverberen en el teatro mientras la mirada del publico denota paz, suavidad y tranquilidad. Busqué a Albert, ¿quieres saber por qué busqué a Albert? Porque de toda la gente que tengo a mi alrededor es con quién yo más me identifico. Allí, si allí está, sentado impretéritamente con una mirada formal que yo conocía perfectamente. Sabes algo Albert, todas nuestras noches codo a codo que caían en el whisky sin hielo son las reflexiones más potentes con las que me quedo. No sé qué tanto tienes que me veo en ti como si fueras un reflejo, algo así como una imagen

especular no superponible. Nuestras dudas, nuestros miedos, la mítica manera de ver la vida, es de las conclusiones que más me llevo. Le has aportado el justo tinte de complejidad a esta obra, eras necesario, por cierto. No te quiero perder, por ningún motivo que pueda existir.

La batuta se mecía de arriba hacia abajo y la mano izquierda sobre los violines, ya era mi turno. Lo puse sobre el hombro y mi barbilla descansaba levemente hacia la izquierda. Esperé la señal para mecer el arco sobre las cuerdas y aunque no podía ver el sonido, sus efectos movían mis hormonas como una carretera de cohetes a la luna. Dopamina, una tempestad de dopamina al ritmo de las escalas.

Las pupilas del público comienzan a dilatarse lentamente como si aumentase la respuesta de lucha o huida, porque así es las 1812 *in crescendo*. De reojo podía notar algunos acomodarse preocupantemente en sus asientos como si el sonido de las tubas, contrabajos y cornos franceses arrasara en una estampida de pegasos. Y esto me recordó mis días de tormentos.

Vibra el arco sobre las cuerdas con la misma fuerza del mar golpeando las rocas, elegantemente afinado pero majestuoso que amedranta, y me veía yo practicando en un baño de tina lleno agua y lágrimas con cereales para el desayuno que tiré contra la pared porque no había caso, no. Eran mis agobios con el mismo volumen de los platos de percusión, caminando yo con el chirrido en los oídos tocando puerta por puerta por si alguien podía socorrer mi auxilio. Froté mis rodillas contra el suelo, sangran sí, pero a nadie le importó, solo a ti Natalia, solo a ti, que has llegado a esta orquesta a enseñarme a tomar el arco con tranquilidad, a susurrarme armonía, aunque Tchaikovski haya puesto cañones para cerrar esta obra. En el clímax de todo este caos escucho tu voz angelical que me conecta a tierra, me conecta tierra.

Natalia, así como me ves, en este momento de fusas y semifusas, corchea tras corchea, moviendo mi cuerpo tensamente, te agradezco porque este ritmo de ardor sincroniza mis manos con tus manos, mi fuerza con tu fuerza, unidas como nunca alimentándome de tu energía. Tengo en mis recuerdos todas las veces que hemos sufrido juntos, y todos los abrazos que nos hemos dado para seguir manteniéndonos de pie, no puedes imaginar lo invencible que seremos, pero solo tú y yo sabemos cuánto duele. Gracias porque mis problemas fueron tan míos como tuyos y los cargaste en tu espalda con la poca fuerza que nos queda. Hoy estas por mí, y mañana yo estaré por ti.

En estos momentos del concierto, lo único que notas es un estallido de sonidos que bailan sincronizadamente, algo así como un espectáculo de fuegos artificiales en el que cada explosión es el final de un compás.

El espectador se relaja y disfruta de la menor entropía, este estado de inercia es un abrazo de blancas que recorre la piel hasta lo más profundo. Una apreciable entelequia que obliga al trance de opioides invadiendo la sangre.

Mientras tanto yo, sigo las notas aunque las tengo casi grabadas en mi memoria, no hay presente para las hojas que han quedado en el pasado y así, compas tras compás no puedo negar que deseo llegar al final.

En el quinto último, giras el reloj para difuminar el último minuto en la arena. En el cuarto, tus dedos se acalambran y potasio se tarda en llegar. En el tercero, la adrenalina se satura y emborracha, caerá como lluvia de invierno. En el segundo te quedas trépido y te preparas, porque sabes que, en el último, la energía entra por la planta de tus pies como una corriente de luz que viaja por el vacío, te golpea de súbito y corre el arco por última vez con gargo y elegancia. El director abre los brazos como señal de que se ha acabado y te quedas impávido.

Estoy conscientemente aturdido y un poco obnubilado oigo los vestigios muy muy a lo lejos. Aunque no pueda distinguir con claridad torcí la mirada al público donde me percaté que Sebastián fue el primero en ponerse de pie para aplaudir con ganas.

Agradezco este momento de inconsciencia que inundó mi mente con tu presencia. Me transporté a Valencia más rápido que las 4 horas que tomaba ir a verte. ¿Habría imaginado que dentro de toda esta tormenta habría un lugar que me dejase como el sol ardiente de junio de Lord Frederic Leighton?, creo que nunca. La habitación era del rococó y el ciego sonido de la estación de trenes adornaba dulcemente la deconstrucción en sueño. Te recuerdo poniendo los vinilos en el tocadiscos y yo por fin olvidándome de toda mi historia pasada. Hay tantas notas musicales entre tú y yo que no caben en una partitura, tan solo una obertura no puede contar nuestros viajes, peripecias y el mundo descubierto a nuestros pies. Te admiro porque ni Calatrava fue capaz de construir un puente tan bonito entre Valencia y Barcelona tal como tú lo has construido.

Sigo un poco aturdido, pero sé que en mis ojos puedes leer un leve lamento de nunca haberte podido brindar toda la energía que mereces, aunque lo poco que he hecho por ti, ha sido con el corazón.

No se cómo, pero ya está toda la orquesta de pie y de cara al público, haciendo una reverencia el teatro vuelve a sonar en mis oídos pregonando el culmine de esta presentación. He volteado para observar a todos aquellos que han caminado conmigo en esta historia, mientras la directora agradecía con una reverencia solemne.

Serra Cucurull y Herrero Rodríguez dirigían esta pieza, que, por cierto, tenía bastante tiempo de preparación. Me sorprende que el público ve un producto final y no el desarrollo en esencia (que a mi juicio es lo más bonito de apreciar). Aquí yo crecí y aquí me formé, bajo la cornisa de dos mujeres de concepción científica y con un claro bagaje en diferentes ámbitos de la concertación, intelectualmente activas y conocedoras de la profunda retórica de la música y su ciencia.

-"Tenéis una mezcla armónica para crear melodías que conjunta a la perfección. Laura, hay algo de ti que nunca olvidaré, toda vez que no se garantiza la ascensión al olimpo de los escenarios estabas tú para acompañarnos en el primer paso. La crin de los arcos se suele cortar con facilidad, pero de tu parte siempre existió un volver a empezar. No te canses de reconocer cuando ves un buen trabajo ("ánimo campeón") ni tampoco de tus críticas constructivas, porque es el único protocolo que tenemos para avanzar. Quizás no lo imaginas, pero tus refuerzos positivos suelen ser un cúmulo de endorfinas que, a mi parecer, es la mejor artillería para combatir las olas de frustraciones.

Dolors, creo no haber visto nunca a alguien luchar por este proyecto como lo he visto en ti. Tienes una fuerza sobrenatural para crear túneles en las montañas y hacer música de la ciencia. Dirigir una orquesta es como tutelar los pensamientos en el cerebro. Una sofisticada red neuronal que funciona melódicamente solo si está en armonía. Gracias por hacer de este aprendizaje una pintura que no me canse nunca de mirar.

Espero de corazón haber representado esta obra tal como queríais porque detrás de todo el esfuerzo había también cariño. Y aunque esté yo solo con un violín en la mano, hoy mis hombros se sostienen por la fuerza mi familia y amigos quienes han escrito toda esta historia.

…Y la adrenalina se fundió en mi sangre depurada hasta el último vestigio, mis músculos temblaron como si no me pudiese mantener de pie. Ahora ya es todo parte de un recuerdo, un montón de notas musicales que bailan en mi mente y que nunca nadie ni nada podrá borrar. La mente es frágil sí, pero dejo en esta partitura una constancia de los mejores años de mi vida.

Gracias.

Menciones especiales.

La gente se había comenzado a acumular fuera del Burgtheater como era de rutina. Me obstiné unos instantes en querer penetrar la muchedumbre porque allí estaban ellos, con una sonrisa que contagia.

Irene, por doquiera ostentaba y derramaba la terapia de alegría más fascinante, fue quién me invitaba a unos viajes de astronauta camino hacia lo más surreal. Porque nuestros diálogos siempre fueron de lo muy extremo a lo más banal. Tengo con ella un montón de fotos que cada vez que las miro me vuelvo a sorprender que exista una chica así, tan excesivamente en todo, gracias Irene por caminar junto a mí.

Con Kevin compartí casi todos mis años del conservatorio, los necesarios para darme cuenta que yo tengo mucho que aprender de él. Ojalá pudiera alcanzarte Kevin, alcanzar el cuarto de tu valentía y un tercio de tu arrojo. Me has dado más lecciones de las que puedes imaginar y tantas historias que tengo para contar. Disfruta estos años que quedan camino a tu meta, pero confío en tu sabiduría de sacar colores de donde no hay.

Paula apareció en esta historia para afinar cada melodía, debo confesar que se robó mi admiración como nadie. Ojalá tuviese voz para llegar a todo el mundo y decir que en cada orquesta debe haber alguien como ella. Noble en un mundo que cuesta y justa en una balanza torcida. Paula es de esas pocas personas que yo diría como ella quiero ser.

Meni vino de Grecia en un abrir y cerrar de ojos, algo así como quien aparece con una conexión que se remota a tiempos ancestrales. Mitológica porque como ella hay pocas. Decidió volar a la casa de la opera de Sidney, lo cual siempre lo contaré con mucho orgullo y ha dejado escrito en mi agenda el día que nos volveremos a abrazar.

Estábamos todos dispuestos para la foto, Pía, Marjorie, Ivonne (quienes están de símil aprendiz) Kevin, Maricarmen y tantos otros con los que competí.

¡Venga va!, poneros todos de perfil y cuando acabe de contar miráis a la cámara.

TRES,…DOS,…UNO…

ABSTRACT

Food intake and whole-body energy balance are regulated by the brain through a sophisticated neuronal network located mostly in the hypothalamus. In particular, the hypothalamic arcuate nucleus (ARC) is a fundamental sensor for the hormones and nutrients that inform about the energy state of the organism. The ARC contains two populations of neurons with opposite functions: anorexigenic proopiomelanocortin (POMC)-expressing neurons and orexigenic agouti-related protein (AgRP)-expressing neurons. Activation of AgRP neurons leads to an increase in food intake and a decrease in energy expenditure. It has been suggested that lipid metabolism in the ARC plays an important role in the central control of whole-body energy balance. Yet it is unclear whether lipid metabolism specifically regulates the activity of AgRP neurons.

Here, we studied mutant mice lacking carnitine palmitoyltransferase 1A (CPT1A) specifically in AgRP neurons (*Cpt1a*$_{\text{AgRP}}^{(-/-)}$ mice). CPT1A regulates the rate-limiting step in the mitochondrial oxidation of fatty acids (FAs) and therefore plays a central role in lipid metabolism. Our results demonstrate that the deletion of *Cpt1a* in AgRP neurons induces sex-based differences on the energy metabolism. Although male and female *Cpt1a*$_{\text{AgRP}}^{(-/-)}$ mice showed a reduction of the body weight gain, both genders afford this reduction in a different way. Male *Cpt1a*$_{\text{AgRP}}^{(-/-)}$ mice showed a reduction of food intake with no changes in the energy expenditure, while female *Cpt1a*$_{\text{AgRP}}^{(-/-)}$ mice increased the energy expenditure with no changes in food intake. Despite these results, the AgRP neuronal activation by fasting conditions or by high levels of ghrelin were impaired in both genders. At a peripheral level, the deletion of *Cpt1a* in AgRP neurons had an impact on different adipose tissues. On the one hand, the lack of *Cpt1a* in AgRP neurons enhanced the brown adipose tissue (BAT) activity. On the other hand, it induced a substantial reduction of white adipose tissues, especially inguinal and gonadal fat pads.

Although AgRP neurons have been associated with solid food consumption, here we also reported that AgRP neurons could be involved in water homeostasis. *Cpt1a*$_{AgRP}^{(-/-)}$ mice showed a reduction of AV/ADH levels and had impaired activation of thirst-related centers. Finally, our results reveal that AgRP neurons require CPT1A to maintain a normal morphology and physiology. The deletion of *Cpt1a* in AgRP neurons does not affect the neuronal viability. However, it interfered in the number of dendritic spines altering their morphology and normal synapses state.

Altogether, our results suggest that CPT1A and FAs oxidation in AgRP neurons impact peripheral energy balance highlighting this pathway as a possible target for therapeutic strategies to decrease body weight. We also provide evidence that AgRP could be involved in the regulation of water homeostasis.

ABBREVIATIONS

AAV	Adeno-associated viruses
aBNST	Anterior bed nucleus of the stria terminalis
ACC	Acetyl-CoA carboxylase
ACE	Angiotensin converting enzyme
ACTH	Adrenocorticotropic hormone
ADH	Antidiuretic hormone
AG	Adrenal gland
AgRP	Agouti-related protein
AMPK	AMP-activated protein kinase
AmpR	Ampicillin resistance gene
ANG	Angiotensin
ANS	Autonomic nervous system
AQP2	Aquaporin-2
ARC	Arcuate nucleus
ARs	Androgen receptor
AT1Rs	Angiotensin II type 1
AT2Rs	Angiotensin II type 2
ATF4	Activating transcription factor 4
ATGL	Adipose triglyceride lipase
AUC	Area under the curve
AVPR2	V2 receptor
BAT	Brown adipose tissue
BBB	Blood-brain barrier
BCA	Bovine serum albumin
BMI	Body mass index
BMR	Basal metabolic rate
BSX	Brain specific homeobox
cAMP	Cyclic AMP
CART	Cocaine and amphetamine-stimulating hormone transcript
CCiT-UB	Científics i Tecnològics de la Universitat de Barcelona
CCK	Cholecystokinene
cDNA	Complementary DNA
CMV	Cytomegalovirus

CNS	Central nervous system
COTs	Carnitine octanoyltransferases
CPTa	Carnitine palmityltransferases
CrATs	Carnitine acetyltransferases
CREB	cAMP response-element-binding protein
CRH	Corticotropin-releasing hormone
CVO	Circumventricular organs
ddNTPs	Dideoxynucleotides
DEE	Diet-induced energy expenditure
DG	Diglyceride
DIO	Double floxed inverted orientation
DMN	Dorsomedial nucleus
DNA	Deoxyribonucleic acid
DOC	Sodium deoxycholate
DTT	Dithiothreitol
ECF	Extracellular fluid
ECL	Enhanced chemiluminescence
EE	Energy expenditure
ERs	Estrogen receptors
eWAT	Epididymal WAT
FAO	Fatty acid oxidation
FAS	Fatty acid synthase
FAs	Fatty acids
FFAs	Free-fatty acids
FFM	Fat-free mass
FM	Fat mass
FOXO1	Forkhead box O1
G6P	Glucose-6-phosphatase
GABA	Gamma aminobutyric acid
Gapdh	Glyceraldehyde-3-phosphate dehydrogenase
GHSR	Growth hormone secretagogue receptor
GI	Gastrointestinal
GPR120	G-protein-coupled receptor 120
GTT	Glucose tolerance test
gWAT	Gonadal white adipose tissue

H&E	Hematoxylin and eosin
HA	Hemagglutinin
HFD	High-fat diet
Hprt	Hypoxanthine phosphoribosyl-transferase
HSB	High salt buffer
Hyp	hippocampus
ICF	Intracellular fluid
ICV	Intracerebroventricular
IL-6	Interleukin 6
IP	Immunoprecipitation
IR	Insulin receptor
iWAT	Inguinal white adipose tissue
KATP	ATP-dependent potassium
Kiss	Kisspeptin
KPBS	Potasium phosphate-buffered saline
LA	Locomotion activity
LB	Luria bertani
LCFA	Long-chain FAs
LD	Lipid droplet
LHA	Lateral hypothalamic nucleus
LT	Lamina terminalis
MBH	Medial basal hypothalamus
MCD	Malonyl-CoA decarboxylase
MCRs	Melanocortin receptors
MIM	Mitochondrial inner membrane
MnPO	Median preoptic nucleus
MOM	mitochondrial outer membrane
mRNA	Messanger ribonucleic acid
MSH	Melanocyte-stimulating hormone
MTS	Mitochondrial targeting signal
NEO	Neomycin
NMDA	N-methyl-D-aspartate
NPY	Neuropeptide-Y
ObR	Leptin receptor
ON	Overnight

OT	Oxitocyn
OVLT	Organum vasculosum of the lamina terminalis
P2Y6	Purinergic receptor 6
PBN	Parabrachial nuclei
PBS	Phosphate buffer saline
PCR	Polymerase chain reaction
PEPCK	Phosphoenolpyruvate carboxykinase
PI3K	Phosphoinositide 3-kinase
PIP_3	Phosphatidylinositol-3,4,5-triphosphate
PLs	Phospholipids
POMC	Proopiomelanocortin
Posm	Serum osmolality
PRV	Pseudorabies virus
PVN	Paraventricular nucleus
qRT-PCR	Quantitative real time polymerase chain reaction
RAAS	Renin-angiotensin-aldosterone system
ROI	Region of interest
Rpl22	Ribosomal protein L22 Rpl2
RQ	Respiratory quotient
SDS	Sodium dodecyl sulfate
SDS-PAGE	Sodium dodecyl sulfate-polyacrylamide gels
SFO	Subfornical organs
SIRT	Sirtuin
SNS	Sympathetic nervous system
SO	Supraoptic
sWAT	subcutaneous WAT
T2D	Type 2 diabetes
TBST	Tris buffered saline with Tween 20
TEE	Total energy expenditure
TG	Triglyceride
TH	Tyrosine hydroxylase
TRH	Thyrotropin-releasing hormone
Uosm	Urine osmolarity
VEGFA	Vascular endothelial growth factor A
VGAT	Vesicular GABA transporter

VHM	Ventromedial nucleus
VP	Arginine vasopressin
VPU	Viral Vector Production Unit
WAT	White adipose tissue
WHO	World health organization
WR	Working reagent
WT	Wild-type

INDEX

1. INTRODUCTION

1.1. OBESITY

Obesity and overweight, together with their associated pathologies, have become one of the most important challenges for national healthcare system worldwide. Since 1980, the prevalence of obesity has doubled in more than 70 countries and continues to grow at a pandemic rate [1]. According to the most recent study providing trends in body mass index (BMI) (kilograms divided by height in meters squared (BMI =W [kg]/H [m^2]) from 128,9 million children, adolescents and adults from all countries in the world, obesity prevalence increased in every country between 1975 and 2016 [2].

The World health organization (WHO) defines overweight as a BMI greater than or equal to 25 kg/m^2 and obesity as excessive fat accumulation that might impair health [3]. It is diagnosed at a BMI ≥ 30 kg/m^2 for men and > 28.6 kg/m^2 for women [3]. The fundamental cause of obesity is a long term energy imbalance between too many calories consumed and too few calories expended [4]. Looking beyond the purely energetic consideration there are also numerous other factors contributing to causation as well as persistence of obesity. Environmental, sociocultural, physiological, medical, behavioral, genetic, epigenetic factors complicate the pathogenesis of obesity [4].

Evolutionarily, humans and their predecessors had to survive periods of undernutrition; therefore, selection pressure most likely contributed to a genotype of overeating, low energy expenditure and physical inactivity [5]. Humans who could stand longer periods of famine and who could store and mobilize energy more efficiently might have reproduced more than those without these adaptations, subsequently leading to the overrepresentation of genetic variants that promote the ability to eat more rapidly, to resorb calories to a higher degree and to expand energy stores in adipose tissue more efficiently [6].

Currently, if we add to the factors previously described the constant exposition to an "obesogenic environment"; we can understand why obesity is continuously increasing. The term "obesogenic environment" refers to conditions of life have on promoting obesity in individuals or populations [7]. On the one hand, many of us live in places where energy dense, highly palatable foods and beverages are abundant and available at relatively low cost. Widespread advertising and sophisticated marketing techniques are designed to keep thoughts of these foods and beverages almost constantly in mind. On the other hand, the lack of recreation areas or places to improved metabolic fitness, unfortunately make people unable to decide to be obese.

Obesity substantially increases the risk of metabolic diseases (for example type 2 diabetes mellitus (T2D) and fatty liver disease), cardiovascular diseases (hypertension, myocardial infarction and stroke), musculoskeletal disease (osteoarthritis), Alzheimer disease, depression and some types of cancer (for example, breast, ovarian, prostate, liver, kidney and colon)[8]. In addition, obesity might lead to reduced quality of life, unemployment, lower productivity and social disadvantages [8,9]. For all these reasons, obesity and its associated health problems have a significant economic impact on the health care system. Medical costs associated with overweight and obesity may involve direct and indirect costs. Direct medical costs may include preventive, diagnostic, and treatment services related to obesity. Indirect costs relate to morbidity and mortality costs including productivity [10]. Therefore, it is extremely urgent to address the issue of obesity prevention and dedicate efforts to prevent obesity amongst individuals, groups or whole communities.

All current approaches for treating obesity including healthy eating, exercising or changing the lifestyle have proven to be a failure rendering obesity with a temporary relief and no cure. Bariatric surgery achieves a sustained weight loss over the years, but it is expensive and associated dangers reduce its clinical indication to morbidly obese patients [11]. Moreover, the endocrine effects of bariatric surgery seem to be more important than the mechanically induced food restriction which has led many

researchers to assess obesity treatment base on the endocrine modification derived from it [12,13]. Thus, it is required to explore the biological mechanisms that cause obesity with the aim of designing interventions to achieve and maintain a healthy body weight. Research efforts have increasingly improved our understanding of how craving for food is disturbed in the brains of individuals with obesity; how adipose tissue, gut or liver hormones regulate appetite and satiety in the hypothalamus; and how dysfunction of adipose tissue causes secondary health problems. The key role of certain brain regions in the regulation of body weight became evident from observations that animals with lesions and humans with tumours affecting the hypothalamus develop abnormal food seeking behavior and obesity [14].

1.2. BRAIN REGULATION OF ENERGY BALANCE

The concept of energy balance is based on the thermodynamic principle that energy cannot be destroyed, and can only be gained, lost, or stored by an organism [15]. Therefore, it is defined as the state achieved when the energy intake equals energy expenditure. If we analyze the definition there are two aspects of this balance, each equally important in maintaining energy homeostasis: energy intake (*i.e.,* food intake) and energy expenditure (*e.g.,* physical activity, metabolism, and core body temperature regulation). Any disturbance of this homeostatic process governing either energy intake or expenditure will almost undoubtedly affect the other arm of the system. If this disruption exceeds the body's ability to regain balance, the risk of diseases related to energy balance such as obesity is increased.

The most important center associated to the coordination of energy balance is the central nervous system (CNS) [16]. Given the reciprocal link between energy intake and expenditure and the fundamental requirement to ensure that adequate energy is available for cellular processes required for survival and reproduction, the CNS control of energy balance is multi-determined. Peripheral signals, neural receptors, and regions of the brain operate with a degree of redundancy to ensure that enough energy exists to sustain life.

When discussing how the brain regulates energy balance, we must consider "the meal" as the fundamental unit of energy intake [16]. The feed-back mechanism works due to our body monitors and releases hunger-related hormone such as ghrelin. Its level typically rise before a meal, when the stomach is empty to stimulate the appetite signals [17]. Once a meal has begun, the brain perceives various components of the meal including the taste and texture of the food, probably communicating the presence of nutrients (*e.g.,* fats and sugars) that promote for further feeding.

Many of these afferent signals relayed to the brain come from: mechanical distension of the gastrointestinal (GI) tract via vagal communication with CNS, nutrients digested per-se *e.g.,* glucose, free-fatty acids (FFAs) and neuroendocrine signal released

from GI and other tissues in response to the digestions. Some of these signals are referred to as *satiation signals*, (*i.e.* cholecystokinene (CCK), insulin, glucagon, leptin) or within-meal intake inhibitory signals. As these satiation signals accumulate, feeding rate slows and eventually *satiety* or meal termination is achieved.

1.3. Hypothalamus and AgRP/NPY neurons

There are numerous brain structures involved in the control of energy balance. Much of evidence has focused on the role of hypothalamus because it is one of the main centers associated to the control of energy body homeostasis.

The hypothalamus is a region of the diencephalon located below the thalamus on each side of the third ventricle. It is composed of many small neuronal nuclei that integrate endocrine, nutritional and sensory signals, which culminate in the generation of precise neuroendocrine, behavioral, and autonomic responses to control body homeostasis. Anatomically, the hypothalamus extends from the anterior commissure, lamina terminalis, and optic chiasm to the caudal limit of the mammillary bodies. Within these anatomical limits, hypothalamic nuclei are organized into the following zones and regions: preoptic area, composed of the medial and lateral preoptic nuclei; lateral zone, includes the lateral hypothalamic nucleus (LHA) and the tuberal nucleus, the medial zone, subdivided into the anterior (or supraoptic) region, which contains supraoptic (SO), paraventricular (PVN), suprachiasmatic, and anterior nuclei; the tuberal region, which contains ventromedial nucleus (VHM), the dorsomedial hypothalamic nucleus (DMN) and the arcuate nucleus (ARC); and finally the third region or mammillary part, which consists of the medial, intermediate, lateral mammillary and posterior hypothalamic nuclei (Figure 1).

One important function of the hypothalamus is the regulation of energy balance and food intake. Experiments done by Hetherington and Ranson over 70 years ago reported that lesions in the VHM nuclei of rats caused hyperphagia and obesity [18]. Later, Anand and Brobeck demonstrated in 1951 that bilateral destruction of the

lateral portion of the LHA causes complete inhibition of food intake [19]. These results gave rise to the “dual-center hypothesis”, which suggests that VHM and LHA are the hypothalamic centers that regulate satiety and appetite respectively [20]. Nonetheless, following studies have further established that ARC nuclei play a more crucial role in the regulation of food intake and energy balance.

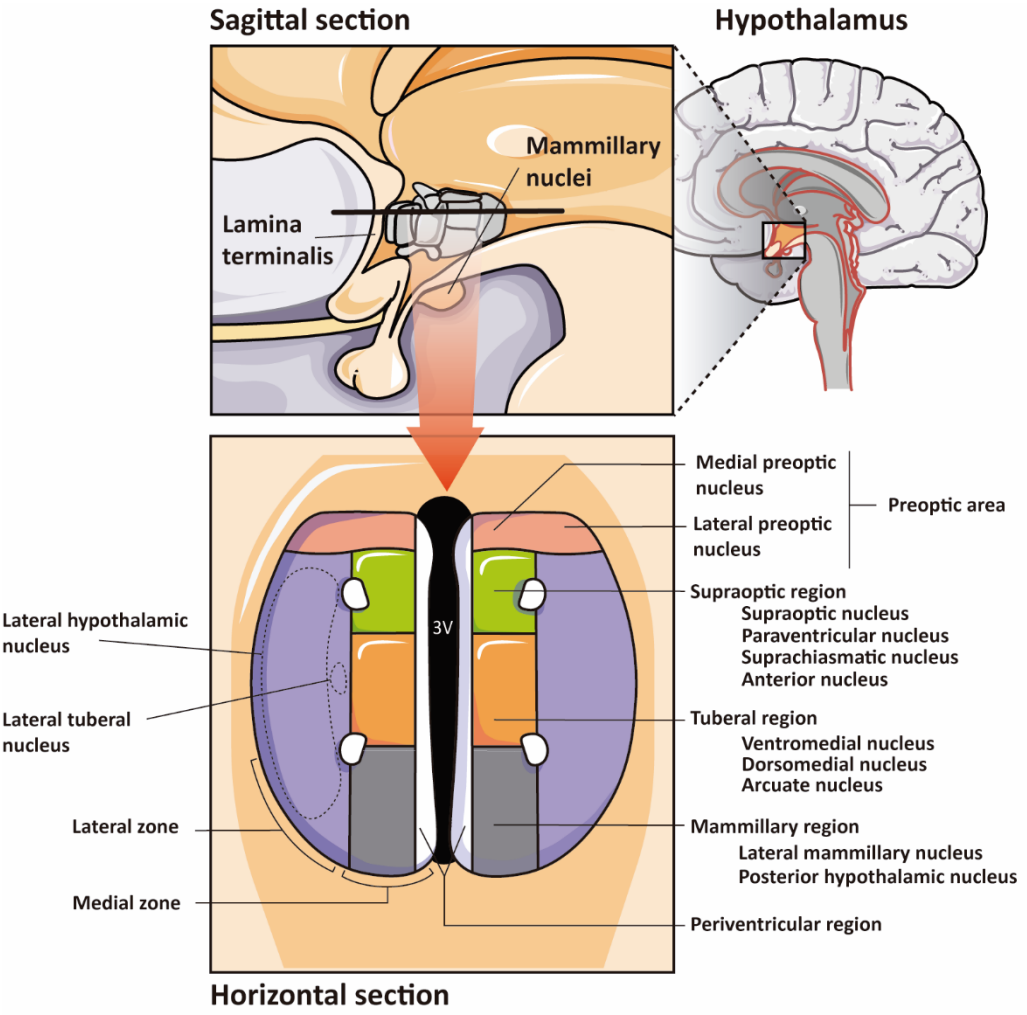

Figure 1. Diagram of hypothalamus nuclei.
Scheme of sagittal and horizontal section of the hypothalamus and nuclei localization.

The relevance of the ARC was identified with the discovery of the melanocortin system, which plays a key role in a number of homeostatic processes [21,22], and reviewed elsewhere [23,24]. The melanocortin system consists of 1) melanocortin peptides (α, β and γ melanocyte-stimulating hormone (MSH) and adrenocorticotropic hormone (ACTH)) derived from the precursor proopiomelanocortin (POMC); 2) five melanocortin receptors (MCRs, MC1R-MC5R, MC3R and MC4R are particularly involved in food intake energy balance regulation), which are widely expressed in the hypothalamus; and 3) the endogenous melanocortin antagonist Agouti-related protein (AgRP). All these components are expressed mainly in two populations of hypothalamic neurons: neurons that co-produce AgRP, neuropeptide-Y (NPY), and gamma aminobutyric acid (GABA) (AgRP/NPY neurons) [25,26] and neurons that co-produce POMC and cocaine and amphetamine-stimulating hormone transcript (CART) (POMC/CART neurons) [27]. Both are located at the base of the hypothalamus in close proximity to fenestrated capillaries.

POMC/CART neurons and AgRP/NPY neurons exert opposite functions and are reciprocally regulated. While POMC/CART neurons express anorexigenic peptides and have appetite-suppressing functions, AgRP/NPY neurons express orexigenic peptides and have an appetite-stimulating role. NPY acts as a neurotransmitter in the brain and is thought to have several functions besides food intake, including regulation of fat storage [28]. The appetite-stimulating response to NPY is mediated by multiple NPY receptor subtypes, which are all G_i protein-coupled receptors. There are six identified NPY receptors, but the Y1 and Y5 isoforms are most strongly associated with the effect of NPY on feeding revised in [29]. Furthermore, AgRP/NPY neurons also release AgRP neuropeptide, a melanocortin antagonist that prevents the binding of α-MSH onto MC3R and MC4R, thus activating hunger [30]. AgRP/NPY neurons also release GABA. GABA is an inhibitory neurotransmitter, and may exert its orexigenic action through GABAergic-mediated inhibition of POMC/CART neurons [31] (Figure 2).

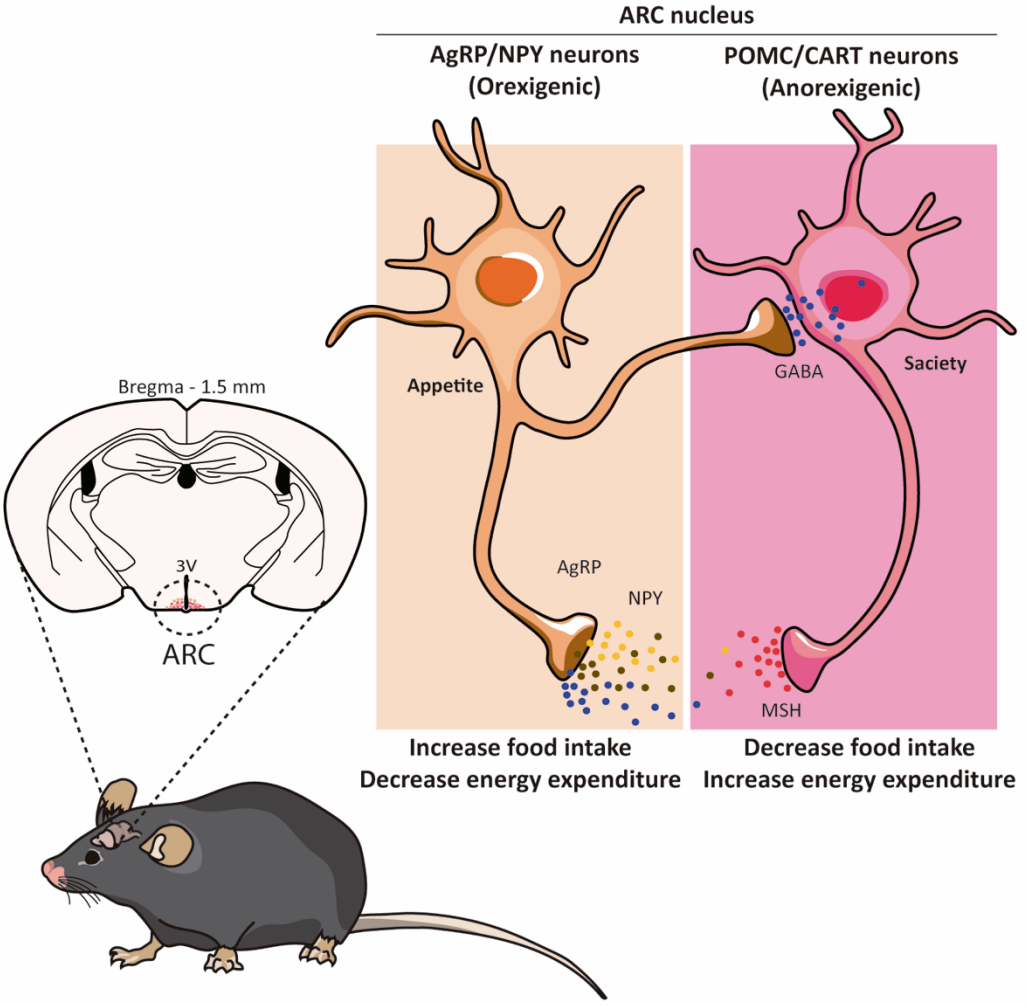

Figure 2. The melanocortin system.
The primary neurons of the melanocortin system are the orexigenic AgRP/NPY neurons and the anorexigenic POMC neurons, which both send projections to a second order neurons to stimulate appetite or satiety. While AgRP/NPY neurons release NPY, GABA and AgRP, POMC neurons express different post-transcriptional products of the Pomc gene, including α-,β-,ɣ-MSH. Both group of neurons are located at the base of the hypothalamus in close proximity to fenestrated capillaries. Neuropeptide Y (NPY), ɣ-amino-butyric acid (GABA), agouti related protein (AgRP), third ventricle (3V), arcuate nucleus (ARC), melanocyte-stimulating hormone (MSH).

1.4. The role of AgRP neurons in food intake

There are numerous neurons distributed in the brain that influence appetite [32], yet AgRP neurons within the hypothalamus are probably the neuronal population that has the strongest and most closely documented association with feeding behavior [33,34]. The first evidence supporting the role of AgRP neurons in food intake control came from experiments showing that AgRP and NPY injection in the brain increase food intake. It was also drawn from the observation that AgRP and NPY release is higher in brain sections of food-deprived mice [35].

These early results have been confirmed recently by using the innovative cell type-specific approaches. For example, optogenetic and pharmacogenetic activation of AgRP neurons result in a robust increase in food intake, even in fed mice [36]. Moreover, ablation of AgRP neurons in adult, but not neonatal, mice results in an acute reduction of feeding and starvation [37–39]**.** The differences observed between neonatal and adult mice suggest that network-based compensatory mechanisms can occur in neonates but not in the adult stage [40]. Surprisingly, deletion of the entire *Agrp* coding sequence using BAC-based targeting vectors did not generate differences in food intake or body weight in adult mice before 6 months of age [38]. Likewise, deletion of *Npy* had little effect on body weight control [42,43]. These observations suggest that GABA, also produced by AgRP neurons, might be a critical neurotransmitter regulating food intake and energy balance. Actually, disruption of GABA signaling by selective inactivation of the vesicular GABA transporter gene (*Vgat*) in AgRP neurons caused a lean phenotype and protected mice from diet-induced obesity [31]. Accordingly, chronic and subcutaneous delivery of bretazenil (a partial $GABA_A$ receptor agonist) prevented starvation in AgRP neuron-ablated mice [44].

GABA is an inhibitory neurotransmitter and thus GABAergic input from AgRP neurons inhibits the activity of several neuronal populations within the brain, including POMC neurons from the ARC. This crosstalk between orexigenic and anorexigenic neurons in the ARC is essential for the precise regulation of food intake [34]. In addition,

GABAergic projections from AgRP neurons also suppress the activity of neurons in the PVN [45]. Because activation of PVN neurons decreases feeding [46], it has been suggested that AgRP neurons increase food intake in part through the GABAergic inhibition of PVN neurons. Another important GABAergic target of AgRP neurons is the parabrachial nuclei (PBN). However, in this nucleus GABA promotes feeding, since administration of bretazenil (a GABA(A) receptor partial agonist) into the PBN prevents starvation in AgRP neuron-ablated mice [44].

Independently of the neurotransmitter released, there are many areas in the brain under the control of AgRP neurons that regulate feeding behavior. Elegant optogenetic experiments by Brüning and colleagues confirmed previous studies showing that AgRP neurons control neurons in the PVN to influence feeding [47]. Likewise, they showed that LHA and the anterior bed nucleus of the stria terminalis (aBNST) dorsomedial nucleus were activated by AgRP projections to promote feeding, while the dorsal vagal complex, dorsal raphe nucleus and aBNST ventral lateral nucleus were not [47]. Overall, this study suggested that AgRP neurons orchestrate the activation and inactivation of various brain areas to promote food seeking and intake.

Now the question is: what is the mechanism by which AgRP neurons are activated upon starvation? A large amount of evidences indicates that ghrelin action on these neurons leads to their activation. Ghrelin is a 28-amino acid peptide produced in the stomach. Ghrelin blood levels increase pre-prandially and decrease post-prandially. Ghrelin increases food intake by activating its receptor GHS-R in AgRP neurons [17,48]. Of note, ghrelin administration increases AgRP firing in brain slices from control mice but not from mice lacking growth hormone secretagogue receptor (*Ghsr)* specifically in AgRP neurons ($Ghsr_{AgRP}^{-/-}$) [49]. Ghrelin increases the mRNA levels of *Npy* and *AgRP* in AgRP neurons, yet the molecular mechanism remains partially unclear [50]. It has been suggested that the AMP-activated protein kinase (AMPK)-Carnitine palmitoyl transferase 1A (CPT1A)- Uncoupled protein-2 (UCP2) axis is a relevant pathway in the ARC, which is involved in ghrelin's control of food intake [51].

AMPK is a downstream target of GHS-R, and upon its activation it inhibits acetyl-CoA carboxylase (ACC), thus decreasing the intracellular levels of malonyl-CoA. Malonyl-CoA is the physiological inhibitor of CPT1A, which is the rate-limiting step in the mitochondrial fatty acid oxidation (FAO) pathway (see more information in section 1.5.2). Increased FAO generates reactive oxygen species (ROS) and subsequent UCP2 activity. Using a mouse model lacking *Ucp2* in all cells, it had been suggested that UCP2 mediates ghrelin's actions on AgRP neurons by lowering free radicals [52]. However, cell-type specific studies are needed to clarify the role of UCP2 in AgRP neurons in regulating food intake (Figure 3).

Another proposed candidate to mediate ghrelin's orexigenic action in the ARC is the NAD^+-dependent class III deacetylases sirtuin 1 (SIRT1). SIRT1 is expressed in the hypothalamus, its function is redox dependent, and it is induced by negative energy balance. In fact, central administration of ghrelin increases SIRT1 activity in the hypothalamus and the blockade of SIRT1 abolished the orexigenic effect of this hormone [53]. Another study showed that the SIRT1/p53 pathway is essential for the orexigenic action of ghrelin [54]. Of note, cell-type specific ablation of Sirt1 ($Sirt1_{AgRP}^{-/-}$ mice) in AgRP neurons determined that this neuronal population mediates the action of SIRT1 on energy balance: $Sirt1_{AgRP}^{-/-}$ mice shows decreased electric responses of AgRP neurons to ghrelin, decreased food intake, decreased lean mass, fat mass, and body weight [53].

Finally, ghrelin stimulates AgRP and NPY neuropeptide expression through the activation of transcriptional factors, such as brain specific homeobox (BSX) protein. BSX needs to interact with another two transcription factors to activate *Agrp* and *Npy* messenger ribonucleic acid (mRNA) expression: forkhead box O1 (FOXO1) for the *Agrp* gene and the phosphorylated cAMP response-element-binding protein (pCREB) for the *Npy* gene [55]. Nonetheless, it has been demonstrated that in rat fibroblast, FOXO formed a complex with SIRT1 in response to oxidative stress [56] and enhances FOXO

transcriptional activity [57], but so far there is no evidence that all these events occur specifically in AgRP neuronal cells (Figure 3).

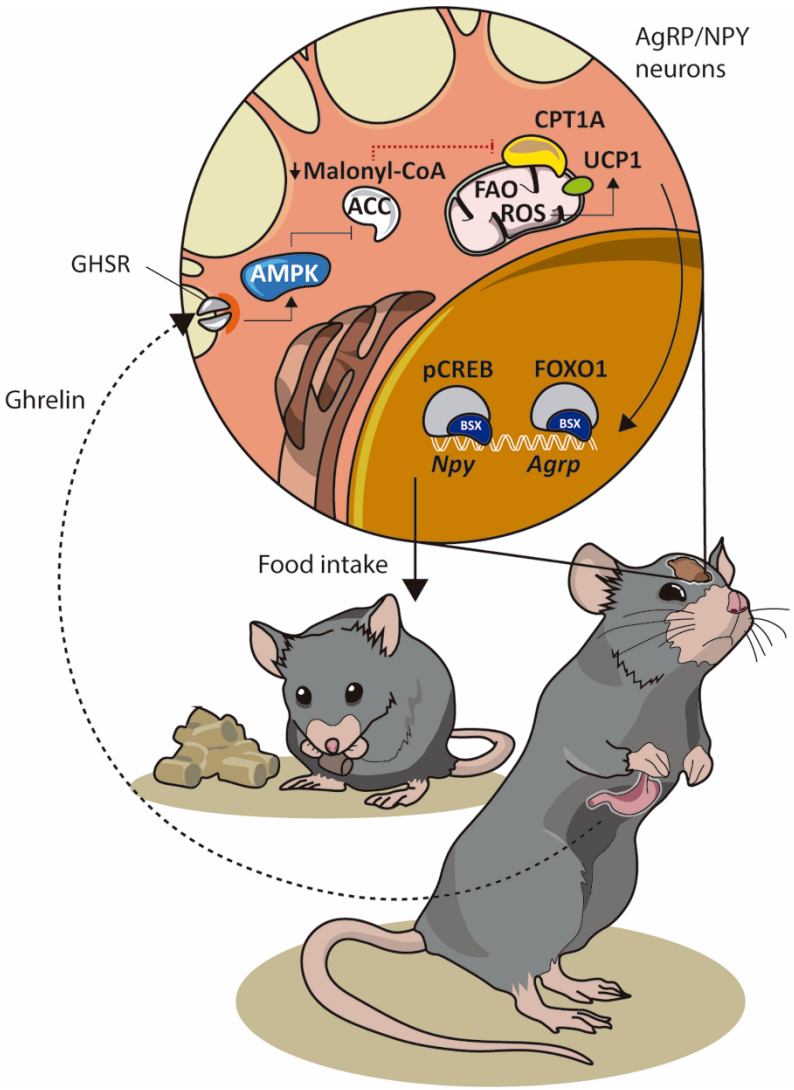

Figure 3. Molecular mechanism leading to ghrelin-induce AgRP activation.
Molecular pathway and mitochondrial metabolism resulting in *Agrp* and *Npy* expression after ghrelin receptor activation. Ghrelin receptor (GSHR), acetyl coenzyme A carboxylase (ACC), 5' adenosine monophosphate-activated protein kinase (AMPK), reactive oxygen species (ROS), carnitine-palmitoyltransferase-1A (CPT1A), uncoupled protein-2 (UCP2), cAMP response-element-binding protein (pCREB), forkhead box O1 (FOXO1), brain specific homeobox (BSX), neuropeptide Y (NPY), agouti related protein (AGRP).

In summary, all the *in vivo* studies have established that AgRP neurons integrate the ghrelin signal to coordinate goal-directed behavior, such as food seeking and intake.

1.5. Feed-back mechanism of AgRP neurons to regulate peripheral metabolism

Once meals are digested, in addition to the neuroendocrine signals, macronutrients such as carbohydrates and lipids serves as a signal to the AgRP neurons and regulate peripheral metabolism and energy expenditure.

1.5.1. Glusose-sensing AgRP neurons to impact peripheral metabolism

Every organism needs to match energy intake and expenditure to be able to subsist. Therefore, from a homeostatic perspective, hunger must be understood as a response emitted from the central nervous system in response to whole-body energy balance. For example, Horowitz M and colleagues showed in 1998 that physiological changes in blood glucose levels affect appetite [58]. Indeed, several decades ago, it had already been demonstrated that specific hypothalamic neurons can sense blood glucose concentrations. Yet, the precise molecular mechanisms underlying this observation are still incomplete.

As mentioned above, activation of AgRP neurons promotes food seeking and intake. After a meal, blood glucose levels increase and, as a result, POMC neurons are activated. While the mechanisms underlying the excitatory actions of glucose on anorexigenic POMC neurons are clear, it is not completely understood yet if and how glucose could directly inhibit AgRP activity as revised in [59,60].

Neurons could sense glucose levels through the ATP-dependent potassium (K_{ATP}) channels, which control potassium flow to depolarize or hyperpolarize the neuron membrane depending on the levels of ATP generated from glucose catabolism [59,61]. The extracellular concentration of glucose in the brain is approximately 2.5 mM during

the fed state and 0.5-0.2 mM during the fasted or hypoglycemic condition. POMC neurons increase spike firing when the concentration of brain glucose changes from 0.1 mM to 2 mM [62], and that is dependent on K_{ATP} channel subunits [63]. Conversely, the expression of a mutated K_{ATP} channel subunit that was insensitive to the ATP in POMC neurons impaired the whole-body response to a systemic glucose load [61].

It is unclear whether K_{ATP} channels are also involved in the glucose-dependent modulation of AgRP neurons. Even though K_{ATP} channels are expressed in AgRP neurons, probably because some of these neurons share a common progenitor with POMC neurons, only a minority of AgRP neurons are glucose responsive [60,62,64,65]. It has been reported that these subsets of neurons are inhibited by an increase in glucose from 1 to 10 mM [66] and appear to be directly activated by decreased glucose levels (from 2.5 mM to 0.1 mM) via K^+ channel closure [67] suggesting that this glucose responsive subset of AgRP neurons has a high impact on the glucose sensing mechanisms.

Yet, AgRP neurons respond to insulin levels. Insulin hyperpolarizes AgRP neurons in wild-type (WT) mice but not in those lacking the insulin receptor (IR) in AgRP neurons specifically ($IR^{\Delta AgRP}$) [68]. Insulin inhibits AgRP neuronal activity by activating the phosphoinositide 3-kinase (PI3K) signaling pathway. The phosphatidylinositol-3,4,5-triphosphate (PIP_3) that is generated activates K_{ATP} channels, resulting in hyperpolarization and a decreased neuronal firing rate, with subsequent reduced release of AgRP [68]. PI3K activation ultimately leads to the exclusion of FOXO1 transcription factor from the nucleus [69]. FOXO1 increases AgRP expression [70], thus insulin action in AgRP neurons ultimately decreases the expression of AgRP. This signaling pathway has also been described in POMC neurons, but in those neurons the exclusion of FOXO1 from the nucleus promotes POMC expression [71]. Taken together, these studies suggest that POMC neurons sense glucose levels, while AgRP neurons respond to changes in insulin concentration.

In addition, AgRP neurons influence peripheral glucose metabolism. For instance, the ablation of these neurons in adult $AgRP^{DTR}$ mice caused a reduction in blood glucose levels 48 hours after the administration of diphtheria toxin [41]. One of the molecular explanations for this phenotype is the decreased hepatic gluconeogenesis observed in this model [68,72]. Accordingly, the acute activation of AgRP neurons using either a chemogenetic or optogenetic approach caused an increase in blood glucose levels due to systemic insulin resistance and decreased glucose uptake in brown adipose tissue (BAT) [47]. At molecular level, several genes in AgRP neurons have been associated with this regulation of whole-body glucose homeostasis. For instance, the deletion of purinergic receptor 6 (P2Y6) specifically in AgRP neurons, improved systemic insulin sensitivity in obese mice [73] and similar results have been observed when the transcription factor activating transcription factor 4 (ATF4) was deleted specifically in AgRP neurons [74].

Taking all this information together suggests that AgRP neurons are able to detect glucose levels and regulate peripheral organ functions to ensure that its energy requirements are met.

1.5.2. AgRP neurons and lipid metabolism

Among the main functions of lipids in the nervous system, of undoubtable importance is their structural role in biological membranes, their participation as bioactive messengers involved in cell signaling and their contribution to energy supply. Around this, the human brain accounts for ~2% of the body mass, but consumes 20% of the total oxygen consumed by the whole body. The high-energy requirement of brain tissue is matched by multiple interactions between neurons, astrocytes, and cerebral blood vessels to guarantee the supply of neurons with sufficient oxygen and oxidizable substrates [75]. As such, it requires a near constant source of metabolites to maintain function.

The general consensus is that this energy requirement is almost entirely satisfied by glucose metabolism [76]. However, it has been shown that approximately 20% of the total energy requirement of the brain is met through the oxidation of fatty acids (FAs) [77]. Even, it was thought for a long-time neuron do not used FAs as a fuel due to they were not able to cross the blood–brain barrier (BBB), but numerous studies have demonstrated that cerebral lipids arise from both local synthesis as well as plasma origin [78–80].

Not only uptake but also the breakdown of lipids has recently gained attention in the field of neuronal research. Some evidences suggest that neuronal triglyceride (TG) lipases are very active and that TGs undergo constant turnover in adult neurons [81]. TG lipase hydrolyzes a TG to one FAs and one diglyceride (DG). DGs are also a precursor of TGs and PLs. Because PLs and TGs share common precursors, neurons likely utilize this strategy to direct the flow of these lipids toward membrane generation or energy production through lipid oxidation depending on needs [82]. Although the oxidation of FAs in neurons is little explored, here we delve into some key aspects of FA utilization for energy and new questions raise of whether FAs could be also a signal to AgRP neurons.

It has been shown that intracerebroventricular (icv) administration of long-chain FAs (LCFAs) inhibits the expression of NPY and AgRP in the hypothalamus, and therefore food intake [83]. Very recently, it has been reported that G-protein-coupled receptor 120 (GPR120) and GPR40, also known as free fatty acid receptor 1, are expressed in the hypothalamus of mice. The majority of cells that express POMC and AgRP also express GPR40 [84]. This receptor binds free FAs, acting as a nutrient sensor [84,85]. Of note, the icv administration of TUG905, which is an agonist of GPR40, reduces body weight [84]. The fact that GPR40 is expressed in AgRP and POMC neurons suggests that these cells could sense the content of FAs in the hypothalamus to regulate food intake and peripheral energy metabolism accordingly.

Besides, most enzymes of the FA metabolic pathways are expressed in the hypothalamus, including AMPK [86,87], ACC, CPT1, fatty acid synthase (FAS), and malonyl-CoA decarboxylase (MCD) [88]. Of note, fasting stimulates hypothalamic AMPK and inhibits ACC and FAS activities, whereas re-feeding induces opposite changes [89,90]. Moreover, pharmacological and genetic manipulation of some of these genes/proteins has a profound impact on food intake and whole-body energy homeostasis. For instance, icv administration of the FAS inhibitor cerulenin reduces feeding and causes weight loss due to the reduction of *Npy* and *Agrp* expression in the hypothalamus [91]. The anorectic effect of this drug requires the accumulation of malonyl-CoA in the hypothalamus, which in turn inhibits CPT1A, a key regulatory enzyme of the FA oxidation pathway.

Additionally, the hypothalamus regulates peripheral lipid metabolism and adiposity. For instance, disruption of melanocortin signaling in the brain promotes lipid uptake, TG synthesis, and fat accumulation in white adipose tissue (WAT) [92]. Conversely, stimulation of MCRs reduces adiposity [93]. Within the hypothalamus, the activity of AgRP neurons impacts peripheral lipid metabolism. In fact, the activation of AgRP neurons promotes lipogenesis via the sympathetic nervous system (SNS) [94]. Additionally, the deletion of carnitine acyltransferase specifically in AgRP neurons increased FA utilization and attenuated the switch to glucose utilization after re-feeding [95]. Moreover, the deletion of ATF4 specifically in AgRP neurons increases lipolysis in epididymal WAT, thus promoting fat loss [74]. Taken together, these results reinforce the metabolic signal that AgRP induce in response to the fuel availability [96,97].

1.5.2.1. Role of CPT1A: sensor of neuronal energy status

Neurons are not energy-storing cells and do not normally contain a significant pool of lipid droplets (LD). Therefore, the available energy is depleted rapidly. This is one factor that makes them especially sensitive to stressful conditions such as

continued stimulation. According to that, oxidation of FAs may be an important source of energy for neuronal metabolism.

FA utilization for energy occurs through FAO, which takes place in the mitochondrial matrix. In order to be oxidized, FAs are converted to fatty acyl-CoA by acyl-CoA synthases with the subtype of enzyme varying by FA composition through two-step thioesterification reaction [98]. Once this reaction takes place, the substrates are transported across multiple mitochondrial membranes to the mitochondrial matrix. This process is catalyzed by a set of proteins known as carnitine acyltransferase [99] .

Carnitine acyltransferases are a large family of enzymes that play a main role in cellular energy metabolism, for example FAO. Catalyzes the formation of a complex between acyl-CoA and carnitine to produce acylcarnitine in the intermembrane space. Depending on their acyl group specificity as well as their localization, three different classes of enzymes which are known as carnitine acetyltransferases (CraTs), carnitine octanoyltransferases (COTs) and carnitine palmityltransferases (CPTs) have been reported.

While CrATs prefer short chain FAs as substrates and are localized in the mitochondrial matrix, the endoplasmic reticulum, and the peroxisome, COT facilitates the transport of medium-chain FAs from peroxisomes to mitochondria through the conversion of acyl-CoAs, shortened by peroxisomal β-oxidation, into acylcarnitine and are mainly found in peroxisomes [100].

The main focus of this project is the CPTs (Figure 4). CPT1 and CPT2 are located in the mitochondrial outer membrane (MOM) and the mitochondrial inner membrane (MIM), respectively. It facilitates the transfer of long-chain acyl groups from the cytoplasm to the mitochondrial matrix, a process that represents the rate-limiting step in β-oxidation. CPT1 is the only acyltransferase that has direct access to the cytosolic pool of acyl-CoA. Mammals express three CPT1 isoforms, CPT1A, CPT1B and CPT1C, which are encoded in different genes and present differential biochemical

characteristics as well as different tissue distribution (Table 1). Nonetheless, only two CPT1 isoforms are expressed in the brain; CPT1A and CPT1C.

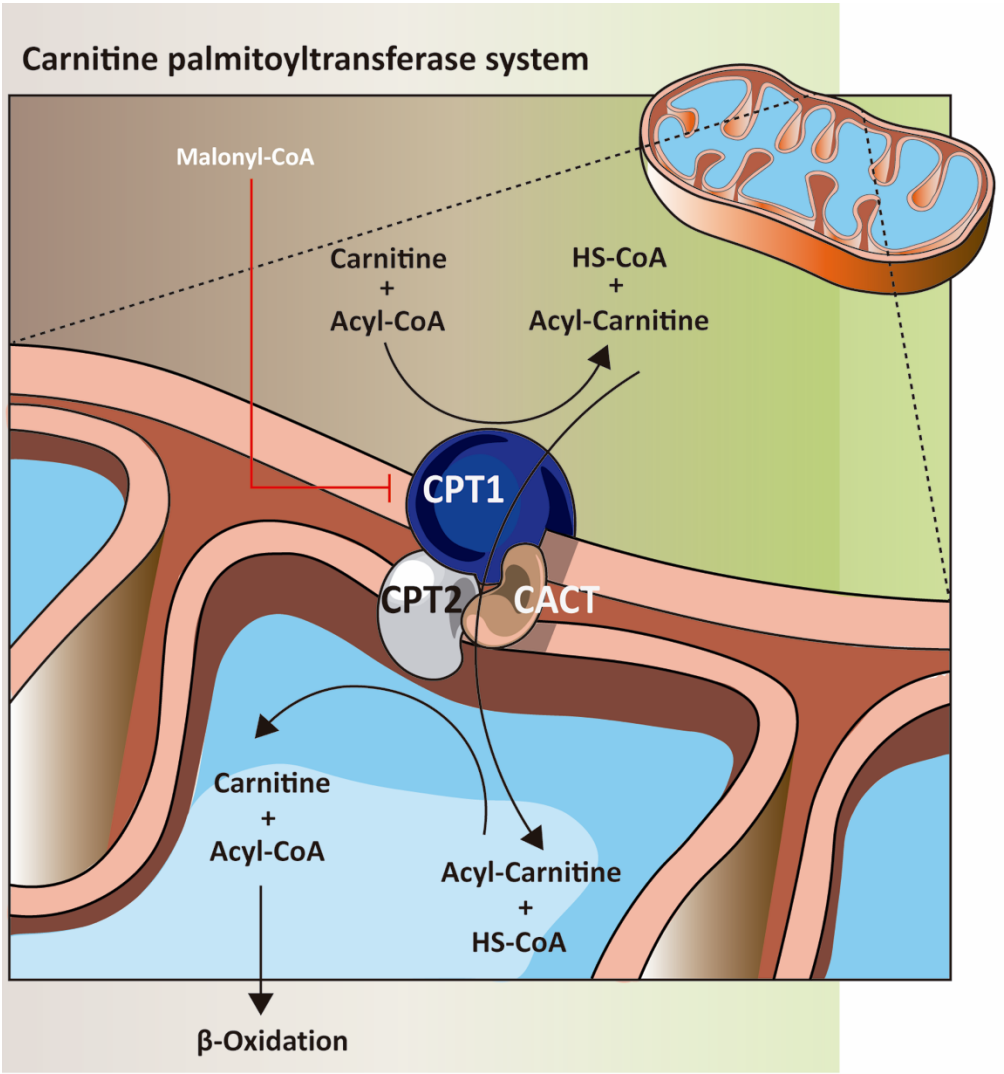

Figure 4. Carnitine palmitoyl transferase system.
Schematic representation of the role of CPT1 in shutting long chain acyl-CoA derivatives through the mitochondrial membrane.

CPT1A is the most widely distributed isoform, it represents the major hepatic isoform but is also expressed in lungs, pancreas, bowel, kidneys, ovaries and brain. Its gene in located in chromosome 11 and codifies for a 773 residues protein whose molecular mass is 88 kDa. CPT1B, has a predicted size of ~88k Da, but folds in such a way that its apparent size is about 82 kDa [101,102]. It is the non-neuronal isoform, is expressed in skeletal muscle, heart, BAT, WAT and testis. Interestingly a profound species- and gender-dependent differences in expression of CPT1A and CPT1B has been reported. For example, CPT1A is expressed in WAT of male mice but not of female mice. CPT1B is expressed in WAT of humans, female mice and male rats, but not in male mice and female rats [103].

Table 1. Comparative summary of all known proteins belonging to the carnitine palmitoyl transferase family.

	CPT1A	CPT1B	CPT1C	Reference
Subcellular location	Outer mitochondria membrane	Outer mitochondria membrane	Endoplasmic reticulum	[104]
Main tissue distribution	Heart, liver, and pancreas	Heart and skeletal muscle	Brain	[104]
Function	Oxidation of long-chain fatty acids, nucleotide synthesis	Oxidation of long-chain fatty acids, nucleotide synthesis	Potential energy sensor in brain	[105,106]
Substrate	Medium and long acyl-CoA esters	Medium and long acyl-CoA esters	Unknown	[103]
Chromosome location	11q13.1-q13.5	22q13.3-qter	19q13.33	[103]

CPT1C is mainly found in the brain, but also in testis [107]. This enzyme has been discovered later than CPT1A and CPT1B and the function of this protein is not yet fully understood. It is encoded by a gene in the chromosome 19, which was described as a CPT1 gene because of its similitude with CPT1A. No orthologous sequences of CPT1C can be found in other species but mammals, which suggests a specific function

in more evolved brains. Functional studies have been hampered by the fact that the enzyme is not active in mitochondria, although it is able to bind to the natural CPT1 inhibitor malonyl-CoA [107]. It has been reported that CPT1C has a prevalent role in the endoplasmic reticulum with a really low transesterification catalytic activity in vitro [108].

1.5.2.2. Role of CPT1A/Malonyl-CoA system

CPT1 is tightly regulated by its physiological inhibitor malonyl-CoA, and thus, CPT1 is the most important regulatory step in mitochondrial FAO. Malonyl-CoA is produced by the condensation of two acetyl-CoA moieties catalyzed by ACC.

Early studies published in 1980 [109,110], described how the sensitivity of the inhibition of fatty acid oxidation or "outer" CPT activity of isolated rat liver mitochondria by malonyl-CoA was markedly decreased in preparations from fasted or diabetic rats compared to those from fed animals. This suggested that the enzyme became less sensitive to the inhibitor when the concentration of the latter was declining (and vice-versa). This inhibition is competitive with respect to palmitoyl-CoA and results in considerable sigmoidicity in the kinetic of CPT1 with respect this substrate suggesting that CPT1 might show regulation of an allosteric manner [111]. The sensitivity for inhibition is different for CPT1A and CPT1B, the latter being about 100-fold more sensitive [99].

In hypothalamus, it has been suggested that malonyl-CoA, a key metabolite in the synthesis and degradation of fatty acids, acts as a molecular messenger of nutritional status in these processes [112] and CPT1A could be the sensor of the neuronal energy status. It has been proposed that in situations of increased malonyl-CoA, it would act by inhibiting CPT1A and limiting the oxidation of long-chain acyl-CoA and this would regulate the expression of orexigenic neuropeptides (NPY and AgRP) and anorectic (POMC and CART). This mechanism is supported by observations where an icv injection of inhibitors of CPT1A activity or a CPT1A riboprobe that causes genetic

inhibition of hypothalamic CPT1A reduced food intake [113]. On the contrary, the orexigenic action of ghrelin would be mediated by an activation of AMPK which in turn would inactivate ACC, thus preventing the synthesis of malonyl-CoA and consequently increasing CPT1A activity [70]. This increase in CPT1A activity would produce an increase in ROS that could be partly responsible for the orexigenic response [52]. All of this points to a key role of CPT1A, but the mechanisms below CPT1A in the different hypothalamic nuclei that lead to the orexigenic response are not yet known.

Studies carried out by our group showed that overexpression of CPT1AM [114] (insensitive to malonyl-CoA) in the VHN of the hypothalamus produces hyperphagia and obesity [115]. This is associated with notable changes in the lipid profile of the mediobasal region (ARC + VHN nuclei) of the hypothalamus and with changes in the expression levels of glutamate and GABA transporters [115]. On the other hand, in the ARC nucleus, the same overexpression of CPT1A does not alter the intake in response to leptin [116], of course, in this nucleus two neuronal types coexist with orexigenic functions (AgRP and NPY neurons) and anorexigenic (POMC neurons) clearly opposed. All this indicates that each hypothalamic nucleus has a differentiated functionality and alterations in specific neurons of these nuclei produce different systemic and food intake effects. The use of genetic tools such as the *Cpt1a*$^{flox/flox}$ mouse obtained in our group helped to develop the main objective of this project and to discern the role of CPT1A in AgRP orexigenic neurons in the ARC of hypothalamus and to confirm CPT1A as a target for therapies against obesity.

1.6. The role of AgRP neurons in energy expenditure

Until now we have analyzed the signals that modulate the activity of AgRP neurons and the effect that they have on food consumption. The specific activation of these neurons produces intense hunger as well as a rapid decrease in energy expenditure. Remarkably, little attention has been paid to the mechanisms producing suppression of energy expenditure by AgRP neurons, leaving the downstream circuitry

mediating this effect unknown. Despite this, a link between AgRP neurons and thermogenesis as a component of the body energy expenditure has been described. Thermogenesis, literally defined as heat production, is an important physiological variable as well as a normal by-product of metabolic processes. It may occur via shivering and nonshivering mechanism in skeletal muscle and by the increase of BAT activity.

According to this, adipose tissues can be classified as WAT, which stores energy in the form of TG, and BAT, which is highly oxidative and contains abundant mitochondria that oxidize FAs to generate heat via the BAT-specific UCP1. In response to specific stimuli, certain WAT depots can undergo a process known as browning described as an increased mRNA expression of UCP1 where the tissue takes on characteristics of BAT.

One of the first experiments that linked food intake with thermogenesis was completed by Rothwell A and Stock M in 1997 [117]. The study demonstrated that food consumption increases the activity of BAT through the SNS, which could be an important compensatory mechanism in case of energy surplus. In addition, caloric restriction and feeding-fasting cycles also regulate body temperature and thermogenesis in BAT [118]. While it is known that sympathetic activity in BAT and WAT controls heat production and energy homeostasis [119], the same neurons that regulate energy intake may also control feeding-induced thermogenesis. It has been demonstrated that the icv infusion of AgRP gradually suppressed sympathetic tone in BAT thus decreasing thermogenesis [120].

Using the optogenetic approach, acute activation of AgRP neurons strongly inhibited the expression of thermogenic genes, including *Ucp1*, in retroperitoneal WAT, and to a lesser extent in inguinal WAT, which indicates that AgRP neurons suppress the browning of WAT [96]. While the inhibition of AgRP neuronal activity by selectively deleting the O-GlcNAc transferase caused WAT browning in those mutant mice [96].

As we mentioned before, ghrelin acts on AgRP neurons through its receptor (GHS-R) to activate food consumption. Deletion of GHS-R specifically in AgRP neurons (*AgRP-Cre*;*Ghsr*^{floxflox} mice) caused increased energy expenditure in mice fed a high fat diet (HFD), and enhanced thermogenic activation in both BAT and subcutaneous WAT [121]. Overall, the role of AgRP neurons in thermogenesis could be an important target to increase energy expenditure and thus fight against obesity.

1.7. WATER HOMEOSTASIS

In order to maintain body homeostasis, it is logical to assume that the increase of food intake would drive the concomitant increase of water consumption. Some evidence demonstrates that animals drink more after meals than at other times and show a drop-in food intake during water deprivation. For example, animals without water do not eat as much food as usual [122]. This physiological feed-back response rises the questions whether hypothalamus could be involved in the fluid balance in response to food consumption. Thus, it is unclear whether AgRP/NPY neurons are involved in fluid intake behavior. In this section, we will describe the fluid balance in order to elucidate whether AgRP/NPY could be involved in the fluid homeostasis.

1.7.1. Body Water Content

Human beings are mostly water, ranging from about 75 percent of body mass in infants to about 50–60 percent in adult men and women, to as low as 45 percent in old age. In young adult males, body water is about 60% of body weight and in young adult females, who have a higher percentage of body weight as fat, about 50% [123,124]. Total body water is generally distributed into two mainly categories: the intracellular fluid (ICF) and extracellular fluid (ECF). The ICF is approximately 40% of the total body weight. It includes all fluid enclosed in cells by their plasma membranes and do not readily adjust rapidly to changes. The ECF comprises approximately 20% of total body weight and further subcategorizes as plasma at approximately 5% of body weight and interstitial space which is approximately 12% of body weight. Finally, about 1-2% of body water is 'trans-cellular water' found in cerebrospinal fluid, the humours of the eye, digestive secretions, renal tubular fluid and urine. Trans-cellular water are separated from the ECF by an endothelium and a continuous epithelial layer [125].

On a typical day, the average adult will uptake about 2,500 ml of water. Although most of the intake comes through the digestive tract, about 230 ml per day is generated metabolically, in the last steps of aerobic respiration. Additionally, each day

about the same volume (2,500 ml) of water leaves the body by different routes; most of this lost water is removed as urine. The kidneys also can adjust blood volume though mechanisms that draw water out of the filtrate and urine [123,126].

1.7.2. Fluid Homeostasis

Fluid homeostasis is the term for maintaining the concentration of the fluids in the body. The unit of solute concentration that are often used in reference to the body fluid are osmolarity and osmolality. While, osmolarity refers to the number of solute particles per 1 L of solvent, osmolality is the number of solute particles in 1 kg of solvent. The latter is the preferred term for biologic systems and is used throughout this and subsequent chapters [127,128].

Human normal plasma osmolality is 275–295 milliosmoles/kg (mOsm/kg) of water while urine osmolality is 50–1,200 mOsm/kg of water. These narrow ranges are maintained by high-gain feedback mechanism involving the hypothalamus, the neurohypophysis, and the kidneys. They determine the hydration state [129]. Consider someone who is experiencing dehydration, there is a net loss of water, which results in insufficient water in blood and other tissues. The water that leaves the body, as exhaled air, sweat, or urine, is ultimately extracted from the plasma. The thirst response is triggered when the plasma osmolality increases to levels above a physiologic threshold [130].

Osmoreceptors in the hypothalamus, which originally were described by Verney [131], sense plasma osmolality and transmits signals that result in a conscious awareness of thirst and elicit the releases arginine vasopressin (VP) /antidiuretic hormone (ADH) through the posterior pituitary gland. VP/ADH signals the kidneys to recover water from urine, effectively diluting blood plasma [131,132]. Decreased blood volume has two additional effects. On the one hand, baroreceptors, blood-pressure receptors in the arch of the aorta and carotid sinuses, detect a decrease in blood pressure that results from decreased blood volume. The heart is ultimately signaled to

increase its rate and/or strength of contractions to compensate the lowered blood pressure [133]. On the other hand, the kidneys have a renin-angiotensin hormonal system that increases the production of the active form of the hormone angiotensin II, which stimulates thirst, but also stimulates the release of the hormone aldosterone from the adrenal glands (AG). Aldosterone increases the reabsorption of sodium in the distal tubules of the nephrons in the kidneys, and water is also reabsorbed with the sodium [134].

1.7.3. Arginine vasopressin (VP) /antidiuretic hormone (ADH)

The gene coding for VP/ADH hormone is expressed in neurons of the SO and PVN of the hypothalamus. *Adh* gene codes for three peptides; the nonapeptide arginine vasopressin, a carrier protein called neurophysin-2, and a small glycoprotein called copeptin [135]. After secretion into the general circulation from the posterior pituitary gland (neurohypophysis), VP/ADH is delivered to the kidney, where it exerts regulatory actions through the V2 receptor (AVPR2) located in chiefly in renal epithelia. Some studies showed that AVPR2 is located in the principal cells of the renal collecting duct, the connecting tubule cells, the distal convoluted tubule cells, and the cells of the thick ascending limb of Henle [136].

The AVPR2 is a G–coupled receptor with physiologic functions that are mediated by the heterotrimeric G-protein Gs, through adenylyl cyclase activation and rise of cyclic AMP (cAMP) intracellular level [137]. This signaling pathways promote the movement and insertion of intracellular aquaporin-2 (AQP2) storage vesicles into the apical membrane. AQP2 is a water channel that allows water to move passively into the cell guided by the osmotic gradient established by NaCl and urea. Thus, it promotes reabsorption of water in the kidney. This creates concentrated, or hyperosmotic, urine and allows our body to conserve water in dehydration periods [138].

Loss of effective blood volume as seen in hemorrhagic or edematous states VP/ADH also has a second action on vascular smooth muscle. ADH binds to V1a

receptors on vascular smooth muscle and activates G protein protein Gq/11; this G protein activates phospholipase C and stimulates calcium mobilization [138].The net effect of this signaling cascade is a vascular smooth muscle contraction leading to increases in total peripheral resistance and consequently blood pressure. This mechanism is synergistic with water reabsorption in that both mechanisms elevate blood pressure. This is crucial in periods where effective arterial blood volume is low in order to maintain tissue perfusion [139].

1.7.4. Renin-Angiotensin-Aldosterone Axis (RAAS)

The renin-angiotensin-aldosterone system (RAAS) is an elegant cascade of vasoactive peptides that control the hemodynamic stability by regulating fluid volume, blood pressure, and sodium-potassium balance [140,141].

One important organ that integrate this system is the kidney, specifically its functional unit, the glomerulus. The glomerulus receives its blood supply from an afferent arteriole of the renal circulation and drains it into an efferent arteriole rather than a venule like in most vascular beds. Within the afferent arterioles, specialized cells called juxtaglomerular cells contain pro-renin. While pro-renin is secreted constitutively in its inactive form, activation of these cells causes the cleavage of pro-renin to renin. A blood pressure decrease due to a negative fluid balance would activate these cells among others. In addition, the activation of these cells occurs in response to ß-adrenergic stimuli or activation by macula densa cells of kidney in response to a decreased sodium load in the distal convoluted tubule [142].

Once renin has been released into the blood, it can act on its target which is angiotensinogen. Angiotensinogen is produced in the liver and is found continuously circulating in the plasma. Renin then acts to cleave angiotensinogen into angiotensin (ANG) I. ANG I is physiologically inactive, but acts as a precursor for ANG II [143]. The conversion of ANGI to ANGII is catalyzed by an enzyme called angiotensin converting enzyme (ACE) found primarily in the vascular endothelium of the lungs and kidneys. It

has effects on the kidney, adrenal cortex, arterioles, and brain by binding to AGN II type 1 (AT1Rs) and type 2 (AT2Rs) receptors, both G protein-coupled receptors [144].

The first effect of ANG II is to promote renal NaCl and water reabsorption and therefore plasma volume expansion. This occurs by at least two mechanisms: 1) direct stimulation of Na^+ reabsorption in the early proximal tubule due to the activation of the Na^+-H^+ antiporter in the luminal membrane. 2) ANG II acts on the adrenal cortex, specifically the zona glomerulosa. There, it stimulates the release of aldosterone, a steroid hormone that causes an increase in sodium reabsorption and potassium excretion at the distal tubule and collecting duct of the nephron through the insertion of luminal Na^+ channels and basolateral Na^+-K^+ ATPase proteins [145]. In addition, AGN II induces arteriolar vasoconstriction and increases the systemic blood pressure by elevating systemic vascular resistance (Figure 5) [141,145].

ANG II also acts on the brain stimulating thirst and increasing water intake [146] (the mechanisms by which will be described in the next section). Furthermore, it stimulates the release of VP/ADH hormone by the posterior pituitary. Finally, decreases the sensitivity of the baroreceptor reflex, which diminishes baroreceptor response to an increase in blood pressure, which would be counterproductive to the goal of the RAAS. The net effect of these interactions is an increase in total body sodium, total body water, and vascular tone.

1.7.5. Neuronal control of thirst

As mentioned before, thirst is the body's defense mechanism that motivates animals to seek fluid and drink it in response to a perceived water deficits [147]. The increases in plasma osmolality or decreases in plasma volume or pressure activate a feedback-controlled variable to restore these parameters to their physiological set-points [148].

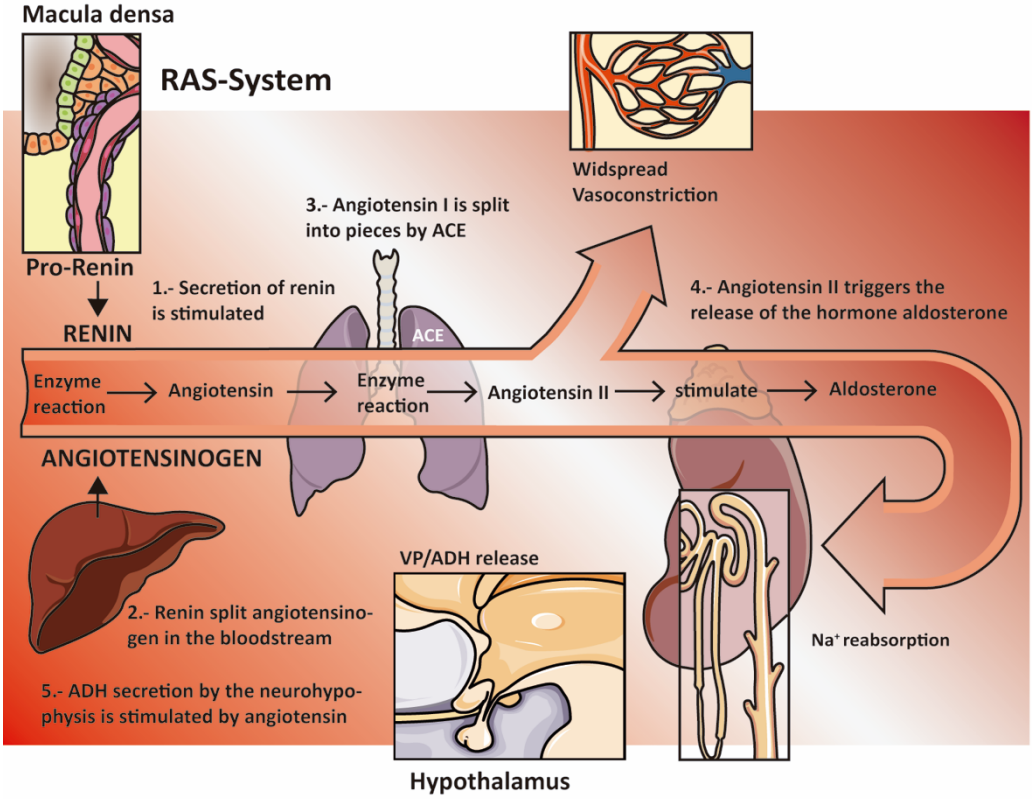

Figure 5. Schematic representation of the Renin Angiotensin cascade.
1.- Secretion of renin is stimulated, 2.- Renin catalyzes the conversion of angiotensinogen into angiotensin I, 3.- Angiotensin I is converted by the angiotensin-converting enzyme (ACE) into angiotensin II, 4.- Angiotensin II controls the secretion of aldosterone which stimulates Na^+ retention and 5.- Antidiuretic hormone (VP/ADH) release that stimulates H_2O reabsorption by the kidney.

Brain plays a crucial role in the orchestration of thirst sensation [149]. It contents a highly-specialized area called lamina terminalis (LT) which is responsible for guiding many of the thirst responses. LT is a small forebrain region that monitors homeostatic signals of fluid balance. It is composed of three small, interconnected structures located adjacent to the third ventricle. Two of these structures –the subfornical organ (SFO) and organum vasculosum of the lamina terminalis (OVLT)– are circumventricular organs (CVO), meaning that they have direct access to the circulation due to the lack of the blood-brain barrier (BBB) [150,151]. Within these structures a group of interoceptives neurons are able to respond to stimuli such as plasma

osmolality, volume, and pressure and then use this information to control thirst [152]. The third component of the LT is the median preoptic nucleus (MnPO), which cannot access the blood directly and is thought to be an integratory center (Figure 6) [149].

Elegant experiments using optogenetics and chemogenetic approaches have allow to elucidate distinct subset of neurons implicated in the control of drinking behavior. In the SFO there is a group of *Nos1, Etv1*, and *Camk2* (SFO^{GLUT}) neurons that triggered a voracious and specific water consumption in response to the photo stimulation [152,153]. It has also been demonstrated that OVLT contains a glutamatergic group of neurons that express the ATR1a ($OVLT^{Agtr1a}$). The photo stimulation of this subset of neurons drive robust water intake. Signals from the SFO and OVLT are thought to converge on the MnPO. In this nucleus, it has been found a group of neurons predominantly glutamatergic that express *Agtr1a* and *Slc17a6* markers ($MnPO^{Adcyap1}$) that also cause a rapid drinking behavior [154].

While these centers work as in interconnected neuronal network, the dynamics of these neurons and the underlying circuitry remain unclear. Some experiments that clarify this were overnight (ON) water restriction, peripheral injection of AGN II or hypertonic saline rapidly and dose-dependently activated SFO^{GLUT} neurons [155]. Optogenetic stimulation of SFO^{GLUT}→ MnPO and SFO^{GLUT}→OVLT projections promote thirst suggesting that SFO is the main structure controlling thirst [155,156].

SFO neurons project to magnocellular cells of the SO and PVN, where ADH/VP is synthetized [138,156]. Although SON^{VP} and PVN^{VP} neurons respond directly to the osmolality changes due to the expression of δ-N TRPV1 channels [157,158], classic models suggest that SFO^{GLUT}→PVN/SO projections mediate secretion of AVP and oxytocin (OXT) into the circulation in a pre-emptively manner [153]. More evidences have been obtained using electrophysiological recordings in genetically identified SON^{VP} neurons under water-restricted condition. It has been observed a rapid decrease in spiking neuronal activity within seconds of presentation of cues signaling water availability, suggesting an anticipatory control of thirst satiation prior

to systemic changes in plasma osmolality [159]. Similar dynamics is also observed in SFO^{GLUT} neurons as they are rapidly inhibited when thirsty mice begin to drink [155] reinforcing the theory that PVN/SO and SFO centers are connected.

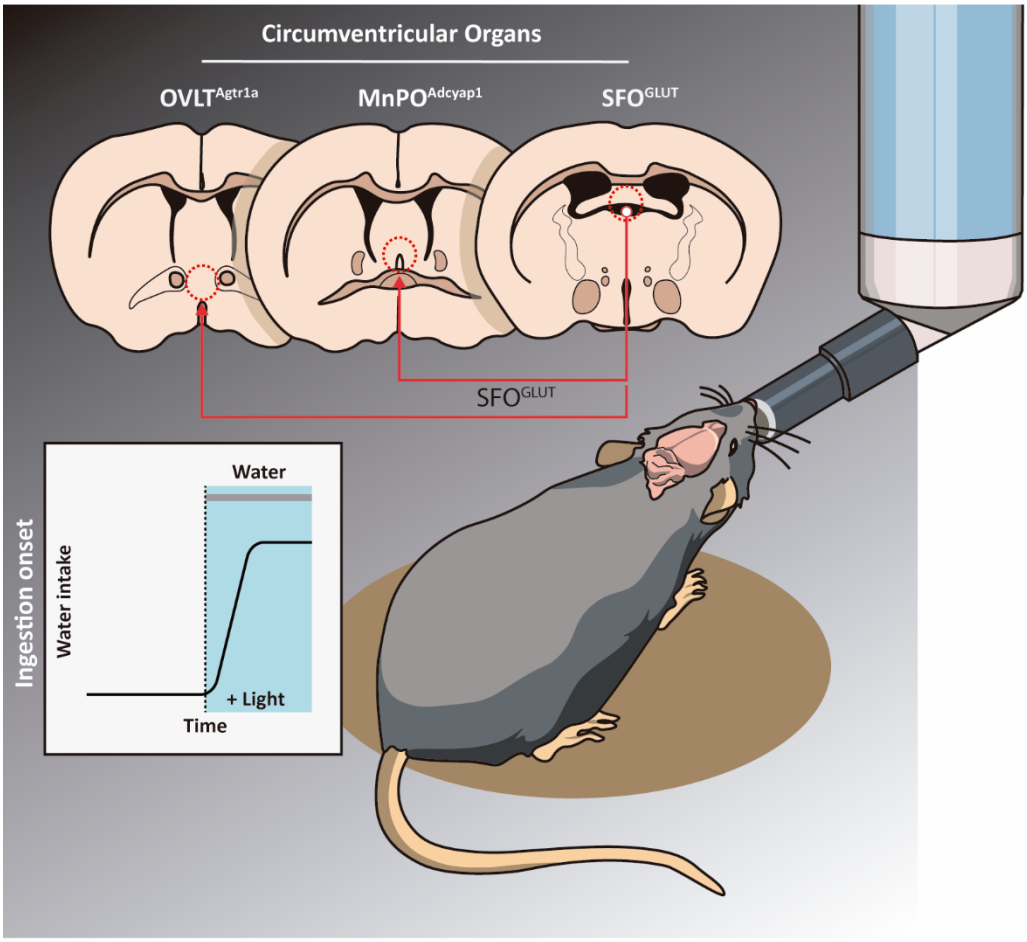

Figure 6. Neuronal populations that regulate thirst.
The image shows mouse brain containing individual population involved in water consumption. The neural stimulation of this single population of neurons trigger a robust increase of water intake as a result of the optogenetic activation.

1.8. ARE THIRST AND HUNGER PROCESSES COORDINATED?

Although there are many longstanding questions about thirst and hunger behavior, very recently new insights about these dynamics have emerged. Due to the anticipatory decrease of the neuronal activity before the osmotic changes of drinking, it has been demonstrated SFO^{GLUT} neurons receive a signal from the gastrointestinal (GI) tract that depends on the osmolarity of the ingested fluid, this was enough to influence drinking behavior [160]. Similar results were observed in SON^{VP} neurons suggesting that GI signal may pre-emptively regulate the fluid homeostasis during eating and drinking.

Taking into account that most stimulus come from a pre-sensing signal before to rich classic hunger and thirst center, and considering that a large number of foods that we consume are more than a half water by weight, is it possible to separate hunger from thirst? Do the stimuli for food intake induce concomitant water drinking? and vice versa. Although food intake and water drinking are traditionally being studied separately, some clues have emerged demonstrating the possible coordination of these two processes.

As we mentioned before ghrelin is one of the most powerful stimuli for food intake acting in hypothalamic centers to stimulate food intake. However, it has been demonstrated that ghrelin and amylin influence the excitability of SFO neurons, supporting a role for SFO in sensing peripheral feeding signals [161]. In contrast to ghrelin, leptin acts within hypothalamic centers to decrease food intake through the expression of leptin receptor (ObR) in target neurons. ObR is also expressed in SFO neurons and play an important role in leptin-induced renal sympathetic excitation, but not in the body weight and food intake [162]. According these results the solely lack of ObR receptors in SFO neurons did not affect the body weight but the selective deletion of AT1aR in the SFO attenuated leptin-induced weight loss suggesting a novel interaction between AGN II and leptin in the control of body weight [163].

It is well-defined the role of ANG in CVO organs [146], but little is known about the effect of ANG in ARC nuclei, where hunger neurons are located. Emerging results

provide evidences that AgRP but no POMC neurons express AT1a receptor and is critical for the control of resting metabolic rate (RMR) and GABA signaling [164]. What is even more surprising is that the dynamic of the feeding circuit has the similar behavior to the thirst. It has been shown that the intragastric nutrients exert a rapid decrease of AgRP neuronal activity suggesting that both centers receive same sensitive inputs to effectively coordinate the food and water ingestion [165].

It has even been demonstrated that ARC may be involved in body fluid balance and circulatory regulation by modulating the activity of SFO. Inputs from ARC neurons converge onto SFO neurons that alter their discharge rate during changes in plasma concentration of Na^+ or ANG II [166]. According to this result, retrograde tracing from SFO neurons has reveal retrograde-labelled neurons in ARC nucleus [155].

Now it is clear that water drinking can occur in the absence of food intake and even under conditions of water restriction some food intake does occur[167]. Eating increases the need of water in order to counteract the increase in blood osmolality caused by the absorption of salts and other osmolytes from food [168]. However, in physiologic conditions there is a believe that coincident behaviors override their independence.

Great progress has been made in understanding the neuronal mechanisms of thirst and hunger but there are important gaps in the physiological integration of both processes. Many of these gaps involve the identity of the specific molecules, neurotransmitters, cell types, and circuits that act as sensors or effectors in the control of drinking and feeding and they should be elucidated.

2. AIMS

The main goal of this doctoral thesis is to analyze the role of CPT1A in AgRP neurons in the control of energy balance and fluid homeostasis. To this end, we have assessed several approaches to get a mechanistic insight, through different specific aims:

Specific Aim I: To study the effect of CPT1A deletion in AgRP neurons of mice on feeding behavior and energy balance.

Specific Aim II: To analyze alterations of liquid homeostasis in mice lacking CPT1A in AgRP neurons.

Specific Aim III: To discern the molecular mechanisms involved in the thirst alteration seen in AgRP neurons CPT1A-deficient mice.

3. EXPERIMENTAL PROCEDURES

3.1. MATERIALS

3.1.1. Animals

The following genomic modified mouse strains were used in the present study:

Cpt1a$^{(loxP/loxP)}$: The mouse strain was designed for conditional knockout carrying the loxP-flanked exon critical for a target gene. The homozygous loxP-flanked allele mice contain two Cre-lox P sequences surrounding the exon 4 of *Cpt1a* gene. Before the exposure to Cre recombinase, CPT1A enzyme is constitutively expressed in all cells. In the presence of Cre recombinase, loxP site-specific excision of exon 4 results in a codon stop in exon 5 avoiding the translation of CPT1A protein. This mouse was obtained in our laboratory [169].

AgRP-CreER^{T2}: Transgenic mice homozygous for the allele that contains deoxyribonucleic acid (DNA) sequences encoding Cre recombinase (*CreER^{T2}*) fused to a triple mutant form of the human estrogen receptor; which does not bind its natural ligand (17β-estradiol) at physiological concentrations but will bind the synthetic estrogen receptor ligands 4-hydroxytamoxifen (tamoxifen). This sequence is under regulatory elements of the mouse *Agrp* gene promoter to allows for spatiotemporal gene manipulation specifically in ARC AgRP neurons following tamoxifen induction. These mice were kindly provided by Prof. Joel K. Elmquist from Southwestern Medical Center in USA [170].

Ribo Tag: Mice homozygous for the RiboTag allele contains a targeted mutation of the ribosomal protein L22 (Rpl22) locus. Consist in a loxP-flanked wildtype C-terminal exon 4 followed by an identical C-terminal exon 4 tagged with three copies of the hemagglutinin (HA) epitope before the stop codon. Prior to exposure to Cre recombinase, RiboTag mice express the wildtype RPL22 protein (15 kDa). When the RiboTag mice are bred with Cre-expressing mice, offspring will carry out the deletion of

the WT exon 4 and replaced with the HA-tagged exon 4. Protein RPL22^{HA} expressed is incorporated into actively translating polyribosomes and allow the immunoprecipitation (IP) with a monoclonal antibody against HA. Ribosome-associated mRNA transcripts from specific cell types can be isolated from the immunoprecipitated polyribosomes and analyzed using standard genomic profiling technologies such as quantitative real time polymerase chain reaction (qRT-PCR) or microarray [171]. These mice were kindly provided by Dr. Albert Quintana and Dr. Elisenda Sanz from the Department of Cellular Biology, Faculty of Medicine of the Universitat Autònoma de Barcelona (UAB).

ZsGreen: mice homozygous for the *ZSGreen* allele, contains a green fluorescent protein (GFP), coupled with the mitochondrial targeting signal (MTS) downstream of a floxed neomycin (NEO) cassette. In the presence of Cre recombinase, loxP site-specific excision of the NEO cassette occurs and this results in expression of the MTS-ZsGreen gene driven by the ubiquitously cytomegalovirus (CMV) promoter (Figure 7).

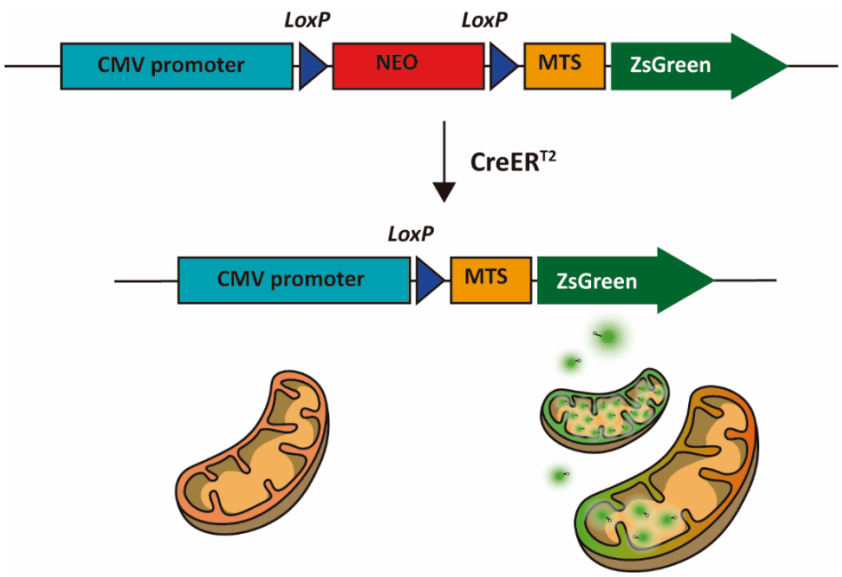

Figure 7. ZsGreen transgene.
The transgene construct contains a cytomegalovirus (CMV) promoter followed by the neomycin (NEO) cassette flanqued by *loxP* sequence. Downstream of the floxed NEO cassette is located the ZsGreen gene sequence coupled with the mitochondrial targeting signal (MTS), which transports the GFP expression to the matrix of the mitochondria.

The MTS used in this construct was cloned from de *Ndufs4* gene that encode the accessory subunit of the mitochondrial membrane respiratory chain NADH dehydrogenase and directs ZsGreen protein to the mitochondrial matrix. ZsGreen-expressing mouse mice were kindly provided by Dr. Albert Quintana and Dr. Elisenda Sanz from the Department of Cellular Biology, Faculty of Medicine of the UAB.

3.1.2. Bacteria

SURE 2 supercompetent cells (Agilent, Cat# 200227) were used for a for high efficiency cloning and plasmid propagation. They allow stable replication of high-copy number plasmids.

3.1.3. Viruses

AAV9-EF1a-DIO-mCherry virus contains the sequence of the gene of the mChrerry fluorescent protein in double floxed inverted orientation (DIO) under the control of EF1a driver-delivery promoter. In the DIO scenario, the mCherry transgene inserted in reverse orientation relative to the 5' promoter is flanked by oppositely oriented loxP and lox2272 sites. Cre recombinase will "flip-exchanged" or FLEXed the mcherry sequence leading to the expression of the mCherry protein. The viruses were produced in Viral Vector Production Unit (UPV) from the Universitat Autónoma de Barcelona (UAB) and their title was ($1x10^{14}$ vp/ul).

AAV2-Syn-DIO-GFP ($1x10^{14}$ vp/ul) was provided by Dr. Albert Quintana, Faculty of Medicine of the UAB. This vector contains the sequence of the presynaptic marker synaptophysin -an integral membrane protein localized into synaptic vesicles- under the control of CMV promoter. In the DIO scenario, the Syn-GFP transgene inserted in reverse orientation will Cre dependently FLEXed allow us to target the presynaptic buttons of specific neurons.

3.1.4. Plasmids

The pAAV-EF1a-DIO-mCherry plasmid (6,304 bp) kindly provided by Dr. Albert Quintana was used for the AAV4-EF1a-DIO-mCherry production. This plasmid contains the sequence of the mCherry fluorescent reporter in double floxed orientation (DIO) under the control of EF1a driver-delivery promoter. The plasmid also contains the ampicillin resistance gene (AmpR). (Figure 8).

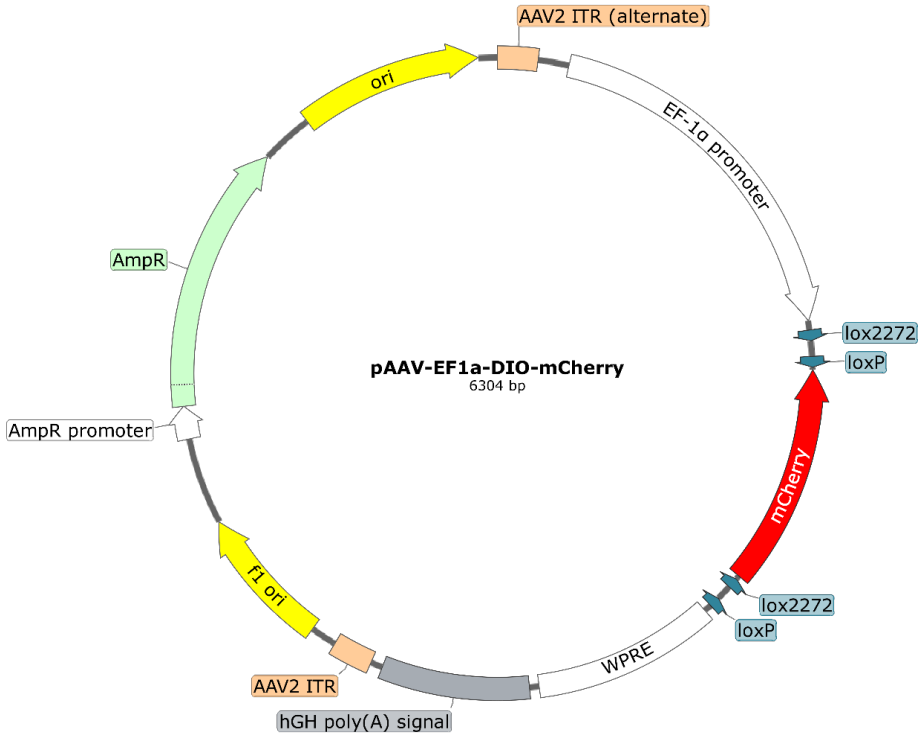

Figure 8. pAAV-EF1a-DIO-mCherry vector circular map (6,304 bp).
EF-1α: Elongation factor 1α promoter, LoxP: Locus of X-over P1, mCherry: Monomeric derivative of DsRed fluorescent protein, WPRE: Woodchuck Hepatitis Virus posttranscriptional regulatory element, hGH poly(A): Human growth hormone polyadenylation signal. AAV2 ITR: Adeno-associated virus inverted terminal repeat, f1 ori: F1 origin of replication. AmpR: Ampicillin resistance promoter and gene for bacterial selection.

3.1.5. Oligonucleotides

The oligonucleotides used in this study were all purchased from Sigma-Genosys. Oligonucleotide names and sequences are listed in table 2.

Table 2. List of the primers used in this study

Oligonucleotides	Source	Sequence
Cpt1a HomArm forward	Sigma-Aldrich	CAGGATCCCTTTGAGCAGCAG
Cpt1a HomArm reverse	Sigma-Aldrich	CAAAGTGGCCCCTAAGGCTAC
AgRP CRE-ERT2 forward	Sigma-Aldrich	CAGATACCATCATCTCTCCC
AgRP CRE-ERT2 reverse	Sigma-Aldrich	CCTTAAACTCGCCCATATATGTGG
AgRP CRE-ERT2 control	Sigma-Aldrich	GCTCTACTTCATCGCATTCCTTG
ZsGreen forward	Sigma-Aldrich	AAAGTCGCTCTGAGTTGTTATCAG
ZsGreen reverse	Sigma-Aldrich	GGAGCGGGAGAAATGGATATG
ZsGreen control	Sigma-Aldrich	TCACTGCATTCTAGTTGTGGTTTG
RiboTag LoxP forward	Sigma-Aldrich	GGGAGGCTTGCTGGATATG
RiboTag LoxP reverse	Sigma-Aldrich	TTTCCAGACACAGGCTAAGTACAC
Cpt1a forward	Sigma-Aldrich	GCTTATCGTGGTGGTGGGTGT
Cpt1a reverse	Sigma-Aldrich	GTTGACAGCAAAATCCTGGGC
Th forward	Sigma-Aldrich	TGTTGGCTGACCGCACAT
Th reverse	Sigma-Aldrich	GCCCCCAGAGATGCAAGT
Leptin forward	Sigma-Aldrich	CAGGATCAATGACATTTCACACA
Leptin reverse	Sigma-Aldrich	CAGGATCAATGACATTTCACACA
Il6 forward	Sigma-Aldrich	CTGCAAGAGACTTCCATCCAGT
Il6 reverse	Sigma-Aldrich	GAAGTAGGGAAGGCCGTGG
Atgl forward	Sigma-Aldrich	TGTAGGTGGCGCAAGACA
Atgl reverse	Sigma-Aldrich	TGTAGGTGGCGCAAGACA
Hsl reverse	Sigma-Aldrich	CGCTCTCCAGTTGAACCAAG
Hsl reverse	Sigma-Aldrich	CGCTCTCCAGTTGAACCAAG
Cpt1b forward	Sigma-Aldrich	TGCCTTTACATCGTCTCCAA
Cpt1b reverse	Sigma-Aldrich	TGCCTTTACATCGTCTCCAA
Ucp1 forward	Sigma-Aldrich	GGCCTCTACGACTCAGTCCA
Ucp1 reverse	Sigma-Aldrich	GGCCTCTACGACTCAGTCCA
Cidea forward	Sigma-Aldrich	GCCTGCAGGAACTTATCAGC
Cidea reverse	Sigma-Aldrich	AGAACTCCTCTGTGTCCACCA
Mmp2 forward	Sigma-Aldrich	TAACCTGGATGCCGTCGT
Mmp2 reverse	Sigma-Aldrich	TAACCTGGATGCCGTCGT
Vegfa forward	Sigma-Aldrich	GGCCTCTACGACTCAGTCCA
Vegfa reverse	Sigma-Aldrich	GGCCTCTACGACTCAGTCCA
Hprt forward	Sigma-Aldrich	TCCTCCTCAGACCGCTTTT
Hprt reverse	Sigma-Aldrich	TCCTCCTCAGACCGCTTTT
18s forwars	Sigma-Aldrich	TGGTTGATCCTGCCAGTAG
18s reverse	Sigma-Aldrich	CGACCAAAGGAACCATAACT
Tbp forward	Sigma-Aldrich	ACCCTTCACCAATGACTCCTATG

Tbp reverse	Sigma-Aldrich	TGACTGCAGCAAATCGCTTGG
ß-actin forward	Sigma-Aldrich	AGGTGACAGCATTGCTTCTG
ß-actin reverse	Sigma-Aldrich	GCTGCCTCAACACCTCAAC
Ucp2 forward	Sigma-Aldrich	CCGGGGCCTCTGGAAAG
Ucp2 reverse	Sigma-Aldrich	CCCAAGCGGAGAAAGGA
Hmg-coa forward	Sigma-Aldrich	GTTGGAGTGTCTCTTACGGTTCTG
Hmg-coa reverse	Sigma-Aldrich	AGTTCTCGAGTCAAGCCTTGATTTA
Pepck forward	Sigma-Aldrich	GTCAACACCGACCTCCCTTA
Pepck reverse	Sigma-Aldrich	CCCTAGCCTGTTCTCTGTGC
G6p forward	Sigma-Aldrich	AGGAAGGATGGAGGAAGGAA
G6p reverse	Sigma-Aldrich	TGGAACCAGATGGGAAAGAG

3.1.6. Antibodies

The Antibodies used in this study and their respectively dilution are listed in in table 3.

Table 3. List of the antibodies used in this study

Antibodies	Source	Sequence	Dilutions
Anti-Rabbit UCP-1	Abcam	Cat# ab10983	1:1,000
Anti-Rabbit β-actin	Sigma-Aldrich	Cat# A3854	1:25,000
Anti-Rabbit HRP	Thermo Fisher	Cat #MA5-15367	1:10,000
Anti-Rabbit c-FOS	Cell signaling	Cat# 2250	1:200
Anti-Rabbit GFP	Abcam	Cat# ab290	1:1,500
Anti-Rabbit HA	BioLegend	Cat# MMS-101R	1:150

3.1.7. Reagents

All chemical reagents and kits used in this project are listed in table 4 including commercial references.

Table 4. List of the primers used in this study

Chemical Peptides and Recominant Proteins	Source	Reference
Tamoxifen	Sigma-Aldrich	Cat# T5648-5G
QuickExtract™ DNA Extraction Solution	Biosearch Technologes	Cat# QE09050
REDExtract-N-Amp PCR ReadyMix	Sigma-Aldrich	Cat# R4775-12ML
Ghrelin, Rat, Mouse, Synthetic	Merck Millipore	Cat# 494127-100UG
Isofluorane	Piramal Healthcare	Cat# 60307-120-25
Trizol reagent	Sigma-Aldrich	Cat# T9424
Nuclease-Free Water	Thermo Fisher Scientific	Cat# AM9937
TaqMan™ Reverse Transcription Reagents	Thermo Fisher Scientific	Cat# N808-0234

LightCycler® 480 SYBR Green I Master	Roche	Cat# 4887352001
Protease Inhibitor Cocktail Tablets	Roche	Cat# 11836153001
PhosSTOP	Roche	Cat# 04906837001
Pierce™ BCA Protein Assay Kit	Thermo Fisher Scientific	Cat# 23227
Pierce™ BCA Protein Assay Reagent A	Thermo Fisher Scientific	Cat# 23228
Pierce™ BCA Protein Assay Reagent B	Thermo Fisher Scientific	Cat# 23224
Bovine Serum Albumin	Sigma-Aldrich	Cat# B2064-50G
Amersham ECL Rainbow Marker - Full range	Merk	Cat# RPN800E
ECL Prime Western Blotting System	GE Healthcare	Cat# RPN2232
Xylazine	Bayer	Cat# 572126.2
Ketamine	Richter Pharma Ag.	Cat# 580393.7
Enrofloxacin 10%	Bayer	Cat# 570216.2
Buprenorfin	Indivior	Cat# 679588
Paraformaldehyde	Sigma-Aldrich	Cat# 158127
Sucrose	Panreach Appliche	Cat# 131621
2-Methylbutane	Merk	Cat# 277258-1L
Tritón X-100	Sigma-Aldrich	Cat# T8787
Fluoromont-G	Thermo Fisher Scientific	Cat# 00-4959-52
RNeasy Mini Kit	Qiagen	Cat# 74104
30% Acrilamide/ Bis Solution 29:1	Sigma-Aldrich	Cat# A7802
Sodium Chloride 0,9%	B. Braun	Cat# 12260029_1019
Glucose 20%	Baxter	Cat# 2B0124P
Fibrilin Heparine 20 UI/ml	Rovi	Cat# 0318
Formalin solution, neutral buffered, 10%	Sigma-Aldrich	Cat# HT501128-4L
Dulbecco's Phosphate Buffered Saline	Sigma-Aldrich	Cat# D1408-500ML
PCR thermocycler	Analytik Jena	N/A
Reax Top	Heidolph instrument	N/A
Proteinase K	Thermo Fisher Scientific	Cat# AM2546
RNAse A	Sigma-Aldrich	Cat# 10109142001
Phenol	Thermo Fisher Scientific	Cat# AM9720
Phenol:Chloroform:Isoamyl Alcohol 25:24:1	Merk	Cat# P3803-100ML
2-Propanol	Sigma-Aldrich	Cat# 190764-1L
Sodium Chloride	Sigma-Aldrich	Cat# S7653-5KG
Ethanol	PanReac AppliChem	Cat# 361086.1611
EDTA	Sigma-Aldrich	Cat# EDS
Tris-base	Merk	Cat# T1503
Agarose D1 LE	Labotaq	Cat# E5000
DNA gene ruler 200 bp	Thermo Fisher Scientific	Cat# SM0241
LB medium	Sigma-Aldrich	Cat# L3022-250G
Yeast extract	Conda	Cat# 1702.00
Bacteriological Agar	Conda	Cat# 1800.00
Tryptone	Conda	Cat# 1612.00
Ampicillin	Sigma-Aldrich	Cat# A9393
HEPES	Thermo Fisher Scientific	Car# BP310-1
Glycerol	Sigma-Aldrich	Cat# 1370281000
Triton X-100	Merck	Cat# 648464-10ML

Sodium Deoxycholate	Merck	Cat# D6750
Glycine	Sigma-Aldrich	Cat# G8898-1KG
Sodium dodecyl sulfate	Merck	Cat# L3771
Bromophenol Blue	Merck	Cat# B5525-10G
β-mercaptoethanol	Merck	Cat# M6250
Tween 20	Merck	Cat# P9416-50ML
Blotto, non-fat dry milk	ChemCruz	Cat# sc-2325
OCT	Tissue-Tek	Cat# 4583
Ethylene glycol	Merck	Cat# 61941
Goat Serum	Sigma-Aldrich	Cat# G9023
PstI	Thermo Fisher Scientific	Cat# ER0611
AatII	Thermo Fisher Scientific	Cat# ER0991
Buffer Tango	Thermo Fisher Scientific	Cat# BY5
Critical Comercial Assay		
Insulin ELISA kit	ALPCO	Cat# 80-INSHU-E01.1
Aldosterone ELISA Kit	LSBio	Cat# LS-F28206-1
Glucose	Monlab	Cat# MO-165086
Vasopressin ADH ELISA Kit	LSBio	Cat# LS-F7592-1
Angiotesnin ELISA Kit	LSBio	Cat# LS-F67331-1
Terminatorv3.1 Cycle Sequencing Kit	Applied Bioqsystems	Cat# 4337455
QIAprep Spin Miniprep Kit	Qiagen	Cat# 27104
RNeasy Lipid Tissue Mini Kit	Qiagen	Cat# 74804

3.2. EXPERIMENTAL PROCEDURES WITH MICE

Mice were kept in the Unitat d'Experimentació Animal facilities of the Universitat de Barcelona under standard laboratory conditions with free access to food (Harlan Ibérca, Cat# 2014) and water at 22 ±2^{o}C and 60% humidity in a 12-hr light/dark cycle. Mice were group-housed to prevent isolation stress unless otherwise stated.

The animal experimentation ethic committee of the University of Barcelona (CEEA-UV) approved all the procedures with mice. Permits 255-19 and 262-19 were obtained from Government of Catalonic, according to Spain and European guidelines directive 2010/63/EU.

3.2.1. Mice identification, genotyping and induction of Cre-ER^{T2} expression

One week after weaning, mice were tagged for identification on the ears. Ear punch codes have been developed as a quick and inexpensive method to label individual animals. Here, we used the scissor punch (Thermo Fisher Scientific, Cat#13-820-063) to tag animal's right or left ear depending on the different combinations.

To genotype the mice, the tissue obtained from the ears was carefully collected from each mouse and properly identified in a 600 µl microcentrifuge tube. Genomic DNA is extracted as described in section 3.3.1 and a polymerase chain reaction (PCR) is performed (section 3.3.3) to confirm the genotype.

To induce gene recombination in CreER^{T2} transgenic mice, tamoxifen (Sigma Aldrich, Cat# T5648-5G) was administrated. A 20 mg/ml of stock solution was prepared by dissolving 100 mg tamoxifen in 5ml of corn oil (Sigma, Cat# C8267-500ML) heated at 42^{o}C (Immersion thermostat Digiterm-100, Selecta) during 30 min. The solution was placed on a rocker (Incubator Shaker, Excella E25) at 37^{o}C ON protected from the light and stored at 4^{o}C.

Adult mice were ip injected with five doses of 150 mg of tamoxifen/kg body weight. The first two injections were coupled with 24 hours of food deprivation (separated by 48 hours) to enhance *Agrp* promoter activity and the last three injection were daily administered with *ad libitum* access to food and water.

3.2.2. Body weight and food intake measurement

One week after the recombination, the food was monitored during the whole experiment. The initial amount of compound pelleted fodder was weighed at the beginning of every week, using the same precision scale. At the following week, remaining pellets were measured again with the same scale, and food was added up to the same amount given the last week. In any case, all mice had *ad libitum* food supply and its consumption was tightly monitored after tamoxifen injection until the sacrifice

of the animals. The body weight was monitored weekly after the recombination until the sacrifice using every week the same precision scale.

3.2.3. Fast-refeeding satiety test.

Animals were induced with tamoxifen at 8-10 weeks old. 4 weeks after tamoxifen induction mice were housed in individual cages 2 days before the beginning of the experiment. Mice were ON fasted for 12 hours and then refeed with a pre-weighed meal. Food intake was measured at 30 min, 1 h, 2 h, 3 h and 4 h after refeeding. All measurements were weighed using the same precision scale [172].

3.2.4. Ghrelin induce-food intake test

Animals were housed in individual cages 2 days before the beginning of the experiment. Mice were food-deprived for 2 h after the dark period and ip injected with ghrelin 0.4 µg/g body weight (Merck Millipore, Cat# 494127-100G) in physiological serum (B. Braun. Cat# 12260029_1019) at 0 min and another dose at 30 min. We monitored eating time and food intake for 1 h after the first injection [17].

3.2.5. Glucose tolerance test (GTT)

For GTT assay mice were ON fasted. The baseline blood glucose concentration from a tail cut was measured using a hand glucometer (Bayer, Contour XT, Cat# 83415194) and it test strips (Bayer, Contour next, Cat# 84191389). A blood sample was collected in a capillary tube (Deltalab, Cat#7301) and keep it in the serum separator tubes (Sarsted, Cat# 201.280) at 4ºC to measure the insulin level. Samples were allowed to clot on ice for 15 minutes and then centrifuged for 15 minutes at 5,700 rpm (Eppendorf® Centrifugue 5415R). The supernatant was withdrawn and frozen at -20^{o}C.

Mice were injected ip with 20% glucose (Baxter, Cat# 2B0124P) at 1.5 mg/g body weight. Blood glucose concentrations were then measured at 15, 30, 60, 90 and 120 min after glucose injection.

3.2.6. Indirect calorimetry

Animals were analyzed for energy expenditure (EE), respiratory quotient (RQ) and locomotion activity (LA) using a calorimetric system (LabMaster; TSE Systems; Bad Homburg, Germany). Briefly, mice were placed in a temperature-controlled (24^{o}C) cage with flowing air for 48 hours before starting the measurements to be adapted to the system. After calibrating the system with the reference gases (20.9% O_2, 0.05% CO_2 and 79.05% N_2), the metabolic rate was measured for 3 days. After that, we extended the experiment for 12 hours under fasting and then 4 hours of refeeding conditions. O_2 consumption and CO_2 production were recorded every 30 min, to indirectly determine the RQ. EE, RQ (VCO_2/VO_2), food intake and LA were measured during the dark and light phase. The LA was assessed using a multidimensional infrared light beam system with the parameters defined by the LabMaster system.

3.2.7. Analysis of BAT thermogenic activity

Heat production was visualized using a high-resolution infrared camera (FLIR T420; FLIR Systems, AB, Sweden). Infrared thermography images were taken from the upper half of the body to specifically visualize BAT activity. The day before of the experiment, mice were ON fasted and shaved in the interscapular area to minimize interference. BAT interscapular temperature was analysed within a fixed area (ROI: region of interest), using the Flir Tools software (Version 4.1). For each image, the average temperature of the skin area was calculated as the average of 3 pictures/animal.

3.2.8. Blood and urine collection

Mice were individually placed in metabolic cages that had a floor area of 370 cm^2 and the dimension of lengh= 207 cm; width = 267 cm and height= 140 mm adapted with a grill at the bottom to collect the urine volume. Mice were housed one day before to initiate the experiment with *ad libitum* access to food and water. The day of the

study, water and urine volumes were measured during 24 hours and urine specimens were taken for osmolality analysis. At the end of the experiment, blood samples were collected in in heparinized tubes through the facial vein method [173]. The blood was centrifuged for 15 minutes at 5,700 rpm at 4°C (Eppendorf® Centrifugue 5415R). The supernatant was withdrawn and frozen at -20°C until the plasma osmolality measurement. At the end of the study all the animals were rehoused in their original cages.

One week later the animals were placed back in the metabolic cages to perform the same protocol under water restriction for 24h. Urine volume was measured, and blood and urine osmolality were also analyzed. Water intake and urine volumes were expressed as values per grams of body weight.

3.2.9. Stereotaxis procedure

Stereotaxic surgery has been an invaluable tool in neuroscience systems. This allows the administration of adeno-associated viruses (AAV) and lentiviruses in a site-specific brain structure through a central injection with an excellent precision. Here, we inject different rAAVs vectors through the stereotaxic surgery.

Mice were anesthetized using 0.1 mg/g ketamine (Richter Pharma Ag., Cat# 580393.7) and 0.01 mg/g xylazine (Bayer, Cat#580393.7) and then placed in a stereotaxic apparatus (Kopf instrument, Model 900 Small Animal Stereotactic Instrument). Once its head was shaved using an electric trimer, a sagittal incision was made through the skin along the midline of the head, and a hole was drilled on the skull at the position of 1.5 mm posterior and 0.3 mm lateral (left and right) to bregma (Bregma point was found in the perpendicular intersection between sagittal and coronal synarthroses). 400 nl of solution, containing either AAV9-EF1a-DIO-mCherry or AAV2-Syn-DIO-GFP was injected slowly using a Hamilton Neuros syringe (5 µL, Neuros Model 75 RN, point style 3, SYR, Cat# 65460-02) and a microinjection pump over 8 min

in ARC. The coordinates for ARC are -1.5 mm posterior, +/- 0.3 mm lateral and -5.8 mm ventral from bregma [174].

Once the procedure was finished, a super glue tissue (3M Vetbond™, Cat# 1469Sb) was used to close the incision. The animals were caged with *ad libitum* food and post chirurgical drug-supplemented water, containing 10% enrofloxacin (Bayer, Cat# 572126.2) and 0.3 g/400 ml buprenorfin (Indivior, Cat# 679588) as antibiotic and analgesic respectively. Daily monitoring was performed to follow up the general state of the operated mice for one week. 3 weeks after rAAVs injection, animals were traded with tamoxifen following the protocol described in section 3.2.1 to activate the recombination.

3.2.10. Procedures to sacrifice

To analyze the gene expression, blood metabolites, protein content and histological morphology of different tissues, mice were ON fasted and induced into anesthesia at a dose of 4% isoflurane (Piramal Healthcare, Cat# 60307-120-25) and then maintained at a surgical plane by continuous inhalation of 2% isoflurane using a calibrated anesthetic delivery machine (Combi-Vet® Rothacher Medical, Switzerland). Blood was rapidly collected in heparinized tubes (Fibrilin, Cat# 0318) from descending aorta using a 25-gauge needle (BD Microlance™ 3 Cat# 300600) and was allowed to clot on ice for 15 minutes and then centrifuged for 15 minutes at 5,700 rpm at 4°C (Eppendorf® Centrifugue 5415R). The supernatant was withdrawn and frozen at -20°C. Liver, inguinal white adipose tissue (iWAT), epididymal white adipose tissue (gWAT), BAT, AG, pancreas, testis and ovaries, kidney, hypothalamus, cortex and hippocampus were collected and rapidly stored at -80°C until processing.

In order to obtain ARC samples, brain was gently placed in a mouse brain matrix (Agnthos, Cat# 69-2175-1) which allows to obtain coronal cuts with a width starting from 1 mm. 3-mm coronal section encompassing most of the ARC nuclei was obtained, taking as a reference the optical chiasm to set them for the dissection. Once the section

was cut, the remaining brain was carefully removed outside the matrix and the section was extracted and horizontally positioned. The area was dissected with a crosswise cut starting the 3rd ventricle till the base of the hypothalamus. Tissue was rapidly stored at -80°C until processing. A piece of tissues was fixed in formalin solution, neutral buffered, 10% (Sigma, Cat# HT501128-4L) for 24 h and then transferred to phosphate buffer saline (PBS) 1X (Sigma, Cat# D1408-500ML) to perform the histological analysis.

To perform immunofluorescent technics, whole animal perfusion fixation was applied. Briefly, animals were deeply anesthetized thorough the ip injection of ketamine (Richter Pharma Ag., Cat# 580393.7) and xylazine (Bayer, Cat#580393.7) anesthetizing Cocktail. Delivery dose was ketamine 0.1 mg/g and xylazine 0.01 mg/g. Once the animal has reached a surgical plane of anesthesia a 25-gauge blunt perfusion needle connected to the perfusion pump (Gilson, miniplus 3) was inserted in the left ventricle. An incision to the animal´s right atrium to create as large an outlet as possible of the fluid was performed. 75 ml of cold PBS 1X was perfused to remove the red blood cells. The PBS 1X was replaced then by 50 ml of 4% paraformaldehyde (PFA) 4% buffered at pH 7.4 (Sigma-Aldrich, Cat# 158127). Once perfusion was complete, the brain was extracted from the skull and post-fixated in paraformaldehyde (PFA) 4% during 4 hours at 4°C. Brains were kept in 30% sucrose (Panreach Applichem, Cat#131621) until they sank. Brains were frozen using pre-cooled 2-metilbutane (Merck, Cat# 277258-1L) at -80°C and stored at -80°C.

In order to isolate mRNA translated in AgRP neurons *in vivo*, RiboTag mice were ON fasted and sacrificed by cervical dislocation. Brain was removed from the skull and gently placed in the mouse brain matrix. A 3 mm of coronal section containing ARC nucleus was obtained. The section was extracted and horizontally positioned. The area was dissected with a crosswise cut starting the 3rd ventricle till the base of the hypothalamus. Tissue was rapidly stored at -80°C until processed.

3.3. MOLECULAR BIOLOGY TECHNIQUES

Molecular biology techniques were used to study DNA, as the repository of genetic information; RNA, another polynucleotide whose functions range from serving as a temporary working copy of DNA to actual structural and enzymatic functions as well as a functional and structural part of the ribosome; and proteins, the major structural and enzymatic type of molecule in cells. Here we describe the different molecular biology techniques used in this project.

3.3.1. gDNA extraction

Ears punches obtained during the mice identification were carefully collected from each mouse and properly identified in a 600 µl microcentrifuge tube. 40 µl QuickExtract™ DNA Extraction solution (Epicenter, Cat# QE09050) was added to each tube. The QuickExtract™ DNA Extraction Solution can be used to rapidly and efficiently extract PCR-ready genomic DNA from almost any sample type using a simple, one-tube protocol. Briefly, the tubes were given a quick spin, to ensure contact between the ear tags and the solution. A 6-min incubation at 65^{o}C (PCR thermocycler FlexCycler, Analytik Jena) and vigorous vortex (ReaxTop, Heidolph Instrument) for mechanical disruption were applied to ease the polynucleotide liberation into the solution. Following that, the tubes were incubated again for 2 min at 92^{o}C using the thermocycler. An ON incubation at 4^{o}C was applied before any other processing of the sample.

3.3.2. Purification of gDNA

gDNA form different tissue collected was extracted using proteinase K method. Briefly, 2.5 µl of proteinase K (0.0001 ng/µl in the reaction) (ThermoFisher Scientific, Cat# AM2546) were used, and the tissue was incubated in 500 µl of lysis buffer (12.2 g of Tris; 1.9 g of EDTA; 2 g of SDS and 11.7 g of NaCl to 1 L solution, pH 8.5) at 55^{o}C for 4

hours. Once digested, 10 µl RNAse A (10 mg/mL) (Sigma-Aldrich, Cat# 10109142001) is added into each tube and incubated at 37°C for 1 h for RNA degradation.

Extraction is started by adding 700 µl phenol (100 mM, Tris-buffered pH 8.0) (ThermoFisher Scientific, Cat# AM9720) and vigourous 10-min shaking. Vortexing should be avoided to keep DNA integrity. Tubes were centrifuged at 16,000 rpm for 15 min and upper phase was placed into a new tube. 700 µl phenol:chloroform:Isoamyl alcohol (25:24:1) (Merk, Cat# P3803-100ML) was added to each tube, which were vigorously shaken for 10 min. At this point, gDNA was isolated and had to be precipitated. To this end, 700 uL 2-propanol (Sigma Aldrich, Cat# 190764-1L) and 15 µl NaCl 5M (Sigma Aldrich, Cat# S7653-5KG) were added to each tube and vigorously mixed. After 10 min, gDNA was precipitated by centrifugation at 16,000 rpm for 15 min. Supernatant was removed avoiding any gDNA pellet disturbance. 100 µl Ethanol (70%) (Panreac, Cat# 361086.1611) was added to each tube for washing and after 15 min centrifugation at 16,000 rpm, ethanol supernatant was removed and the gDNA was left to dry out. Once it was dry, the gDNA pellet was resuspended with 100 µl Tris-EDTA 10 mM solution and stored at 4°C at least ON before any further processing. gDNA yield was quantified using NanoDrop 1000 Spectrophotometer (Thermo Scientific, ref. ND-1000).

3.3.3. Polymerase chain reaction (PCR)

PCR reaction was conducted in a 20 µl final volume containing 10 µl of REDExtract-N-Amp PCR ReadyMix (Sigma-Aldrich, Cat# R4775-12ML) which include all the reagent needed for PCR amplification, 1.5 µl of 10 µM forward and reverse primers, 1 µl of gDNA and nuclease free water (Ambion, Cat# AM9937) up to complete the final volume. PCR conditions were applied depending on the gene analyzed and PCR products were visualized by electrophoresis in 1–2% agarose (Labotaq, Cat# E5000) gels using the Gene Ruler DNA Ladder Mix 100 bp (ThermoFisher scientific, Cat# SM0241) as molecular DNA marker.

For *Cpt1a Flox* gene: *Cpt1a HomArm* forward and reverse primers were used (table 2). The initial denaturation was at 94°C for 5 min, denaturation at 94°C for 30 sec, annealing at 56°C for 30 sec, and extension at 72°C for 60 sec, for 30 cycles and final extension at 72°C for 5 min. The DNA fragments obtained for WT *Cpt1a* amplified allele was 990 bp, for *Cpt1a* flox allele was 1.030 bp and for recombined gDNA was 219 bp.

For AgRP-*CreER^{T2}* gene: *AgRP CRE-ER^{T2}* forward reverse and control primer were used (table 2). The initial denaturation at 94°C for 5 min, denaturation at 94°C for 30 sec, annealing at 56°C for 30 sec, and extension at 72°C for 60 sec, for 30 cycles and final extension at 72°C for 5 min. For WT allele AgRP-*CreER^{T2}* gene, the obtained amplicon was 514 bp long and for AgRP-*CreER^{T2}* allele was 323 bp long.

For *RiboTag* gene: *RiboTag loxP* forward and reverse primers were used (table 2). The initial denaturation at 95°C for 2 min, denaturation at 95°C for 20 sec, annealing at 57°C for 20 sec, and extension at 72°C for 30 sec, for 30 cycles and final extension at 72°C for 5 min. WT mice generate a 260 bp long and the RiboTag allele 290 bp.

For *ZsGreen* gene: ZsGreen forward and reverse primers were used (table 2). The initial denaturation at 95°C for 2 min., denaturation at 95°C for 30 sec, annealing at 55°C for 30 sec, and extension at 72°C for 30 sec, for 30 cycles and final extension at 72°C for 5 min. The amplicon obtained for WT *ZsGreen* mice was 600 bp and for *ZsGreen* allele was 500 bp long.

3.3.4. Sequencing

In order to confirm tissue-specific recombination of the *Cpt1a*-floxed allele in the hypothalamus, the gDNA from different tissues from control and recombined animals was purified according to the section 3.3.2. The PCR protocol (Section 3.3.3) using *Cpt1a HomArm* forward and reverse primers was applied to detect the recombined band of 219 bp.

This PCR product was extracted from the gel and sequenciated. We took advantage of a variation of DNA sequencing technologies developed in mid-1970's [175], materialized in our case in the BigDye Terminator v3.1 Cycle Sequencing Kit (Applied Biosystems, Cat# 4337455). This method requires chain-terminating dideoxynucleotides (ddNTPs) which cause DNA polymerase to stop DNA extension, when one of these ddNTPs is incorporated. Each of the four ddNTPs is labelled with a different fluorescent dye which allows assessing the nucleotide incorporated in a particular position in the DNA polymer along the whole sequence.

The reaction mix used for each primer was the following: 8.65 µl ddH2O, 1 µl Ready BigDye Reaction Mix, 3 µl BigDye Sequencing Buffer, 2 µl Oligonucleotide 10 µM, 7 µl gDNA containing 1 ug of sample. The reactions were further processed at the Genomic Services Unit from the Centres Científics i Tecnològics de la Universitat de Barcelona (CCiT-UB) to obtain the sequence chromatograms.

3.3.5. SURE 2 supercompetent cell transformation

In the electrotransformation process, a high-voltage electric field is applied briefly to cells, apparently producing transient holes in the cell membrane. To perform the transformation, 75 ng of the pAAV-EF1a-DIO-mCherry DNA plasmid was added to 40 µl of recently thawed competent cells and incubated on ice during 3 minutes. Then, mix was transferred into a cuvette and 2 pulses of 2,500 V was applied using the electroporator (Electroporator 2510, Eppendorf). One ml of Luria bertani medium (LB) (Sigma Aldrich, Cat# L3022-250G) containing 10 µl of 500 µM glucose was added to the mix and transferred into a transparent sterile tube. The mix was incubated for 1 h at 37^{o}C with moderate shaking. Cells were centrifuged at 1,400 rpm 3 min (Eppendorf® Centrifugue 5415R) at room temperature to remove the supernatant. The pellet was suspended in remaining medium and load into ampicillin-LB plate (10 g/L tryptone, 5 g/L yeast extract and 5 g/L NaCl, 2% (w/v) agar, 100 mg/L ampicillin) and ON incubated at 37^{o}C.

3.3.6. Plasmid DNA purification

QIAprep Spin Miniprep Kit (QIAGEN, Cat# 27104) was used to obtain a high-copy number of pAA-EF1a-DIO-mCherry plasmid. Briefly, competent *E. coli* previously transformed was incubated in LB medium containing ampicillin with vigorous shaking at 37°C for 14-15 hours. 1-5 ml bacterial was centrifuged at > 8,000 rpm (Eppendorf® Centrifugue 5415R) for 3 min at room temperature. The pellet was resuspended in 250 µl of Buffer P1 and transferred to a microcentrifuge tube. 250 µl of Buffer P2 was added and mixed vigorously until the solution became clear. 350 µl of Buffer N3 was added and centrifuged for 10 min at 13,000 rpm. 800 µl of the supernatant was transferred to QIAprep 2.0 spin column and centrifuged for 30–60 sec at 13,000 rpm to discard the flow-through. The column was washed by adding 0.75 ml Buffer PE and centrifuged again at 13,000 rpm to discard the flow-through. The QIAprep 2.0 spin column was transferred to a new collection tube and centrifuged again at 13,000 rpm to remove residual wash buffer. Finally, to elute DNA, 50 µl Buffer EB was added in the QIAprep 2.0 spin column placed in a new collection tube and centrifuged during 1 min at 13,000 rpm. The DNA of the purified plasmid was quantified in the NanoDrop-ND-1000 Spectrophotometer (Thermo Scientific, ref. ND-1000) and stored at -20°C.

3.3.7. Total RNA extraction and quantification

Depending on the sample, RNA was extracted using Trizol reagent (Sigma-Aldrich, Cat# T9424) or with a specific kit. For fatty tissues or high lipid content tissues, RNA was extracted using the RNeasy Lipid Tissue Mini Kit (QIAGEN, #74804) following the manufacturer's instructions. For any other tissue Trizol reagent was used according to the manufacturer's protocol with minor modification.

Briefly, 50-100 mg of high-lipid content tissues was added to 1 ml QIAzol lysis reagent and 30-70 mg of non-lipid tissue was added to 1 ml trizol. After addition of the appropriate lysis reagent, the tissues were disrupted using beads (QIAGEN, Cat# 69989 or cat# 69997) and a Tissuelyser LT (QIAGEN, Cat# 85600) for 3 minutes at 50 Hz. A

homogenization by pipetting up and down was applied. Then, 0.2 ml clorophorm was added to separate the aqueous phase after centrifugation for 15 minutes at 12,000 rpm at 4°C.

On the one hand, to extract RNA from adipose tissues with RNeasy Lipid Tissue Mini Kit were accomplished according to the manufacturer's protocol and using the column system. On the other hand, for any other tissue and according to the trizol protocol, RNA was precipitated using 0.5 ml of isopropanol and centrifuged for 10 minutes at 12,000 rpm at 4°C (Eppendorf® Centrifugue 5415R). The remaining pellet remaining was washed with 75% ethanol and centrifuged for 5 minutes at 7,500 rpm at 4°C several times and eluted in a small volume (10-30 µl) of Nuclease-free water. Finally, RNA samples were heated to 55-60°C for 10-15 minutes using a thermoblock (JP Selecta EN, Temblock, Cat# 7462200), quantified using a NanoDrop-ND-1000 Spectrophotometer and stored at -80°C until processing.

3.3.8. cDNA synthesis by reverse transcription

RNA was reverse transcribed to complementary DNA (cDNA) by using Taq Man® Reverse Transcription reagent (ThermoFisher Scientific, Cat# N808-0234) following the manufacturer instruction. Briefly, the reaction was performed from 1,000 ng of RNA stock samples and were incubated with the kit reagents and RNAse free water up to a final volume of 20 µl. The mix was incubated in the thermocycler for 10 minutes at 25°C, 30 minutes at 48°C and 5 minutes at 95°C. The cDNA obtained was diluted with RNAse nuclease free water up to a concentration of 10 ng/µl.

3.3.9. Quantitative real time PCR

In conventional PCR (see section 3.3.3), the amplified product, or amplicon, is detected by an end-point analysis, by running DNA on an agarose gel after the reaction

has finished. In contrast, real-time PCR allows the accumulation of amplified product to be detected and measured as the reaction progresses, that is, in "real time".

Real-time detection of PCR products is made possible by including in the reaction a fluorescent molecule that reports an increase in the amount of DNA with a proportional increase in fluorescent signal.

Quantitative real time polymerase chain reaction (qRT-PCR) was performed using Power SYBR Green PCR Master Mix adapted for LightCycler 480 (Roche, Cat# 4887352001), according to the manufacturer's indication in the LightCycler 480 instrument II (Roche, Cat# 05015243001).

4.5 µL of the diluted cDNA were mixed with 5.5 µl of PCR mix containing 2X SYBR green PCR Master Mix reagent (Roche, Cat# 4887352001) and 10 µM primer mix (10 µM primer forward and µM primer reverse). The qRT-PCR reactions were done in duplicate in a 384 well plate (MicroAmp™ Optical 384-Well Reaction Plate, ThermoFisher, Cat# 4309849). The plate was incubated at 95°C for 5 minutes, followed by 45 cycles at 95°C, 60°C and 72°C 10 seconds each. cDNA levels from liver tissue were normalized with β-actin. BAT and WAT were normalized with Hypoxanthine phosphoribosyl-transferase (*Hprt*) or β-actin. Finally, for cDNA extracted from AgRP neurons the housekeeping gene used was Glyceraldehyde-3-phosphate dehydrogenase (*Gapdh*). Primers used in this project are showed in the table2

3.3.10. Protein extraction

Tissue was disrupted by adding 1 ml or 500 µl of protein extraction buffer to 30-70 mg of non-fat tissues or 50-100 mg of fat tissues, respectively. The protein extraction buffer contains 30 mM HEPES pH 7,4, 150 mM NaCl, 10% glycerol, 1% Triton X-100, 0.5% sodium deoxycholate (DOC), Mini Protease Inhibitor Tablet (Roche, Cat# 11836153001) and PhosSTOP Phosphatase Inhibitor Tablet (Roche, Cat# 04906837001). To disrupt the tissue Tissulyser LT was used during 3 minutes at 50 Hz. Lysates were then kept shaking at 4°C for 15 minutes for proteins solubilisation. The

samples were centrifuged at 13,000 rpm for 15 minutes at 4°C (Eppendorf® Centrifugue 5415R) and the supernatant was collected avoiding the pellet and the thin lipid layer at the top of the solution. Samples were diluted 1:2 and stored in aliquots of 200 µL at 4ºC before the protein content quantification by bicinchoninic acid (BCA) protein method.

3.3.11. Protein quantification by BCA method

The protein concentration was determined using the Pierce™ BCA Protein Assay Kit (Thermo Fisher Scientific, Cat# 23227) following the manufacturer instruction. Briefly, the assay was performed in a 96 well plate (Creiner bio-one, Cat# 655101). To prepare BCA working reagent (WR), Pierce™ BCA Protein Assay Reagent A (Thermo Scientific, Cat# 23228) and Pierce™ BCA Protein Assay Reagent B (Thermo Scientific, Cat #23224) were mixed 50:1.

To prepare the diluted albumin standards a 2 mg/ml bovine serum albumin (BSA) (Sigma Aldrich Cat# B2064-50G) stock were diluted within a range of 0 to 2 µg/µl (0, 0.2, 0.4, 0.8, 1.6, 2 µg/µl). Then, 10 µL of the diluted protein samples were mixed with 10 µL of water. Both the standards and samples were added in duplicate. Finally, 200 µL of the BCA WR were dispensed in each of the wells and the plate was incubated at 37°C protected from the light for 30 minutes. The plate was cooled down at room temperature and it was read in a microplate reader Varioskan Lux (Varioskan LUX multimode microplate reader, Thermo Fisher scientific) at 562 nm at endpoint.

3.3.12. Western Blot

A western blot is a laboratory method used to detect specific protein molecules from among a mixture of proteins. This mixture can include all of the proteins associated with a particular tissue or cell type. Western blots can also be used to evaluate the size of a protein of interest, and to measure the amount of protein expression.

3.3.12.1. Electrophoresis

Once the protein concentration was determined, a stock of samples was prepared at a final concentration of 1.5 µg/µl by adding the proportional part of water and 6X loading buffer, [375 mM Tris-HCl pH 6.8, 9% (w/v) sodium dodecyl sulfate (SDS), 50% (v/v) glycerol, 0.03% (w/v) bromophenol blue, 9% (v/v) β-mercaptoethanol, 10%(v/v)]. Samples were denaturalized at 95°C (P selecta, Cat# 7462200) for 5 minutes and kept on ice or stored at -20°C for later use.

Electrophoresis is performed in a system of sodium dodecyl sulfate-polyacrylamide gels (SDS-PAGE) formed by a stacking gel to concentrate the proteins and a separating gel that separates them according to the molecular weight. The gels were prepared with 8-10% acrylamide (Sigma-Aldrich, Cat# A7802), depending on the molecular weight of the protein to be studied. The gels composition was performed in the Mini-PROTEAN® Spacer Plates (Bio-Rad, Cat# 1653312) or criterion emptycCassettes (Bio-Rad, Cat# 3459901, Cat# 3459902) as shown in the Table 5. Polymerized gels were covered with a running buffer [25 mM Tris-HCl pH 8.8, 192 mM glycine and 0.1% (w/v) SDS] and, 15 to 30 µg of total protein per well were loaded depending on sample type. In addition, 7 µl of the marker Amersham™ ECL™ Rainbow™ Marker - Full range (GE Healthcare, Cat# RPN800E) was loaded into the first well of the gel.

The electrophoresis was performed using the Mini-PROTEAN® Tetra Vertical Electrophoresis Cell (Bio-Rad, Cat# 1658004) or Criterion Gel Electrophoresis Cell (Bio-Rad, Cat# 1656001) systems.

Table 5. Gel Composition for Western Blot. The volume depends on the gel concentration.

	Separating gel (8% polyacrylamide)	Stacking gel (5% polyacrylamide)
1.5 M Tris-HCl pH 8.9, 0.4% SDS	2.6 ml	-
0.5 M Tris-HCl pH 6.8, 0.4% SDS	-	1.3 ml
Polyacrylamide 40%	2 ml	0.64 ml
ddH2O	5.3 ml	3 ml
TEMED	4 µl	5 µl
10% Ammonium persulfate	100 µl	25 µl

The migration was first performed at 25 mA until all the samples reached the stacking gel (5% polyacrylamide). Then, the intensity was increased up to 35-45 mA until the electrophoresis front reached the end of the separating gel (10% polyacrylamide).

3.3.12.2. Transference

Once the electrophoresis was finished, the stacking gel was removed and the separated proteins contained in the separating gel were transferred to a 0.45 µm nitrocellulose membrane (Bio-Rad Laboratories, Cat# 1620115). The transference sandwich was formed by the gel and the nitrocellulose membrane surrounded by a sponge and a same-size piece of whatman paper at each of the sides. It was submersed in transfer buffer [25 mM Tris-HCl, 190 mM glycine, 0.2% SDS (m/v), 20% Methanol (v/v)]. The transfer was performed using Mini Trans-Blot Cell (Bio-Rad) or Criterion™ Blotter with Wire Electrodes (Bio-Rad, Cat# 1704071) and applying an intensity of 250 mA during 90 minutes in cold conditions.

The membrane was rinsed and washed with 1X Tris buffered saline with Tween 20 (TBST) [10 mM Tris-HCl, pH 7.4, 150 mM NaCl, 0.1% Tween 20] 3 times for 5 minutes in orbital shaker (Polymax 1040, heidolph). Once washed, non-specific binding sites were blocked with blocking solution containing 5% non-fat milk (ChemCruz, Cat# sc-

2325) in 1X TBST during 1 hour at room temperature in orbital shaker. After this time, the membrane was rinsed and washed again 3 times for 5 minutes in TBST in orbital shaker.

3.3.12.3. Antibody incubation and immunodetection

The nitrocellulose membranes were incubated ON at 4°C in orbital shaker with the corresponding first antibodies diluted in blocking solution or 5% BSA, (all antibody used in this project are listed in table 3). The next day, the membranes were rinsed and washed three 3 times for 5 minutes in TBST in orbital shaker.

The second antibody was diluted in blocking solution and incubated for 1 hour at RT in orbital shaker. Then, the membrane was rinsed and washed 3 times for 5 min in TBST in orbital shaker. After the second antibody incubation, protein detection was performed by enhanced chemiluminescence (ECL). The membranes were incubated for 2-5 minutes with the sufficient covering amount of ECL substrate (ECL™ Prime Western Blotting System, GE Healthcare, Cat# RPN2232). Then, the membrane is drained and developed with the film developer system ImageQuant LAS 4000 mini (GE Healthcare Life Sciences). The images obtained were processed with the program Image J (v1.50b, NIH) to quantify the average of optic density of all the immunoreactivity bands.

3.3.13. Hematoxylin and eosin staining

Tissues were rapidly fixed in 10% formalin solution, neutral buffered, for 24 h and then transferred to PBS 1X. Samples were sent to the histology service of the Animal Experimentation Unit of the University of Barcelona, School of Medicine for processing. Briefly, the tissues were then paraffin-embedded and the resulting blocks were cut into 5–10 µm sections and stained with hematoxylin and eosin (H&E) to assess tissue histology [176]. Photomicrographs were obtained using a microscope camera (Leica MC 190 HD Camera) and microscope (Leica DM IL LED Tissue Culture Microscope).

3.3.14. Assessment of urine and serum osmolality

Urine osmolarity (U_{osm}) and serum osmolality (P_{osm}) were measured on 20 µl samples by the freezing-point depression technique using an Advanced Osmometer (3320 Micro-Osmometer, Advanced Instruments). A control (Clinitrol 290) and a set of calibration standards (50, 850 and 2,000 mosm/kg H_2O) were used before running each batch.

3.3.15. Plasma blood and urine analysis

Plasma Insulin (Insulin ELISA kit Alpco, Cat# 80-INSHU-E01.1), Aldosterone hormone (Aldosterone ELISA Kit, LSBio, Cat# LS-F28206-1), VP/ADH hormone (Vasopressin ADH ELISA Kit, LSBio, Cat# LS-F7592-1), Angiotensin (Angiotesnin ELISA Kit, LSBio, Cat# LS-F67331-1), glucose (Monlab, Cat# MO-165086) were all measured according to manufacturer's instructions.

3.3.16. Immunohistochemistry

In order to determine the tissue distribution of an antigen of interest, free-floating brain section immunofluorescence was performed. Frozen brains were embebed in OCT (Tissue-Tek, Cat#4583) and slices of 30 µm thickness of were obtained by microtome (Leica SM2000R). Tissue slices were stored at 4^{o}C in cryoprotectant solution [30% (w/v) sucrose, 30% (v/v) ethylene glycol, 250 ml PBS] until the immunostaining was performed.

Tissue slices were washed 3 times for 5 min in PBS 1X to remove the cryoprotectant solution. All steps were done with gentle agitation on a shaker (Thermo-Shaker, PST-100HL). Slices were permeabilized in potassium phosphate-buffered saline (KPBS) [0,9% (p/v) NaCl, 52 mM Potassium phosphate dibasic, 9.6 mM potassium dihydrogen phosphate], containing 0.1% Tritón X-100, 2 times for 10 min and blocked for 1 hour with blocking solution (KPBS containing 0.1% (v/v) Tritón X-100, 3% (w/v) BSA, and 2% (v/v) of goat serum (Sigma-Aldrich, Cat# G9023). The primary antibody in

blocking solution was incubated 1 h RT and ON at 4°C. Slices were then washed 3 times for 10 min with KPBS 0.1% Triton X-100 and incubated with the secondary antibody in blocking solution during 2 h RT and protected from the light. Finally, the samples were washed 3 times for 10 min with KPBS Triton X-100 0.1% and mounted onto superfrost plus slides, (Thermo-fisher, Cat# J7800AMNT) with fluoromont-G containing DAPI, (Thermo-fisher, Cat# 00-4959-52) and coverslipped. (Primary and secondary antibodies are listed in the table 3 showing the dilution used in each incubation).

3.3.17. Paraventricular (PVN) and subfornical organs (SFO) cFos quantification

cFos-positive cells in PVN and SFO sections were quantified using Fiji software. Immunostained slices were scanned under a 20x objective of a fluorescent microscope (Leica DM IL LED Tissue Culture Microscope) equipped with a high-sensitive camera (Leica MC 190 HD Camera) and LAXZ software (version 3.3) was used to obtain the images. High quality images were obtained using a confocal microscope (LSM 800, Carl Zeiss). To select the same PVN and SFO sections in each animal, the images of the slice were overlaid with corresponding Atlas maps of mouse brain [174]. This enabled to outline different brain regions. Brightness and contrast adjustments were applied to all images and the images were transformed to 8-bit images. Black and withe thresholding was used to improve the cFos positive cell visualization. PVN and SFO section was selected and the number of particles was measured using Fiji software, consistent with previous published studies [177].

3.3.18. Synaphotphysin amplification

In order to amplify the AAV2-Syn-DIO-GFP signal in different target areas of the brain, immunostaining of brain slices containing AAV2-Syn-DIO-GFP was performed. Target pre-synaptic areas were scanned under a 20× objective of a fluorescent microscope (Leica DM IL LED Tissue Culture Microscope) equipped with a high-sensitive

camera (Leica MC 190 HD Camera) and LAXZ software (version 3.3) was used to obtain the microscopy images. High quality images were obtained using a confocal microscope (LSM 800, Carl Zeiss). To select the target areas in each animal, the images of the slices were overlaid with corresponding Atlas maps of mouse brain [174]. For the measurement of the intensity level of synaptophysin fluorescence a region of interest (ROI) was drawn including whole PVN section. Measurement tool of imageJ was applied to obtain information average pixel intensity.

3.3.19. Dendritic spines analysis

For detailed morphological analyses of dendritic spines, samples were obtained by Zeiss LSM 800 confocal microscope using a 1003 Plan Apo TIRF DIC-oil immersion objective (total magnification of 63x). To visualize the mCherry protein in AgRP neurons, the samples were excited with a 587 nm laser wave length and the fluorophore emission was captured by a 610 band-pass (BP) filter. A Z-stack was obtained for each dendrite extended from the apex of the cell soma. For each animal, 20 dendrites (segmented by 50 µm) were analyzed. Z-stacks were used to achieve three-dimensional reconstruction. The dendritic spine density in each dendritic segment was quantified using Fiji software and expressed as dendrite number/50 µm.

3.3.20. Adipocyte area measurement

To quantify the adipocyte cells area three representative images from each adipose tissue section were taken with a 20x objective using a high-sensitive camera (Leica MC 190 HD Camera). Images were analyzed with adiposoft software, a fully automated open-source for the analysis of white adipose tissue cellularity in histological sections [178]. Each image was calibrated to 4.65 pixel per micron using a 20x objective and Leica microscope. Any adipocytes with visible alterations in the membranes was “closed” digitally prior to continuing with the automated area quantification. To quantify the adipocyte area, images are analyzed and adipocytes

highlighted if they meet the following 3 criteria: (1) the boundaries for sizing of cell were 40-40,000; (2) the adipocyte has a shape factor of 0.35–1 (a shape factor of 0 indicating a straight line and 1 a perfect circle); and (3) the adipocyte does not border the image frame. When measurement was obtained, results were represented as frequency distribution and the average of total area counted.

3.3.21. Transcriptomic analysis by RiboTag technique

To the cell-specific characterization of the transcriptional RNA in a physiologically relevant context we took advantage of the developed RiboTag mouse line [171]. This approach allows us to epitope-tag ribosomes from solely AgRP neurons and isolate cell-specific mRNAs that are actively being translated in the adult mouse *in vivo*.

3.3.21.1. Immunoprecipitation (IP)

Punches containing ARC nucleus from ON fasted mice were homogenized and IP was performed. To homogenize the tissue, 350 µl of homogenization buffer (HB) [50 mM Tris, pH 7.5, 100 mM potassium chloride, 12 mM magnesium chloride, 1% NP-40 and RNAase-free H_2O] supplemented with 1mM dithiothreitol (DTT), 1X protease inhibitor, 200 U/ml RNase inhibitors, 0.1 mg/ml ciclohexamide and 1 mg/ml heparin, was added to the sample (Important prepare the supplemented HB same day of the experiment). To improve the homogenization a 30G insulin needle was used to aspirate up and down 4-5 times avoiding make bubbles). The homogenized was transferred to a new eppendorf and kept on ice for 5 min. The samples were centrifuged at 13,000 rpm for 10 min at 4^{o}C (Eppendorf® Centrifugue 5415R). 50 µl of the supernatant was collected (input) and stored at -80 ^{o}C.

In an ice-cold low-binding eppendorf, 3 µl of HA-antibody (Mouse monoclonal anti-HA, Cat# MMS-101R) was added to the leftover supernatant and samples were incubated in a cold room spinner for 2 hours.

During this incubation period, the Dynabeads prot G (ThermoFisher Scientific, Cat# 10004D) were prepared. This procedure consisted in to wash 1 time 200 µl of dynabeads with 1 ml of HB. To do so, the 200 µl of dynabeads were added to a tube already placed in the magnet. The liquid was aspirated and 1 ml of HB was added. The beads were put on ice (without magnet) until used.

Once the incubation of the sample containing the HA-Antibody was finished, it was transferred to the tube containing the dynabead. To perform this step, the magnet was placed on ice and the tube containing the dynabead was put on the magnet. The HB medium was aspirated and immediately the sample with the HA-antibody was added. The tubes were taken out from the magnet and spin during 2 hours in a cold room spinner.

After the IP, the beads were washed 3 time with 1 ml of high salt buffer (HSB) [50 mM Tris pH 7.4, 300 mM KCl, 12 mM $MgCl_2$, 1% NP-40, 1 mM DTT, 100 µg/ml Cyclohexamide, RNAase free H_2O]. For each wash, the samples were centrifuged 5 min 13,000 rpm (Eppendorf® Centrifugue 5415R).

Finally, in order to extract the RNA from the tagged neurons the RNeasy Plus micro kits (QIAGEN, Cat# 74034) was applied following the manufacturer instruction. Briefly, samples were treated with 350 µl of RLT buffer (QIAGEN, Cat# 74034) and 3.5 µl β-mercaptoethanol to lysate the cells. Samples were centrifuged at 13,000 rpm for 3 min (Eppendorf® Centrifugue 5415R) and the supernatant was transfer to a gDNA eliminator spin column placed in a 2 ml collection tube. The samples were centrifuged again 30 seg at 10,000 rpm and the column was discarded. 350 µl of ethanol 70% was added to the flow-through and mixed by pipetting. The sample was transferred to an RNeasy MinElute spin column placed in a 2 ml collection tube and centrifuged for 15 seg at 10,000 rpm (Eppendorf® Centrifugue 5415R). The flow through was discarded and 700 µl of RW1 was added to RNeasy MinElute spin column. Samples were centrifuged again 15 seg at 10,000 rpm (Eppendorf® Centrifugue 5415R) to wash the spin column membrane. Same step was repeated by adding 500 µl of RPE buffer and

then ethanol 80%. Finally, 14 µl of RNAse-free water was directly added to the center of the spin column membrane and centrifuged for 1 min at 13,000 rpm to elute the RNA.

3.3.21.2. RNA quantification by ribogreen assay

Quant-iT RiboGreen RNA reagent is an ultrasensitive fluorescent nucleic acid stain for quantitating RNA in solution. The RNA obtained from the IP was measured following the manufacturer instruction of Quant-iT RiboGreen RNA kit (Thermo Fisher scientific, Cat# R11490). Briefly, working solution according to the low range assay was prepared. The RNA standard was diluted to create a 6-point standard curve (0, 0.5, 1. 5, 25, 50 ng/ml). Samples and standard curve was measured in a microplate reader at 488 excite and 520 emission.

3.3.21.3. cDNA synthesis by SuperScript IV

SuperScript IV (ThermoFisher Scientific, Cat# 11750150) is designed to synthesize first-strand cDNA directly from mammalian cell lysates without requiring the initial isolation of RNA. This cDNA synthesis kit has been optimized for small cell samples, ranging from 10,000 cells down to a single cell.

To perform the retro transcription, we follow the instruction of the manufacturer. Briefly, 0.27 ng of RNA from the samples and the input were incubated with 5X SuperScript IV RT buffer, 100 mM DTT, RNAseOUT Recombinant RNase inhibitor and the SuperScript IV Reverse transcriptase (200 U/µl). The samples were incubated at 23^{o}C for 10 min, 50^{o}C for 10 min and 80^{o}C form 10 min. Samples were stored at -20^{o}C until the qRT-PCR was performed.

3.4. Bioinformatics and statistical analysis

Statistical significance was determined using Prism 8.0 software from GraphPad. Two-way ANOVA, followed by post-hoc analysis with Tukey-Kramer test in

the multiple comparison analysis was applied when more than two groups were compared and t-student was performed when two groups were compared. Data is expressed as mean +/- SEM. P value lower than 0.05 is considered significant.

Fiji Image-J1.33 software (NIH; Bethesda, MD, USA) was used to count c-Fos positive cells, GFP-syn and to process electron microscopy images and western blot analyses. Adipocyte area was calculated with the MRI_Adipocytes_Tools of ImageJ software. The number of animals used in each experimental setting and analysis are specified in each figure legend.

4. RESULTS

4.1. Generation of mice with *Cpt1a* deletion in AgRP neurons

In order to evaluate the role of CPT1A in the control of food intake and energy homeostasis we generated the time-dependent conditional AgRP-*Cpt1a* knockout mice (*Cpt1a*$_{AgRP}^{(-/-)}$). *Cpt1a*-floxed and tamoxifen-inducible AgRP-CreER^{T2} mice were bred to generate *Cpt1a*$_{AgRP}^{(-/-)}$ and their control littermates (*Cpt1a*$^{(flox/flox)}$, *Cpt1a*$^{(+/+)}$; AgRP-CreER^{T2}).

To confirm the recombination in the ARC nucleus, Cre recombinase activity was evaluated. The AAV9-EF1a-DIO-Cherry virus expressing the mCherry reporter activated by "Cre-on" system was administered by stereotaxis allowing to distinguish the Cre-expressing neurons from neighboring neurons. The AAV9-EF1a-DIO-Cherry at a dose 1,23x10^{13} gc/ml was bilaterally injected in ARC nucleus of *Cpt1a*$_{AgRP}^{(-/-)}$ male and female mice at 8-10 weeks old (Figure 9A,B). In order to achieve the maximal efficiency of AAV delivery, the time of infection was set up at 3 weeks. After 3 weeks' of AAV administration, mice were induced using tamoxifen protocol (mentioned in section 3.2.1). One week later animals were sacrificed and the brain was fixed and analyzed. Both male and female *Cpt1a*$_{AgRP}^{(-/-)}$ mice showed an AgRP Cre-dependent mCherry signal limited to the ARC nucleus. No other signal was detected in neighborhood nuclei of the hypothalamus (Figure 9C).

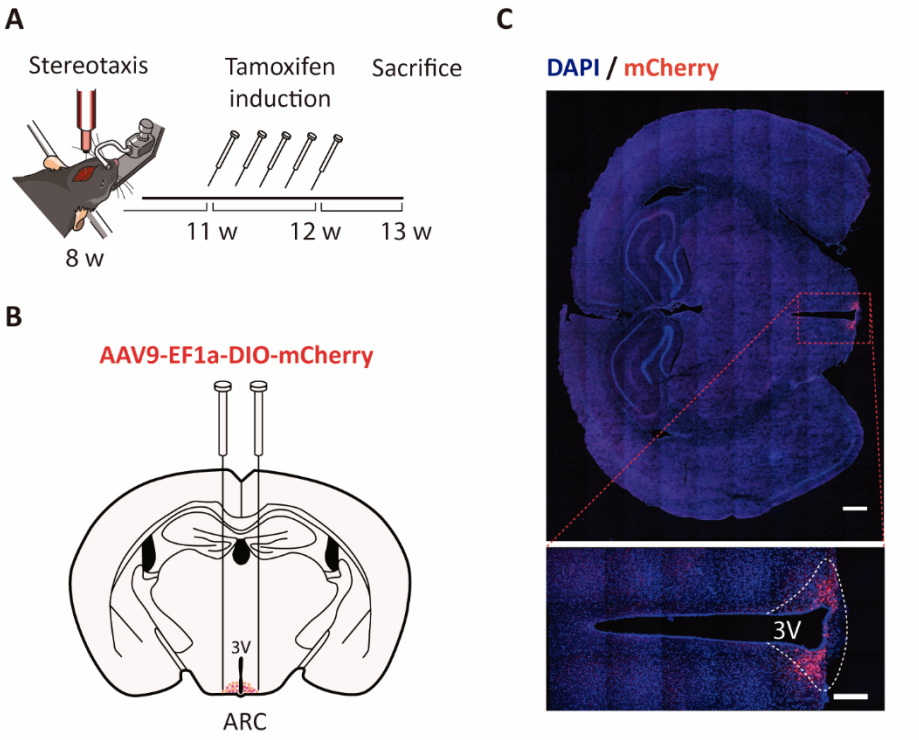

Figure 9. Validation of Cre-mediated recombination in AgRP neurons.
(A) Scheme of the time-course of the experiment. (B) Bilateral injection of 400 nl at dose 1,23 x 10^{13} gc/ml of AAV9-EF1a-DIO-mCherry into the ARC of AgRP-Cre-ER^{T2} mouse. (C) Representative histological slice of Cre-dependent mCherry expression in the ARC nucleus; Scale bar 500 µm (upper image), 200 µm (bottom image).

Tissue specific recombination of *Cpt1a* floxed allele was confirmed by conventional PCR analysis. At 8-10 weeks old male and female *Cpt1a*$_{AgRP}^{(-/-)}$ mice and control littermates were induced with tamoxifen (Figure 10A). After sacrifice, gDNA from different tissues and brain areas were obtained and *Cpt1a* recombination was analyzed by PCR using the Hom Arm primers (described in section 3.3.3).

The PCR product of the loxP-flanked region containing the CPT1A exon 4 is 1,030 bp. The Cre recombination of this sequence produced a 219 bp product (Figure 10B). No recombined DNA amplicons were observed in all the tissues analyzed in control animals. Surprisingly, we did not observed the 219 bp amplicon in ARC and in any of the tissues analyzed from *Cpt1a*$_{AgRP}^{(-/-)}$ mice (Figure 10C). Importantly, it has been

reported that ARC nucleus contains just 9,965 ± 66 AgRP neurons which are evenly distributed along the anterior to posterior ARC axis [179]. Taking into account this information, the isolation of the gDNA from the ARC nucleus could content high proportion of non-recombined gDNA coming from the parenchyma vs low amount of recombined gDNA from AgRP neurons. Therefore, we only could detect the *Cpt1a* WT amplicon (1,030 bp).

To avoid the DNA amplification of the *Cpt1a* WT amplicon (1,030bp) we digested the gDNA with the restriction enzymes *PstI* (Fermentas, Cat #ER0611) and *AatII (Fermentas, Cat# ER0991)*, which were not present in the *Cpt1a* recombined sequence (Figure 10D). gDNA from the ARC nucleus was incubated during 1 hour at 37^{o}C and after that the same PCR program was applied. The *Cpt1a* recombined amplicon of 219 bp was only observed in the samples from ARC nucleus (Figure 10E).

The 219 bp amplicon obtained from the ARC nucleus of *Cpt1a*$_{AgRP}^{(-/-)}$ mice was excised from the agarose gel, purified and sequenced to confirm the *Cpt1a* recombination (Figure 10F).

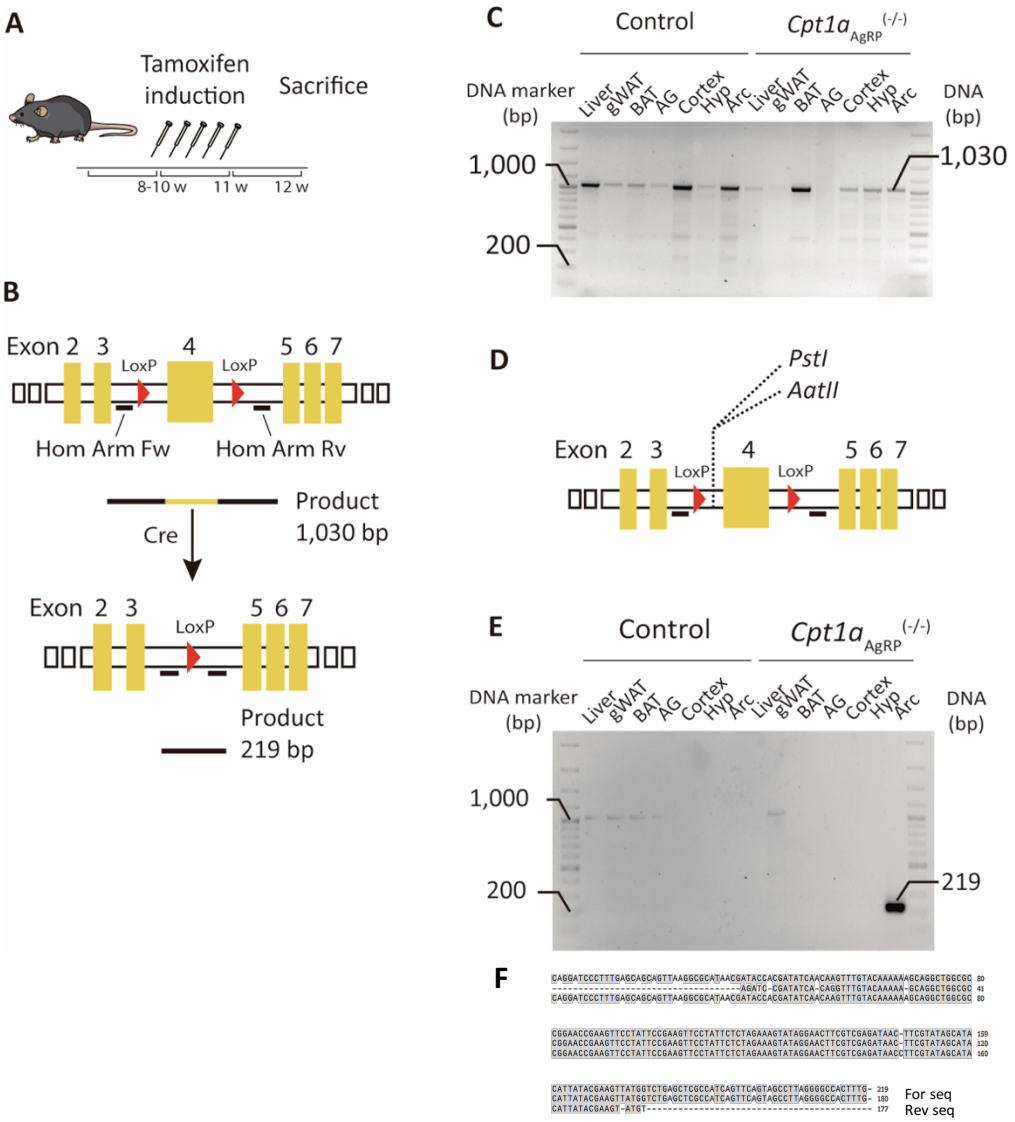

Figure 10. Validation of the *Cpt1a* exon 4 deletion.

(A) Scheme of the experiment. (B) Scheme of Cre-mediated recombination product showing the floxed band (1,030 bp) containing the *LoxP* sequences surrounding the exon 4 of *Cpt1a* gene. After the Cre recombination, product resulted in a DNA fragment of 219 bp. (C) Representative PCR analysis of gDNA from liver, gonadal white adipose tissue (gWAT), brown adipose tissue (BAT), Adrenal Gland (AG), Cortex, Hypocampus (Hyp) and Acuate nucleus (Arc). (D) Scheme of restriction enzyme. *PstI* and *AatII* cutting regions to avoid *Cpt1a* amplicons from unrecombined gDNA. (E) Representative PCR analysis of gDNA from liver, gonadal white adipose tissue (gWAT), brown adipose tissue (BAT), Adrenal Gland (AG), Cortex, Hypocampus (Hyp) and Acuate nucleus (Arc) treated with *PstI* and *AatII* from $Cpt1a_{AgRP}^{(-/-)}$ mice (n = 3-5 mice). (F) Annealing of the sequenced band extracted from the gel. The upper band is the query signal annealed with the sequence obtained with the forward and the reverse Hom Arm primers, gray bars represent the match between signals.

Very recently, it was demonstrated that AgRP is also expressed in cromaffin cells of the adrenal medulla of AG [180]. Thus, we examined this tissue in order to detect whether the *Cpt1a* deletion could alter the phenotype and AG functionality. AG from *Cpt1a*$_{AgRP}^{(-/-)}$ and control littermates were analyzed after 3 month of induction by tamoxifen. No histological disruption was observed in both medulla and cortex (Figure 11A) and no statistical changes in AG weight normalized by body weight of each mouse were detected (Figure 11B,D). Given the difficulty to isolate the cortex from the medulla of AG, we analyzed the gDNA of the whole tissue. We could not observe *Cpt1a* recombined amplicons in AG from male and female *Cpt1a*$_{AgRP}^{(-/-)}$ mice (Figure 11C) probably due to the low copies of recombined *Cpt1a* product.

Furthermore, we measured the level of *Cpt1a* mRNA levels in the whole AG tissue. No differences in the mRNA levels of *Cpt1a* were observed between genotypes (Figure 11C,E). Next, we analyzed the adrenal medulla integrity by measuring the mRNA levels of tyrosine hydroxylase (*Th*). No significant changes were observed between genotypes (Figure 11F,H). Adrenal cortex function was also evaluated analyzing the levels of plasma aldosterone. Adrenal cortex functionality was not impaired since the blood levels of aldosterone were enhanced in both sexes of *Cpt1a*$_{AgRP}^{(-/-)}$ mice (Figure 11G,I). All these results together suggest that AG maintain their integrity and function.

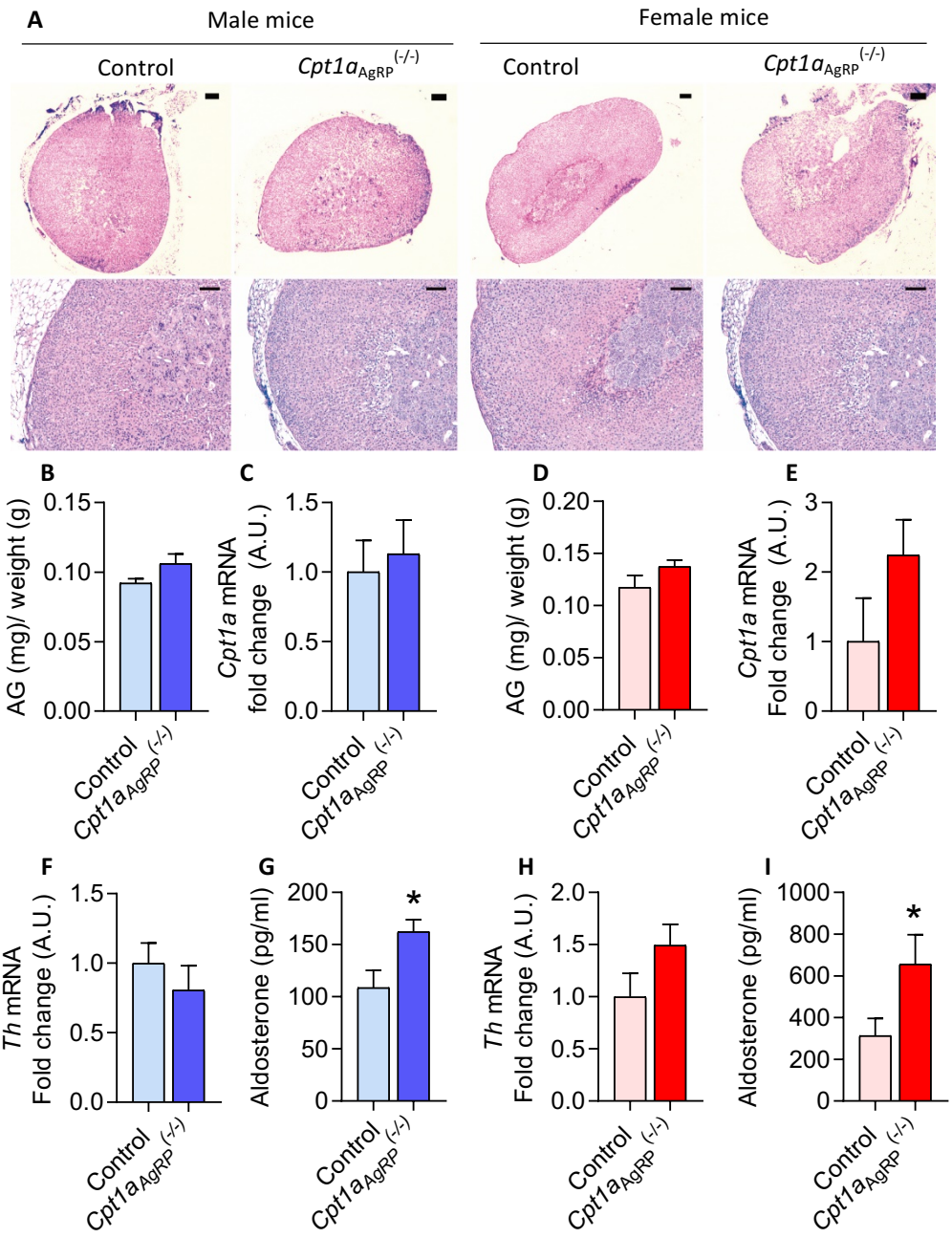

Figure 11. Analysis of Adrenal Gland after *Cpt1a* deletion in AgRP neurons.
(A) Representative H&E staining of male and female adrenal gland. Scale bar 500 µm (magnification 4X) and 100 µm (magnification 20X). (B) Weight of the left and right adrenal glands in male and (D) female. (C) *Cpt1a* mRNA levels in adrenal gland (AG) from male and (E) female. (F) Tyrosine hydroxylase (*Th*) mRNA levels in adrenal gland from male and (H) female. (G) Plasmatic aldosterone levels of male and (I) female mice. Data are expressed as mean ± SEM; n = 8-10; Student's T * $p < 0.05$.

4.2. *Cpt1a* deletion in AgRP neurons influences the feeding behavior differently in male and female

In order to analyse whether lipid metabolism in AgRP neurons influence feeding behaviour we studied the phenotype effect of *Cpt1a* deletion in this population of neurons. Male and female $Cpt1a_{AgRP}^{(-/-)}$ and control littermate were induced with tamoxifen at 8 weeks old. Both male and female $Cpt1a_{AgRP}^{(-/-)}$ mice appeared markedly smaller at 3 months of age compared to their littermates (Figure 12A,B). Body weight was weekly monitored until the mice sacrifice. Both $Cpt1a_{AgRP}^{(-/-)}$ male and female mice increased significantly less than the control littermates (Figure 12C,D). Interestingly, this reduction of the body weight gain was higher in male mice than female. While $Cpt1a_{AgRP}^{(-/-)}$ male mice showed reduction of approximately 35% of their body weight (43.82 ± 4.691g *vs.* 28.37 ± 2.059 g, **** p <0.001), female $Cpt1a_{AgRP}^{(-/-)}$ mice educe a 22% (28.13 ± 3.321 g *vs.* 21.78 ± 1.062 g, **** p <0.001).

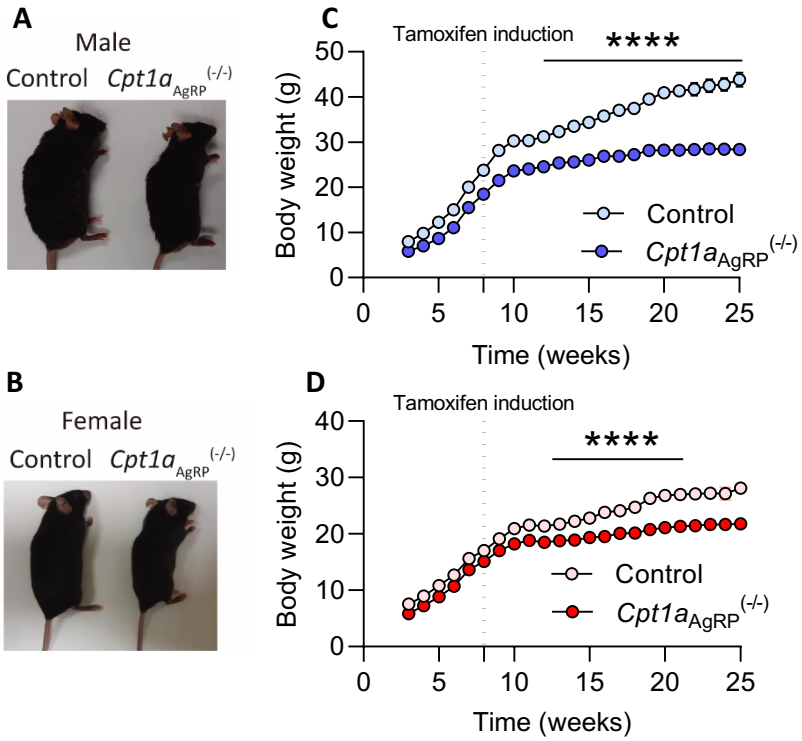

Figure 12. Deletion of *Cpt1a* in AgRP neurons affects feeding behavior
(A) Representative image of male *Cpt1a*$_{AgRP}^{(-/-)}$ and (B) female mice compared with their control littermates after 3 month of tamoxifen induction. (C) Body weight in *Cpt1a*$_{AgRP}^{(-/-)}$ male and (D) female mice and control littermates. Data are expressed as mean ± SEM; n = 6-9 male and n = 8-12 female; Data were analyzed by 2-way repeated measures ANOVA followed by Šidák's post hoc test. **** $p < 0.001$.

Next, we studied the feeding behaviour. First, we measured the food consumption under normal chow diet during one month. Interestingly, we found gender-based differences in food and feeding behaviours. Food intake in *Cpt1a*$_{AgRP}^{(-/-)}$ male mice was significantly lower compared with their control littermates and this differences became evident after 21 days after tamoxifen induction (Figure 13A,B). Surprisingly, no differences were observed in female *Cpt1a*$_{AgRP}^{(-/-)}$ mice in the same period. (Figure 13C,D).

This result was confirmed with the food intake measurement obtained from TSE metabolic system. This monitoring system facilitates accurate control and measurement of food intake. After a period of acclimation both male and female

Cpt1a$_{AgRP}^{(-/-)}$ mice reveal the same behaviour previously described. While *Cpt1a*$_{AgRP}^{(-/-)}$ male mice showed a reduction of the food intake (Figure 13E), *Cpt1a*$_{AgRP}^{(-/-)}$ female mice did not reveal statistical changes (Figure 13G). Importantly, *Cpt1a*$_{AgRP}^{(-/-)}$ male mice showed this food intake reduction during dark phase (9.620 ± 5.464 g *vs.* 3.946 ± 0.5305 g, * p < 0.05), which is the most active phase for mice.

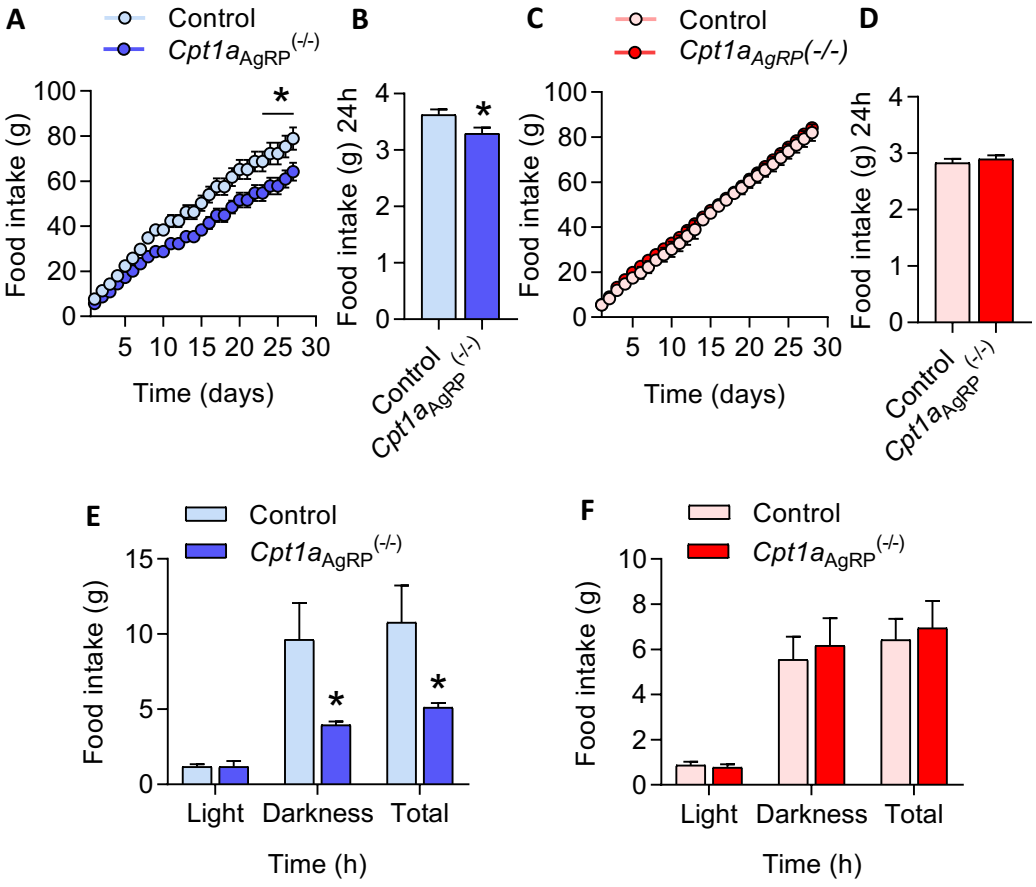

Figure 13. Deletion of *Cpt1a* in AgRP neurons affects differentially food intake depending on gender. **(**A) Analysis of cumulative food intake in male and (C) female mice measured during one month after tamoxifen induction. (B) 24 hours of food consumption in male and (D) female. (E) Analysis of food intake measured by TSE system during light and dark phases in male and (F) female mice. Data are expressed as mean ± SEM; n = 8-10 for A, B, C, D experiment and n = 5 for E, F experiment. Data were analyzed by 2-way repeated measures ANOVA followed by Šidák's post hoc test. * < 0.05 (A,C) and Student's T, * p < 0.05 (B, D, E. F)

Given the important role played by AgRP neurons in the regulation of feeding and energy balance, there is great interest in understanding the factors that regulate their activity. Fasting and ghrelin, a hormone that increases during fasting, are considered key factors to activate AgRP/NPY neurons [181,182]. To know if CPT1A is a downstream factor involved in the signaling pathway of fasting and ghrelin in the food intake induction we measured food intake in both conditions.

Mice were ON fasted and we evaluated the cumulative food intake during the refeeding period for 4 hours (Figure 14A). Results showed that both male and female *Cpt1a*$_{AgRP}^{(-/-)}$ mice reduced food intake during the refeeding period (Figure 14B,C) and the reduction of cumulative food intake is more pronounced in *Cpt1a*$_{AgRP}^{(-/-)}$ male than female mice (Figure 14B,C).

In order to analyze the effect of ghrelin on *Cpt1a*$_{AgRP}^{(-/-)}$ mice, two ip injections of ghrelin were administered at 0 and 30 min. Food consumption and the eating time were evaluated during 1 hour after the first dose of ghrelin administrated. Male (Figure 14D) and female (Figure 14F) *Cpt1a*$_{AgRP}^{(-/-)}$ mice showed less food consumption compared with their control mice. While total food consumed by *Cpt1a*$_{AgRP}^{(-/-)}$ male mice was reduced by 31.5 % (0.2280 g ± 0.049 *vs.* 0.1560 g ± 0.045, * $p < 0.05$), *Cpt1a*$_{AgRP}^{(-/-)}$ female mice showed only 23.5 % reduction (0.6817 g ± 0.1402 *vs.* 0.5214 g ± 0.0829, * $p < 0.05$) respect to their littermates.

Consistent with these results male *Cpt1a*$_{AgRP}^{(-/-)}$ mice spent less time consuming food than their littermates and the same tendency was observed in *Cpt1a*$_{AgRP}^{(-/-)}$ female mice (Figure 14E,G). Interestingly, it seems that female mice are more sensitive to ghrelin hormone as the control female mice food ingestion was 3-fold more than male control mice (0.6817g ± 0.1402 *vs.* 0.2280g ± 0.049).

Altogether, these results reinforce the importance of CPT1A downstream in ghrelin's pathway specifically in AgRP neurons and suggest that males are more prone to reduce food intake *at libitum* conditions than females but both sexes have impaired food intake in fasting conditions and in high ghrelin levels.

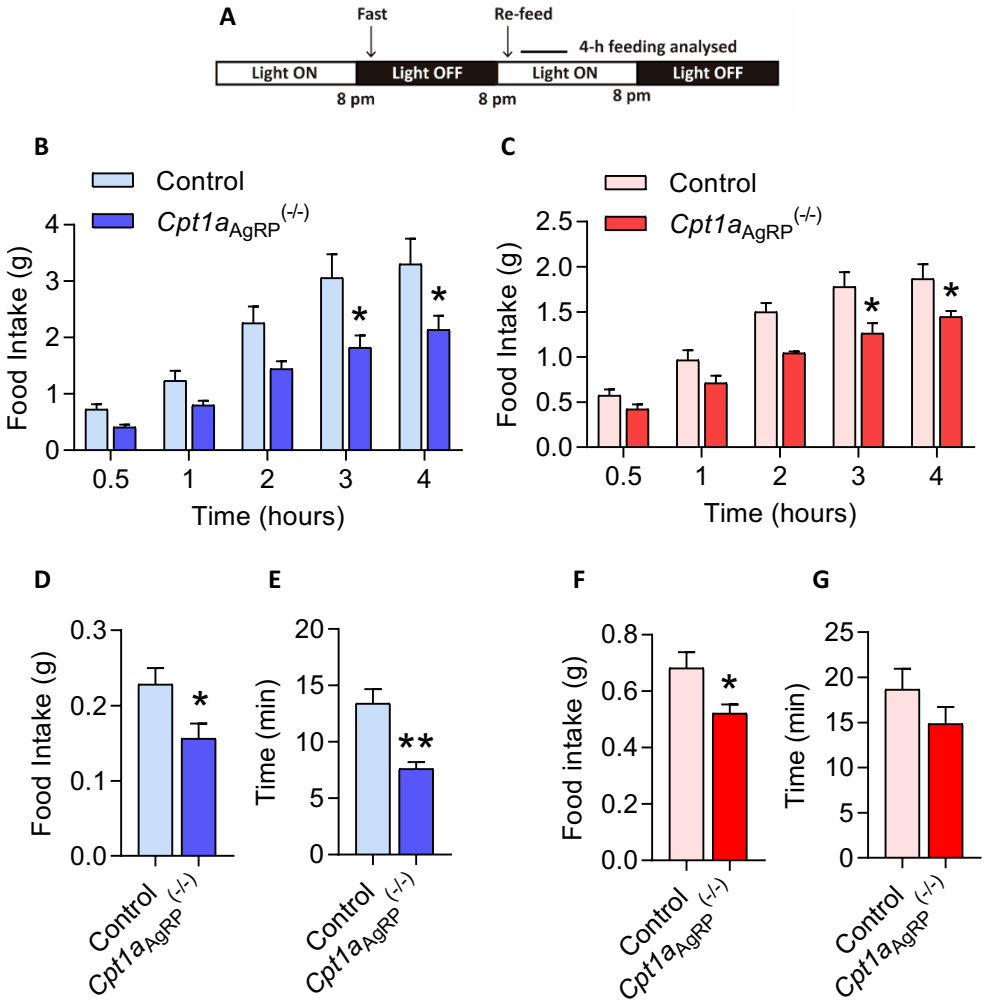

Figure 14. Deletion of *Cpt1a* in AgRP neurons affects the food intake induced by fasting and ghrelin. (A) Scheme of the experiment design of the Fast-refeeding assay. (B) Response to fasting-refeeding in male and (C) female. (D) Cumulative food intake measured after 1 hour of ghrelin ip administration in male and (F) female mice and time that (E) male and (G) female mice spent eating after ghrelin injection. Data are expressed as mean ± SEM; n = 8 (B,C); n = 5-6 (D, E F, G). Data were analyzed by 2-way repeated measures ANOVA followed by Šidák's post hoc test. * < 0.05 (A,C). Student's T, * $p < 0.05$, ** $p < 0.01$.

4.3. *Cpt1a* deletion in AgRP neurons increases energy expenditure in females but not in males

Several studies have determined that AgRP intervention mediates an effect in EE [183,184]. Thus, in order to evaluate the involvement of lipid metabolism in the EE regulations through AgRP neurons, male and female *Cpt1a*$_{AgRP}^{(-/-)}$ and control littermate mice were subjected to the TSE system to measure the metabolic energy by indirect calorimetry. Mice were acclimated for 48 hours and metabolic rate was measured for 3 days at *ad libitum* and in conditions of 12 hours fasting followed by 4 hours of refeeding (Figure 15A).

No differences in the EE profile in male mice were observed and surprisingly, male *Cpt1a*$_{AgRP}^{(-/-)}$ mice tend to show a reduction of EE during light, darkness and fasting phases being this difference significant in the re-feed state (Figure 15B,C).

Conversely, we found an increase of EE in female *Cpt1a*$_{AgRP}^{(-/-)}$ mice compared with their control littermates in all phases analyzed (Figure 15D,F). While the total EE in control female mice was 1.557 ± 0.07 Kcal/h/g lean mass, female *Cpt1a*$_{AgRP}^{(-/-)}$ mice showed an increase of 1.24-fold (1.945 ± 0.364 Kcal/h/g lean mass) compared with their control littermates, suggesting that CPT1A deletion in AgRP neurons impact in EE in a different manner depending of gender.

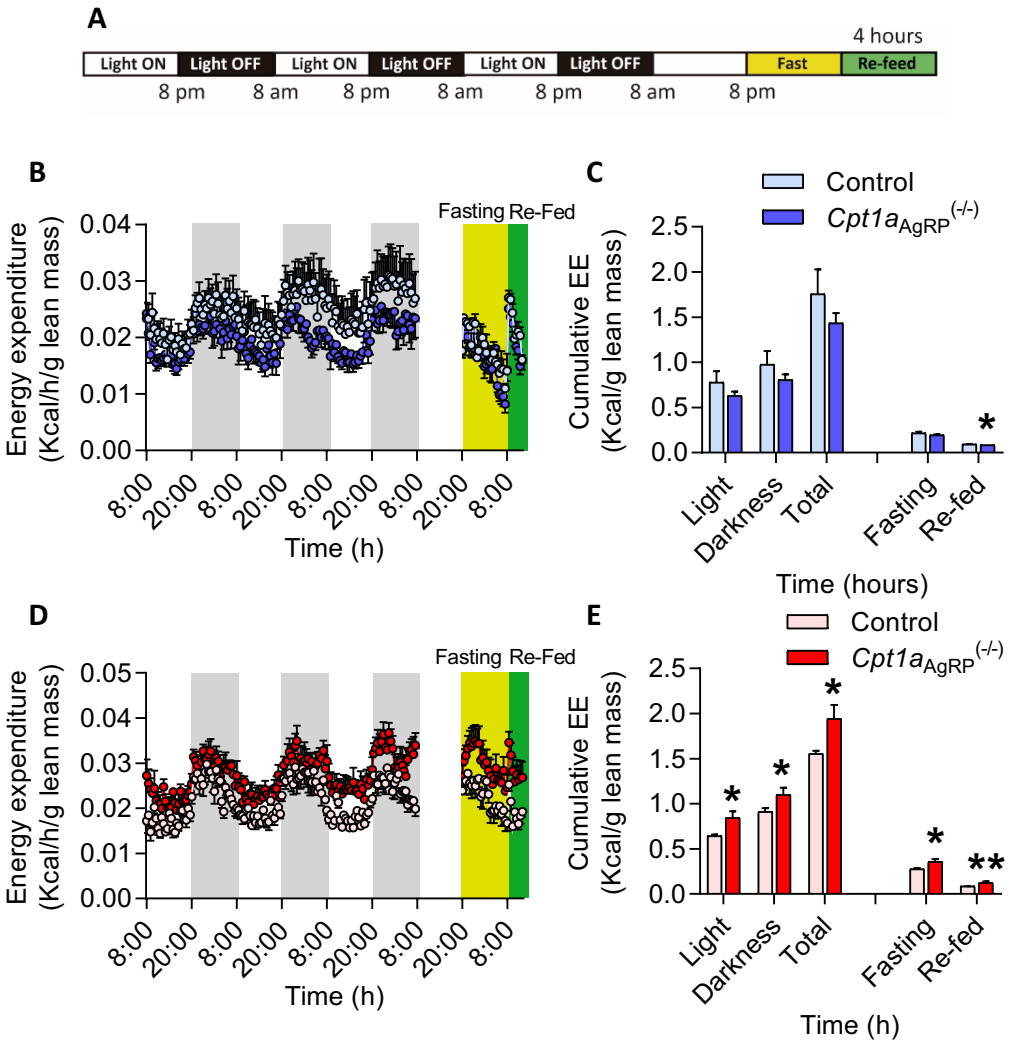

Figure 15. Deletion of *Cpt1a* in AgRP neurons affects energy expenditure depending on gender. (A) Scheme of the experiment design. (B) Energy expenditure (EE) registered by TSE system during light, dark cycles and fast and re-feeding in male and (D) female. (C) Average of EE in light and dark cycles and during fast and refeeding in males and (E) female. Data are expressed as mean ± SEM; n = 5-6; Student's T, * $p < 0.05$, ** $p < 0.01$.

Respiratory quotient (RQ; *i.e.,* carbon dioxide output/oxygen uptake), is the ratio of the volume of carbon dioxide produced when a substance is oxidized, to the

volume of oxygen used. The oxidation of carbohydrate results in RQ of 1.0; of fat, 0.7; and of protein, 0.8.

This ratio is useful to know which substrate is being used at a specific time. The analysis of RQ index provided by the TSE system was done in the same condition described for the EE (Figure 16A). Results did not reveal significant differences between male *Cpt1a*$_{AgRP}^{(-/-)}$ mice and control littermates measured during light, darkness and total phases (Figure 16B). Interestingly, although there were not differences during light and darkness phases in female mice, female *Cpt1a*$_{AgRP}^{(-/-)}$ mice showed an RQ of approximately 0,95 during fasting and refeeding (Figure 16C) suggesting that female *Cpt1a*$_{AgRP}^{(-/-)}$ mice is metabolizing more carbohydrate instead lipid and proteins during these conditions.

In order to analyse the ambulatory behaviour, LA (beam breaks) was recorded during all phases previously described. Male and female *Cpt1a*$_{AgRP}^{(-/-)}$ and control littermates mice did not reveal significant differences in LA (Figure 16D,E). However, female mice seem more active than male during darkness period independently of CPT1A deletion in AgRP neurons.

All these results together suggest that *Cpt1a* ablation in AgRP neurons influences differentially the EE profile in male and female. While female *Cpt1a*$_{AgRP}^{(-/-)}$ mice showed an increase of EE no differences were observed in male mice. In addition, female *Cpt1a*$_{AgRP}^{(-/-)}$ mice metabolize more carbohydrates during metabolic stress such as fasting and keep this state during the refeeding period. Finally, *Cpt1a* deletion in AgRP did not affect the LA.

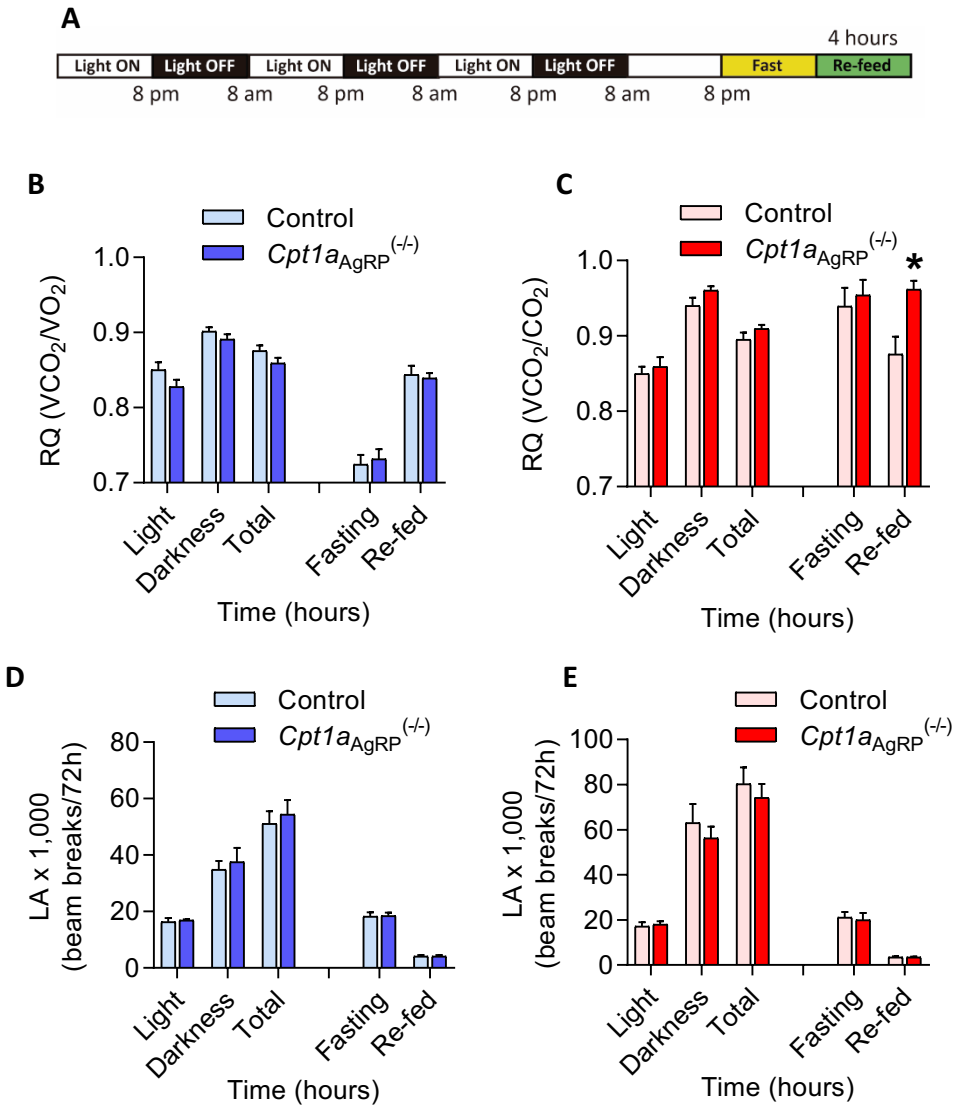

Figure 16. Deletion of *Cpt1a* in AgRP neurons does not affect the RQ index and locomotion activity. (A) Scheme of the experiment design. (B) Respiratory quotient (RQ) registered by TSE system in male and (C) female. (D) Locomotion activity (LA) registered by TSE system in male and (E) female. Data are expressed as mean ± SEM; n = 5-6; Student's T, * $p < 0.05$.

4.4. *Cpt1a* deletion in AgRP neurons regulates peripheral metabolism and adiposity

It is well stablished that AgRP neurons coordinate nutrient partitioning through the ability to orchestrate peripheral organs activity. To specifically address the role of lipid metabolism in AgRP neurons and their impact on peripheral organs we analysed different targeted tissues. Male and female *Cpt1a*$_{AgRP}^{(-/-)}$ and control littermates mice were sacrificed 3 month after tamoxifen induction and gWAT, iWAT, BAT liver, pancreas, testis and ovaries were studied.

4.4.1. *Cpt1a* ablation in AgRP neurons increases BAT activity

During the last decade, great attention has been emerged in the study of brain-SNS-BAT axis. In 2016, Brüning and colleagues have shown that AgRP neurons acutely control glucose metabolism through the modulation of BAT activity [185]. The group found that switching on AgRP neurons reduced sympathetic activation of BAT and dramatically altered its gene profile. Considering this information, we wondered whether modifying the lipid metabolism in AgRP neurons would affect the BAT activity.

We analyzed BAT morphology and thermogenic activity after 3-months of tamoxifen induction. The day before sacrifice, the temperature of interscapular area was measured as an indicator of BAT thermogenic activity. Results showed a clear reduction of BAT weight both in male and female *Cpt1a*$_{AgRP}^{(-/-)}$ mice compared with their control littermates (Figure 17A,B). While in male *Cpt1a*$_{AgRP}^{(-/-)}$ mice the weight reduction is approximately 40%, in female *Cpt1a*$_{AgRP}^{(-/-)}$ mice the reduction was approximately 80% of the normal BAT weight suggesting that BAT from female mice are more sensitive to the deletion of CPT1A in AgRP neurons.

When we analysed the histology of the tissue, we observed an apparent reduction of the LD content independently of the gender (Figure 17C). Using image J and adiposoft software to analyse LD area, we observed a 47% and 44% lipid droplet reduction in male and female *Cpt1a*$_{AgRP}^{(-/-)}$ mice respectively respect to their control

littermates (Figure 17D,E). Interestingly, the comparison between sex control groups showed that male mice have larger areas of LD compared to female mice.

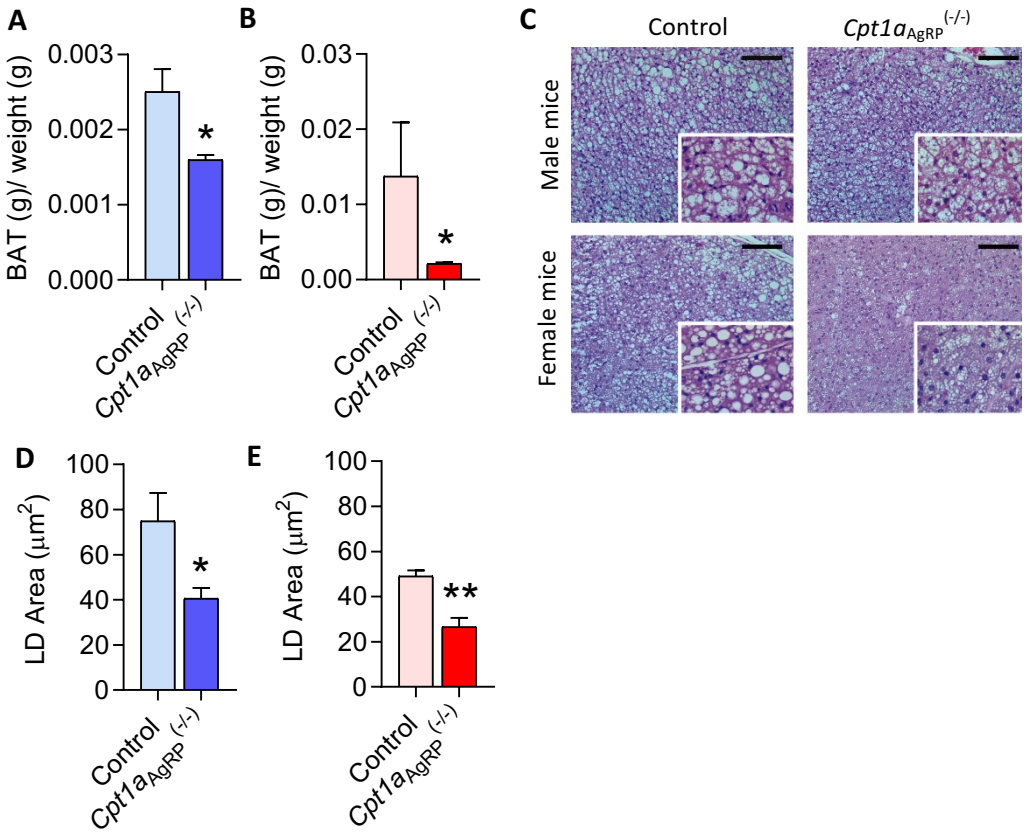

Figure 17. Deletion of *Cpt1a* in AgRP neurons affect the LD content in BAT
(A) Weight of brown adipose tissue of male and (B) female mice. (C) Representative images of BAT sections stained with H&E in male and female mice. Scale bar 100 µm (magnification 20x). (D) Lipid droplet (LD) quantification by using image J in male and (E) female. Data are expressed as mean ± SEM; n = 8-10; Student's T, * $p < 0.05$, ** $p < 0.01$.

The reduction of the LD content could suggest that tissue is burning lipids to produce heat. We took the advantage of the thermography camera to measure the temperature of interscapular area where BAT is located (Figure 18A). As we expected, both genders showed an increase of the BAT skin surface area (Figure 18B,C). Whereas

male *Cpt1a*$_{AgRP}^{(-/-)}$ mice increased 0.4 degrees (37.97 ± 0.3033 °C *vs.* 38.37 ± 0.3394 °C, * p = 0.05) compared with their control littermates, this difference is clearly higher in female mice. Female *Cpt1a*$_{AgRP}^{(-/-)}$ mice increased 1.05 °C compared to their control littermates (36.5 ± 0,7276 °C *vs.* 37.80 ± 0.4375 °C, ** p = 0.01).

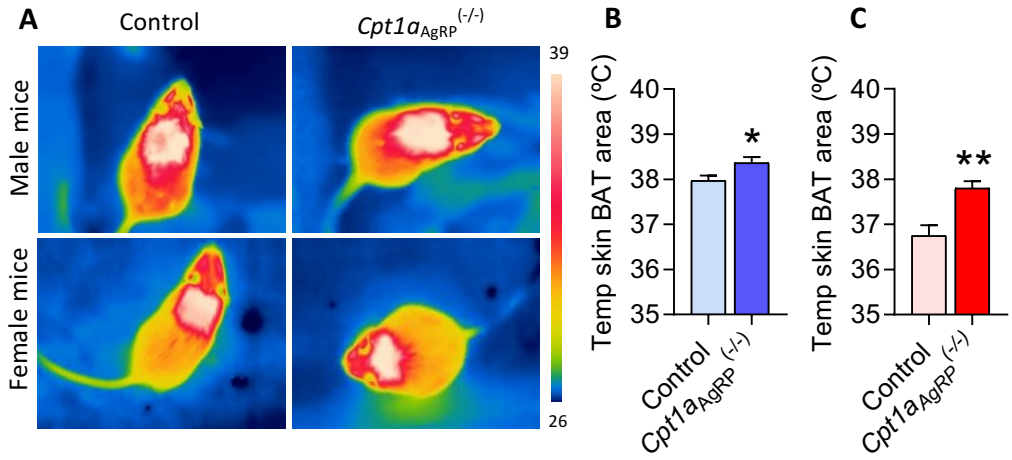

Figure 18. Deletion of *Cpt1a* in AgRP neurons activates BAT activity.
(A) Representative infrared thermal images and temperature of the skin BAT area in (B) male and (C) female mice. Data are expressed as mean ± SEM; n = 8-10; Student's T, * p < 0.05, ** p < 0.01.

To go deeper in this result, we analysed the gene expression profile of thermogenic genes and key enzymes involved in lipid and glucose metabolism. Consistent with the increased BAT temperature, female *Cpt1a*$_{AgRP}^{(-/-)}$ mice showed an important increase of mRNA levels of lipolytic genes *Atgl* (50-fold) and *Hsl* (10-fold) and FA oxidation gene *Cpt1b* (Figure 19B) suggesting an accelerated TG breakdown to produce FAs as a fuel. In contrast, male *Cpt1a*$_{AgRP}^{(-/-)}$ mice showed a slightly increase of *Atgl* and *Cpt1b* mRNA levels (Figure 19A). We also found an important induction of *Glut4* mRNA levels in BAT from female *Cpt1a*$_{AgRP}^{(-/-)}$ mice that is not observed in male *Cpt1a*$_{AgRP}^{(-/-)}$ mice (Figure 19A,B).

One important protein that provide thermogenic capacity to the BAT is UCP1. It uncouples respiration from ATP synthesis and therefore induces energy dissipation

in the form of heat. In order to confirm the BAT activation in *Cpt1a*$_{AgRP}^{(-/-)}$ mice, we also measured the mRNA levels of *Ucp1,* a highly expressed gene in thermogenic activated cells. While male *Cpt1a*$_{AgRP}^{(-/-)}$ mice reveal a slightly increase of *Ucp1* expression, no changes were observed in female mice. However, when we analysed the protein levels of the UCP1 by western blot we observed an increase in 50% and 25% of UCP1 protein levels in female and male *Cpt1a*$_{AgRP}$ mice respectively compared to their littermates mice (Figure 19C,D). We also found an increase in the thermogenic marker gene *Cidea* in female *Cpt1a*$_{AgRP}^{(-/-)}$ mice respect to their control littermates (Figure 19A,B), which is not observed in the male mice. We also found an enhanced expression of the *Mmp*2 in female *Cpt1a*$_{AgRP}^{(-/-)}$ mice respect to their control littermates suggesting an activation of BAT tissue remodelling.

These results suggest that that alterations in lipid metabolism in AgRP neurons cause an important activation of BAT thermogenesis mainly in female mice.

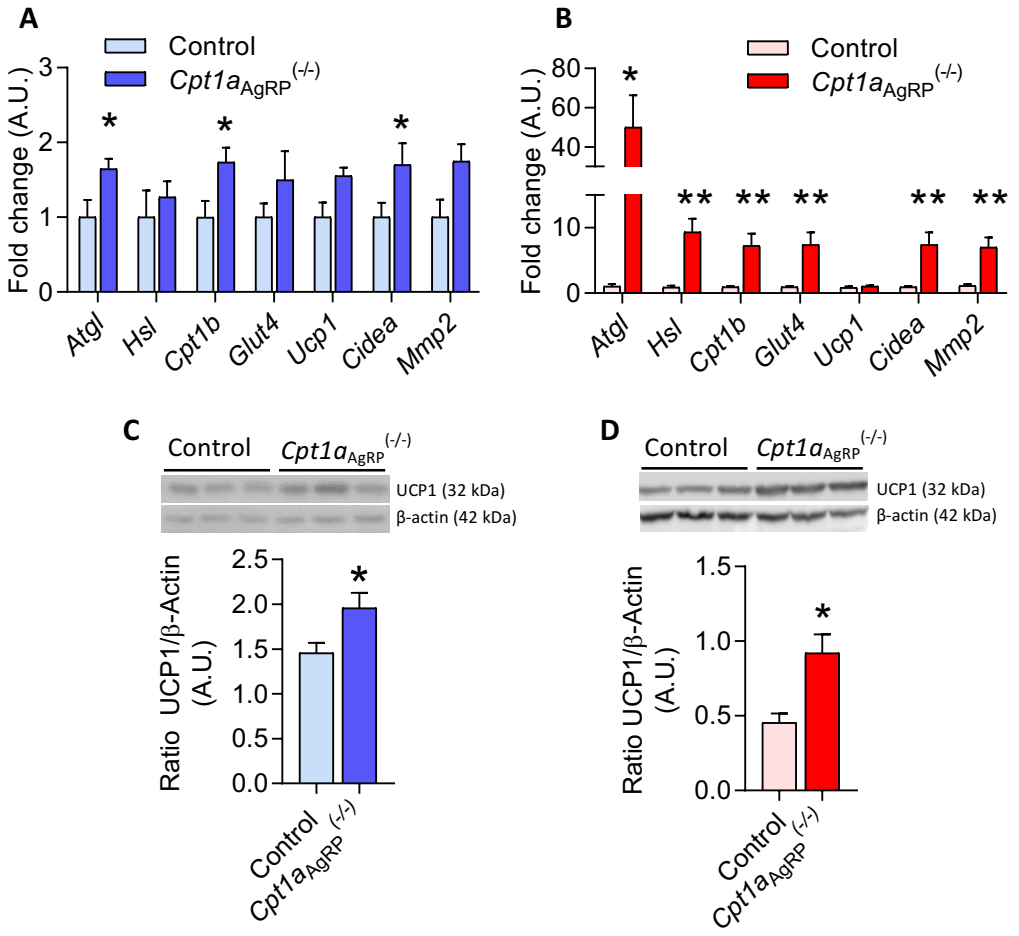

Figure 19. Deletion of *Cpt1a* in AgRP neurons upregulates thermogenic gene expression.
(A) Analysis by qRT PCR of the mRNA levels of *Atgl, hsl, Cpt1b, Glut4, Ucp1, Cidea* and *Mmp2* of male and (B) female. (C) Representative western blot of UCP1 protein from BAT (30 µg) in male and (D) female normalized by β-actin. Data are expressed as mean ± SEM; n = 8-10; Student's T, * $p < 0.05$, ** $p < 0.01$.

4.4.2. *Cpt1a* ablation in AgRP neurons reduces lipid content in white adipose tissue

It has been demonstrated a cross-talk between AgRP neurons and WAT. On the one hand, it has been repoted that leptin release from WAT inhibits hypothalamic *Npy* and *Agrp* gene expression [186] and on the other hand fasting and activation of AgRP affect fat depot quantity [96].

In order to evaluate whether lipid metabolism in AgRP neurons is at the same time a signal that modulates lipid depots in WAT we focus on the weight, morphological and expression analysis of iWAT and gWAT. We analysed WAT depots 3 months after tamoxifen induction.

Both male and female *Cpt1a*$_{AgRP}^{(-/-)}$ mice showed an important reduction of the tissue weight compared with their control littermates (Figure 20A,B). Our result shows that male *Cpt1a*$_{AgRP}^{(-/-)}$ mice reduces a 46.5% the gWAT weight (0.02353 ± 0.008962 *vs.* 0.01257 ± 0.004709, * $p < 0.05$) and female *Cpt1a*$_{AgRP}^{(-/-)}$ mice this reduction is 48.3% (0.02319 ± 0,01299 *vs.* 0.01120 ± 0.002996, * $p < 0.05$)

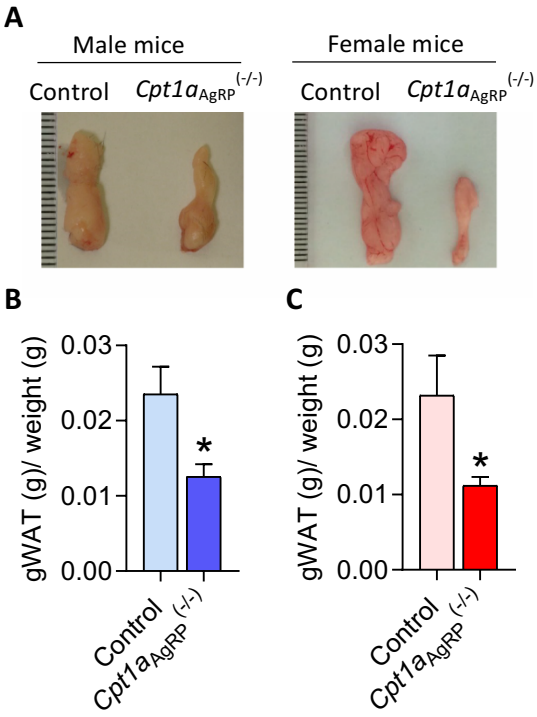

Figure 20. Deletion of *Cpt1a* in AgRP neurons reduces the fat mass in male and female mice. (A) Representative image of gonadal white adipose tissue (gWAT) from male and female mice. (B) gWAT weight in male and (C) female mice. Data are expressed as mean ± SEM; n = 8-10; Student's T, * $p < 0.05$.

To analyse adipocyte morphology, H&E staining was performed and the adipocyte area was measured using imageJ and adiposoft software (described in section 3.3.20). gWAT exhibits larger adipocyte areas compared with iWAT, 3,000 *vs.* 1,000 μm^2 in control male mice (Figure 21A,C) and 1,700 vs 1,450 μm^2 in control female mice (Figure 21E,G). The average of adipocyte area of gWAT from male $Cpt1a_{AgRP}^{(-/-)}$ mice was reduced by 70% respect to their control littermates (Figure 21A), whereas iWAT showed a reduction of 56.7% (Figure C). According to the frequency distribution of adipocyte areas, it was possible to observe that adipocyte from male $Cpt1a_{AgRP}^{(-/-)}$ mice tent to cluster in smaller areas compared with the control littermates both gWAT and iWAT (Figure 21B,D).

Similar results were observed in female mice. Female $Cpt1a_{AgRP}^{(-/-)}$ mice showed a reduction in the averages of adipocyte areas both in gWAT and iWAT. However, on the contrary with male $Cpt1a_{AgRP}^{(-/-)}$ mice, higher reduction was observed in iWAT, since female $Cpt1a_{AgRP}^{(-/-)}$ mice reveal a reduction of 76% of the adipocyte areas (Figure 20E,G). This result was consistent with the analysis of the frequency distribution, since higher frequency of smaller adipocytes (<500 μm^2) correspond to the 80% of the tissue (Figure 20F,H).

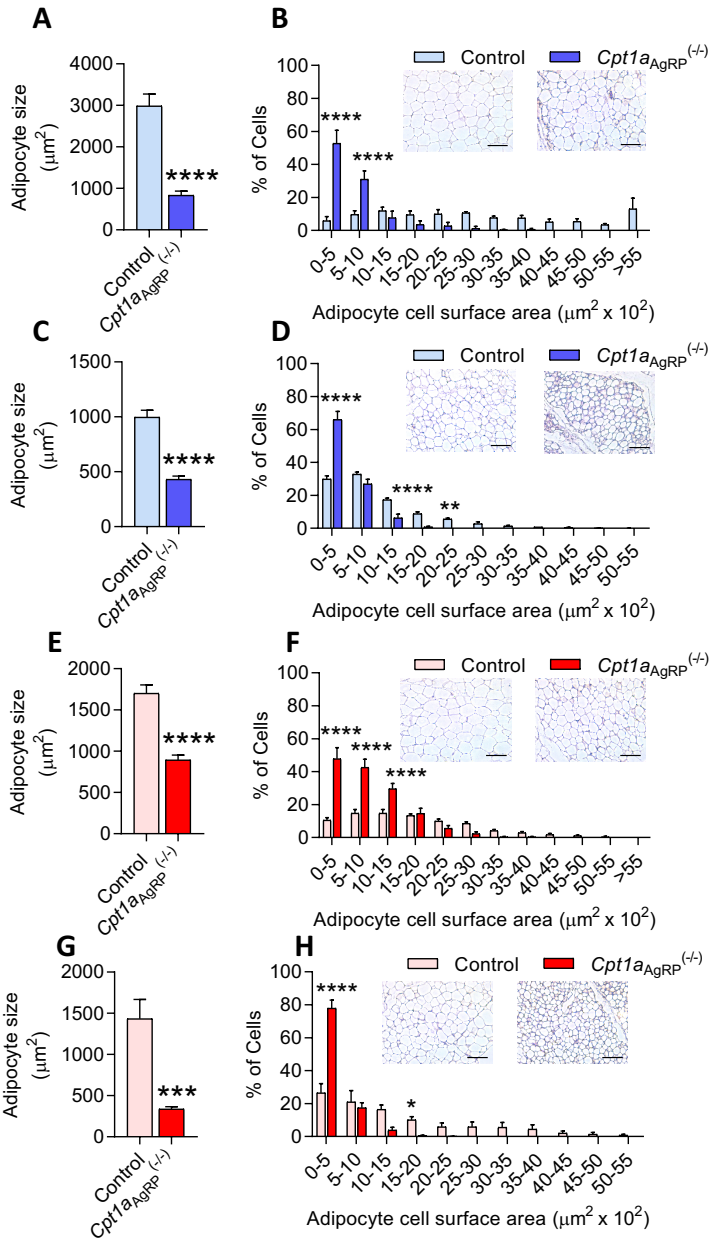

Figure 21. Deletion of *Cpt1a* in AgRP neurons reduces the lipid area in WAT.
(A) Average of adipocyte area of gonadal white adipose tissue (gWAT) in male and (E) female mice. (B) Morphometric analysis of adipocyte area distribution in gWAT of male and (F) female mice. (C) Average of adipocyte area of inguinal white adipose tissue (iWAT) in male and (G) female mice. (D) Morphometric analysis of adipocyte area distribution in iWAT of male and (H) female mice. Data are expressed as mean ± SEM; n = 8-10; Data were analyzed by 2-way repeated measures ANOVA followed by Šidák's post hoc test. * $p < 0.05$, ** $p < 0.01$, *** $p < 0.001$, ****$p < 0.0001$, (B, D, F, H) and Student's T, *** $p < 0.001$, **** $p < 0.0001$.

We next assessed gene expression of different key regulators of adipocyte physiology by qRT-PCR in gWAT and iWAT. The mRNA analysis in gWAT reveals that male *Cpt1a*$_{AgRP}^{(-/-)}$ mice have an increased of *Atgl* (lipolysis), *Vegfa* (angiogenesis), *Mmp* (matrix remodeling) gene expression with no changes of *Il-6* (inflammation) and *Leptin.* On the other hand, female *Cpt1a*$_{AgRP}^{(-/-)}$ mice shown a reduction of *Leptin* gene expression with no changes in the other genes analysed (Figure 22A,B).

The same analysis in iWAT reveals that male *Cpt1a*$_{AgRP}^{(-/-)}$ mice increased the mRNA level of *Ucp1* and tended to increase the *Atgl* gene expression with no changes in *leptin*, *Cpt1a* and *Il-6*. However female *Cpt1a*$_{AgRP}^{(-/-)}$ mice showed an statistical increase of *Atgl*, *Ucp1* with no changes in *leptin* and *Cpt1a* levels*. Il-6* exert a statistical reduction in this tissue (Figure 22D,E).

Interestingly, the increase of *Ucp1* mRNA levels in iWAT both male and female *Cpt1a*$_{AgRP}^{(-/-)}$ suggest a browning induction and a conversion of white adipocytes into beige adipocytes. This result is consistent with the presence of multilocular adipocyte observed in H&E analisis (Figure 22C).

All these results together showed that *Cpt1a* ablation in AgRP neurons impact in the lipid content of WAT by reducing the lipid droplet content and inducing browning.

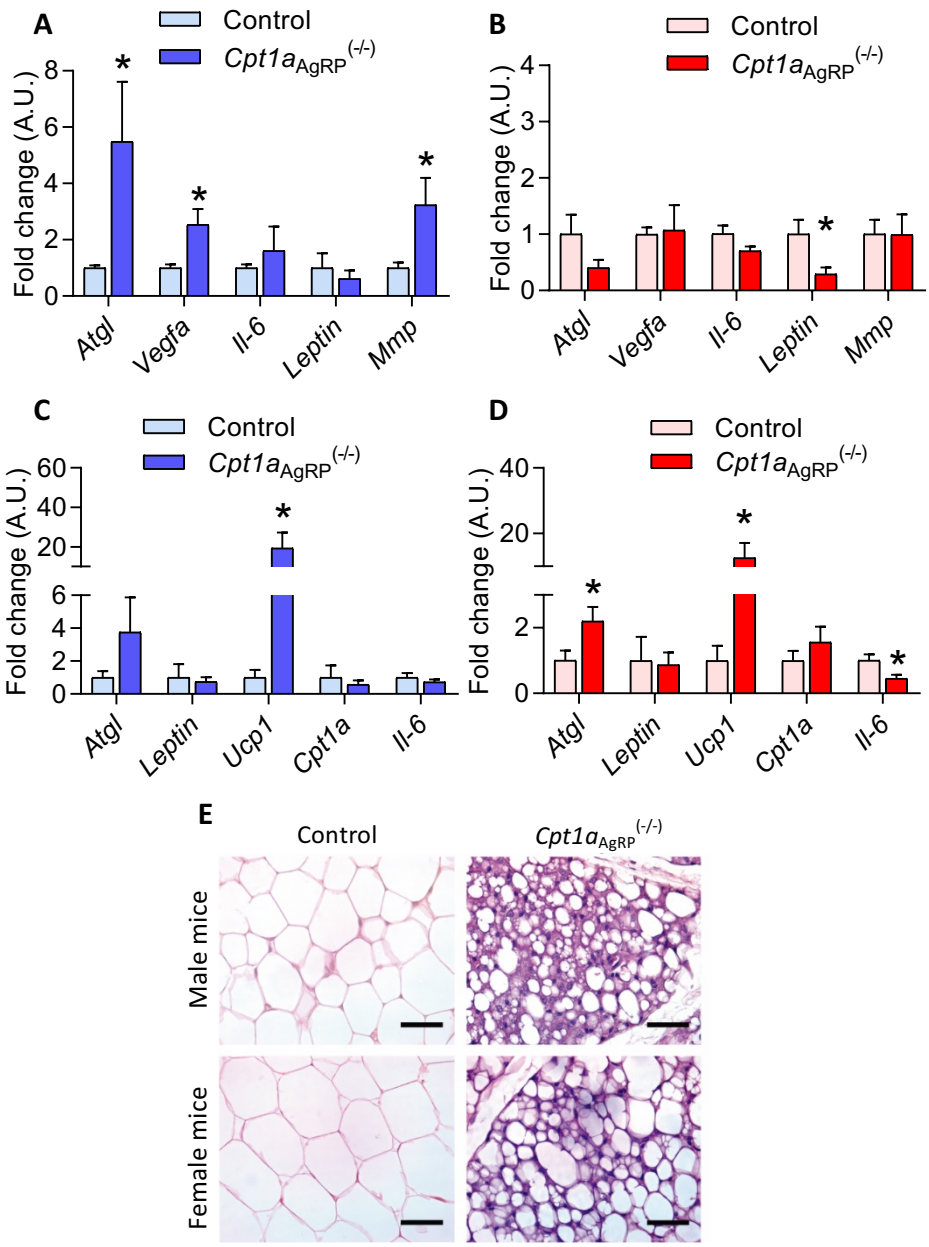

Figure 22. Deletion of *Cpt1a* in AgRP neurons stimulate browning in inguinal WAT.
(A) Analysis by qRT-PCR of *Atgl, Vegfa, Il-6, Leptin* and *Mmp genes* in gonadal white adipose tissue (gWAT) of male and (B) female mice. (C) mRNA levels of *Atgl, Leptin, Ucp1, Cpt1a* and *Il-6* in iWAT of male and (D) female mice. (E) Representative images of inguinal white adipose tissue (iWAT) sections stained with H&E in male and female mice. Scale bar 50 µm. (magnification 40x). Data are expressed as mean ± SEM. N = 6; Student's T, * $p < 0.05$.

4.4.3. *Cpt1a ablation in AgRP neurons increases the expression of Cpt1a in liver*

It has been extensively demonstrated that AgRP expressing neurons in the hypothalamus contribute to the hepatic physiology, but little is known whether lipid metabolism in these neurons is necessary to modulate the hypothalamus-liver axis. The histopathologic analysis of the liver was also performed at 3 months after tamoxifen induction. Liver from male and female *Cpt1a*$_{AgRP}^{(-/-)}$ mice did not reveal histological disruption (Figure 23A) and no differences were observed in the tissue weigh normalized by the body weight respect to the control littermates (Figure 23B,D). In order to analyse metabolic alterations in liver we measure mRNA levels of the key enzymes involved in lipid and glucose metabolic pathways. Both male and female of *Cpt1a*$_{AgRP}^{(-/-)}$ mice showed an increase in *Cpt1a* liver expression (Figure 23C,E) suggesting an enhancement of FAO in the liver. Only male *Cpt1a*$_{AgRP}^{(-/-)}$ mice increased of *Ucp2* expression in liver respect to their littermates (Figure 23C). To assess the hepatic glucose production, *Pepck* and *G6p* gene expression were measured. Interestingly both enzymes were significantly higher in *Cpt1a*$_{AgRP}^{(-/-)}$ male mice (Figure 23C) and the same tendency was observed in female *Cpt1a*$_{AgRP}^{(-/-)}$ mice (Figure 23E) suggesting an increased gluconeogenesis.

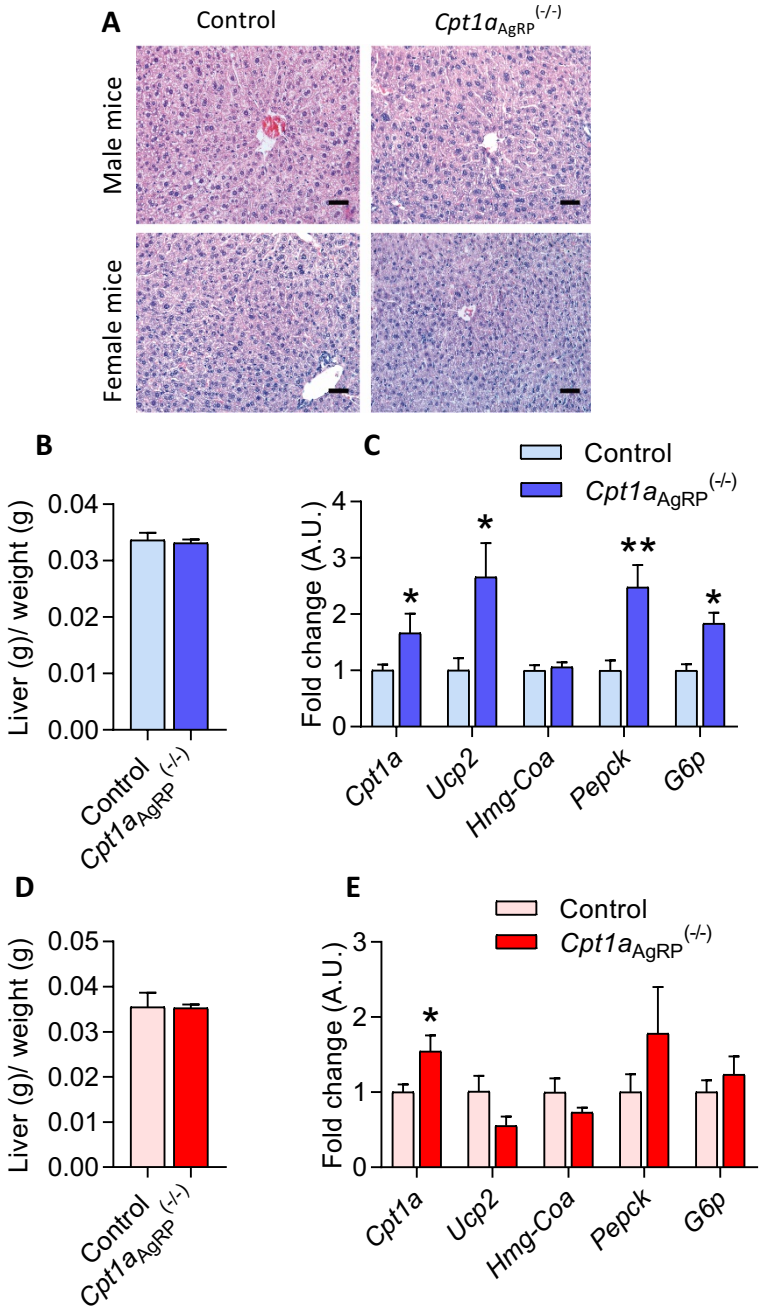

Figure 23. Deletion of *Cpt1a* in AgRP neurons upregulates *Cpt1a* expression in liver.
(A) Representative hematoxylin and eosin (H&E) staining of livers from male and female mice. Scale bar 50 µm (magnification 20x). (B) Liver weigh of male and (D) female mice. (C) Analysis by qRT-PCR of *Cpt1a, Ucp2, Hmg-Coa, Pepck* and *G6p* genes of male and (E) female. Data are expressed as mean ± SEM; n = 8-10; Student's T, * $p < 0.05$, ** $p < 0.01$.

4.4.4. *Cpt1a* ablation in AgRP neurons does not induce histological disturbances in pancreas, testis and ovaries

Other tissues analysed in *Cpt1a*$_{AgRP}^{(-/-)}$ mice were pancreas, testis and ovaries. We did not found histological changes in *Cpt1a*$_{AgRP}^{(-/-)}$ mice respect to their control littermates (Figure 24).

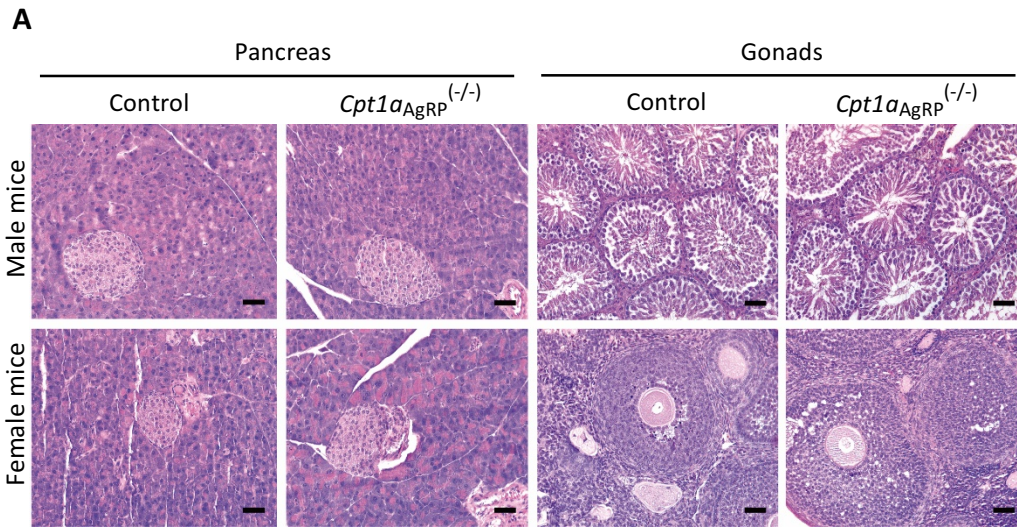

Figure 24. Deletion of *Cpt1a* in AgRP neurons does not affect peripheral tissues.
(A) Representative hematoxylin and eosin (H&E) staining of pancreas and testis from male mice (upper panel) and pancreas and ovaries from female mice (Lower pannel). Scale bar 50 µm (magnification 20x); n = 8-10.

4.5. CPT1A of AgRP neurons is involved in the thirst behaviour through CPT1A

Hunger and thirst are defined as sensations that promote food and water ingestion respectively. Despite AgRP neurons have been always associated to the solid food consumption, little is known if this hunger-neurons could be involved in fluid consumption or fluid balance.

The first finding that pushed us to study the fluid balance was the evident increase of water intake in *Cpt1a*$_{AgRP}^{(-/-)}$ mice. First, we measured the amount of water

consumed during 24 hours in *Cpt1a*$_{AgRP}^{(-/-)}$ mice compared with their control littermates 1 month after tamoxifen induction (when the phenotype became evident). While male *Cpt1a*$_{AgRP}^{(-/-)}$ mice mice increases 51.17% the water intake compared with their control littermates, female mice increase a 52.83% (Figure 25A,B) .

We also observed a clear increase of the urine output measured at 24 hours using metabolic cages. Male and female *Cpt1a*$_{AgRP}^{(-/-)}$ mice showed 4.23 and 4.25-fold increase of urine volumes respectively, suggesting a compensatory homeostasis in response to the increase of drinking in *Cpt1a*$_{AgRP}^{(-/-)}$ mice (Figure 25C,D).

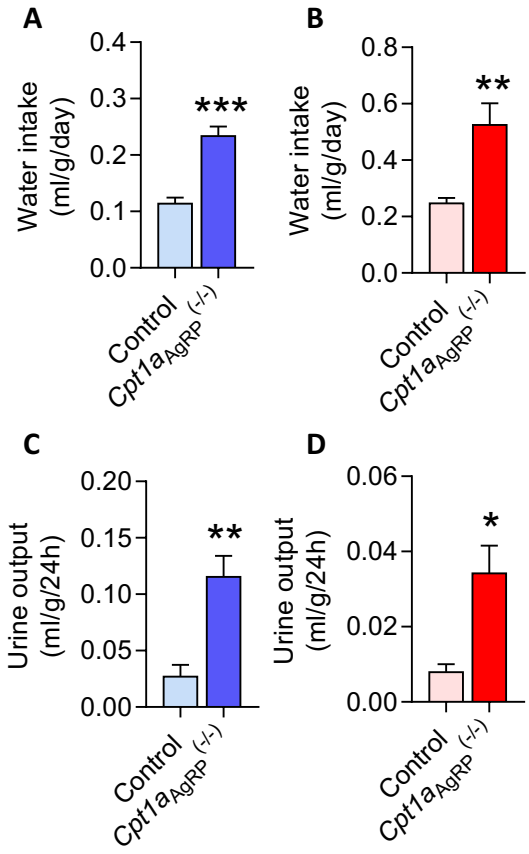

Figure 25. Mice lacking *Cpt1a* in AgRP neurons display an increase of water consumption.
(A) Total amount of 24 hours of water intake in male and (B) female. (C) 24 hours of urine collection in male and (D) female. Data are expressed as mean ± SEM; n = 5-7; Student's T, * $p < 0.05$, ** $p < 0.01$, *** $p < 0.001$.

4.6. *Cpt1a* deletion in AgRP neurons does not induce diabetes in *Cpt1a*$_{AgRP}^{(-/-)}$ mice

Since the increase of the urinary frequency (polyuria) and thirst (polydipsia) are two of the three classical symptoms of diabetes we determine whether *Cpt1a*$_{AgRP}^{(-/-)}$ mice were developing this disease. 2 month after tamoxifen induction a GTT was performed. Mice were ON fasted and the basal insulin level was measured. Glucose was monitored during 2 hours after an ip glucose administration. Male *Cpt1a*$_{AgRP}^{(-/-)}$ mice exhibit lower levels of glucose at 60 and 90 min than their control littermates suggesting an improvement of the glucose tolerance (Figure 26A). On the contrary no differences were observed in the GTT of female mice, even female *Cpt1a*$_{AgRP}^{(-/-)}$ mice showed a lower levels of glucose at 15 min compared with their littermates (Figure 26D). These results were accompanied with no changes in the basal insulin level in both male and female mice (Figure 26B,E).

In order to confirm the absence of diabetes in *Cpt1a*$_{AgRP}^{(-/-)}$ mice, the glucose level in urine was measured. An increase of glucose in the urine, also referred as glycosuria, indicates an impaired renal proximal tubular reabsorption due to higher levels of circulating plasmatic glucose. Results showed no statistical significant differences of urine glucose levels independent of the gender between *Cpt1a*$_{AgRP}^{(-/-)}$ mice and their control littermates, reinforcing the absence of diabetes (Figure 26C,F). In addition, the histological analysis of kidney did not reveal apparent changes of the cortex and medullary regions (Figure 26G).

Altogether these results suggest that CPT1A in AgRP neurons do not induce a diabetic state despite the polyuria and polydipsia detected.

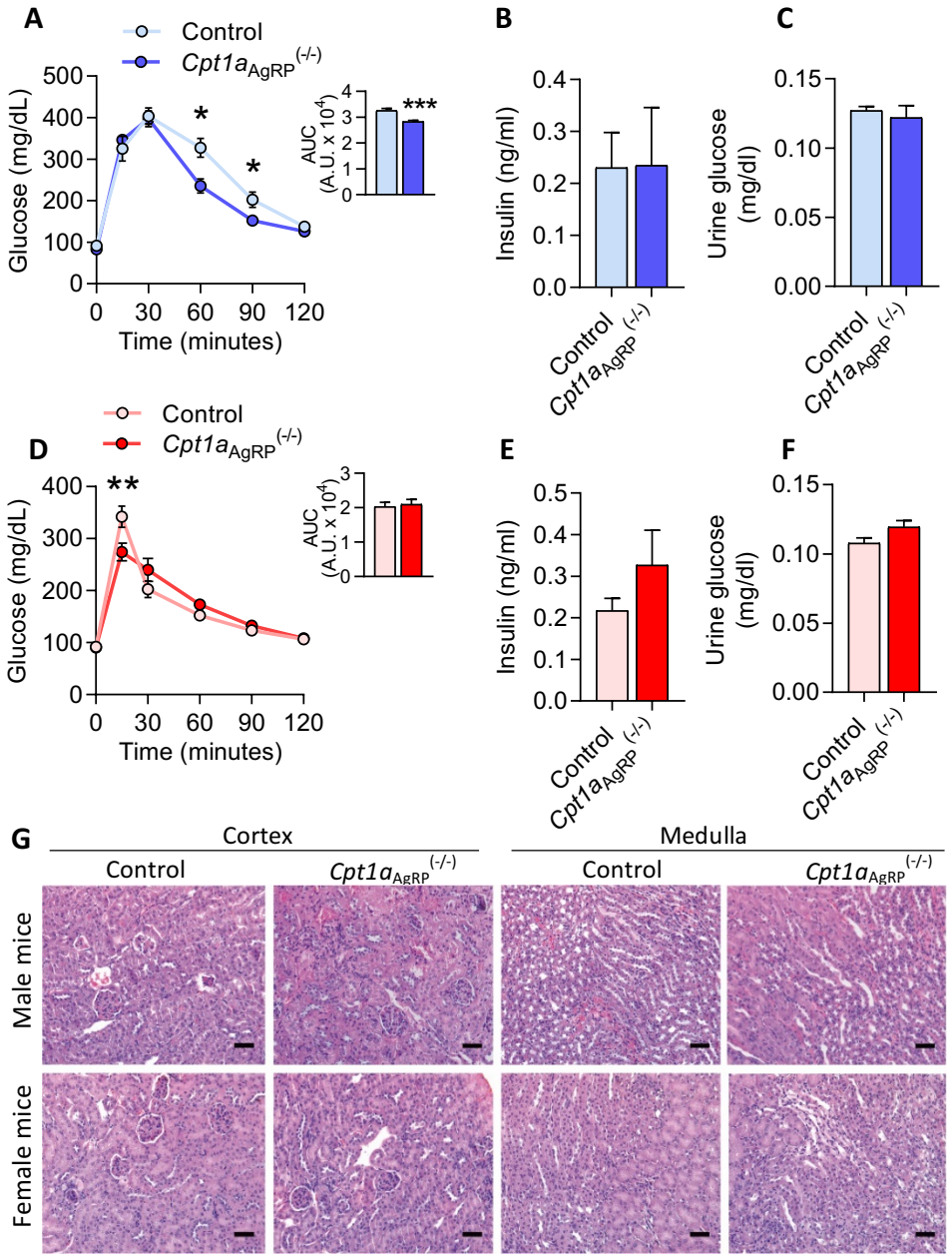

Figure 26. *Cpt1a* deletion in AgRP neurons does not induce a diabetic state.
(A) Glucose tolerance test (GTT) and AUC (area under the curve) quantification (right) in male and (D) female mice. (B) Fasting insulin levels in male and (E) female mice. (C) Urinary glucose levels in male and (F) female mice. (G) Representative hematoxylin and eosin (H&E) staining section of the cortex (left panel) and medulla (right panel) of the kidney from male and female mice. Scale bar 50 µm (magnification 20x). Data are expressed as mean ± SEM; n=8-10 (A, D); n = 5-8 (B,C,E,F); Data were analyzed by 2-way repeated measures ANOVA followed by Šidák's post hoc test. * $p < 0.05$, ** $p < 0.01$ (A,D).

4.7. *Cpt1a* deletion in AgRP neurons influences the circulating level of vasopressin (VP)/ antidiuretic hormone (ADH).

In order to gain deep into the increase of water consumption triggered by the *Cpt1a* deletion in AgRP neurons we measured the VP/ADH hormone which is an important regulator of the fluid balance. VP/ADH is a nonapeptide hormone synthesized in magnocellular neurones cell bodies of the PVN and SO nuclei of the posterior hypothalamus. It is released from the posterior pituitary in response to plasma osmolality and volume changes. Due to the increase of water consumption and the concomitant increase of urine output, VP/ADH was measured at basal state. Plasma samples were obtained from $Cpt1a_{AgRP}^{(-/-)}$ and control littermates mice after 3-months of tamoxifen induction and the circulating levels of VP/ADH hormone was evaluated.

We observed different AV/ADH blood levels depending on the gender. Male mice have higher blood levels of the hormone than female mice (410.2 ± 28.97 pg/ml *vs.* 227.7 ± 21.24 pg/ml) (Figure 27). In addition, we observed a reduction of VP/ADH in $Cpt1a_{AgRP}^{(-/-)}$ independently of gender. While male $Cpt1a_{AgRP}^{(-/-)}$ mice showed a reduction of 25% of circulating levels of AV/ADH the reduction in female $Cpt1a_{AgRP}^{(-/-)}$ mice was higher and raised to 33.6% suggesting a major impairment in female $Cpt1a_{AgRP}^{(-/-)}$ mice to reabsorb water at the kidney than in male.

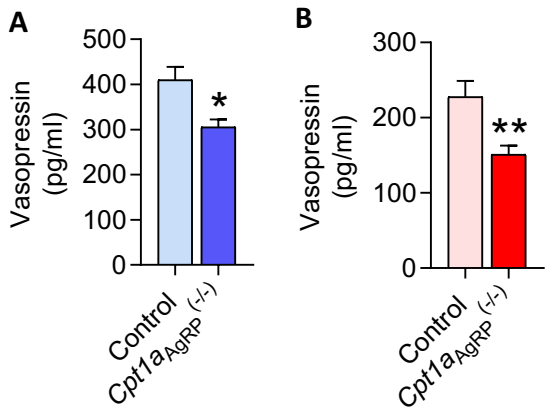

Figure 27. Deletion of *Cpt1a* in AgRP neurons reduces the plasmatic level of VP/ADH.
(A) Plasmatic level of vasopressin hormone in male and (B) female mice. Data are expressed as mean ± SEM; n = 6-9; Student's T, * $p < 0.05$, ** $p < 0.01$.

4.8. Effect of *Cpt1a* deletion in AgRP neurons on serum and urine osmolarity

Since osmolality is one of the most important stimuli to the VP/ADH hormone release, we measured this variable in order to elucidate whether $Cpt1a_{AgRP}^{(-/-)}$ had an impairment in the osmolality regulation. Thus, animals were keep in *ad libitum* access to food and water consumption, then we challenge the mice to 24 hours of water restriction, and the serum and urinary osmolality were measured. Serum and urine samples were collected from $Cpt1a_{AgRP}^{(-/-)}$ and control littermates mice with *ad libitum* access to food and water and under 24 hours of water restriction with *ad libitum* access to food.

Serum osmolality did not reveal statistical significant changes in *ad libitum* access to water (Figure 28A,B). When the mice were challenged to 24 hours of water restriction we did not find changes in the serum osmolality (Figure 28A,B) suggesting that $Cpt1a_{AgRP}^{(-/-)}$ mice were able to maintain the serum osmolality.

Analysis of the urinary osmolality reveals that male and female $Cpt1a_{AgRP}^{(-/-)}$ mice have lower osmolality compared with the control littermates in *ad libitum* access

to water suggesting an impairment in the urinary concentration. Under the condition of 24 hours of water restriction mice try to concentrate the quantity of urine produced to increase the osmolality. Although male *Cpt1a*$_{AgRP}^{(-/-)}$ mice increased the osmolality, only 3 samples were possible to obtain in this condition. No urinary samples were obtained from female mice under 24 hours of water restriction, thus it was not possible to analyse the urine osmolality in female mice under this condition.

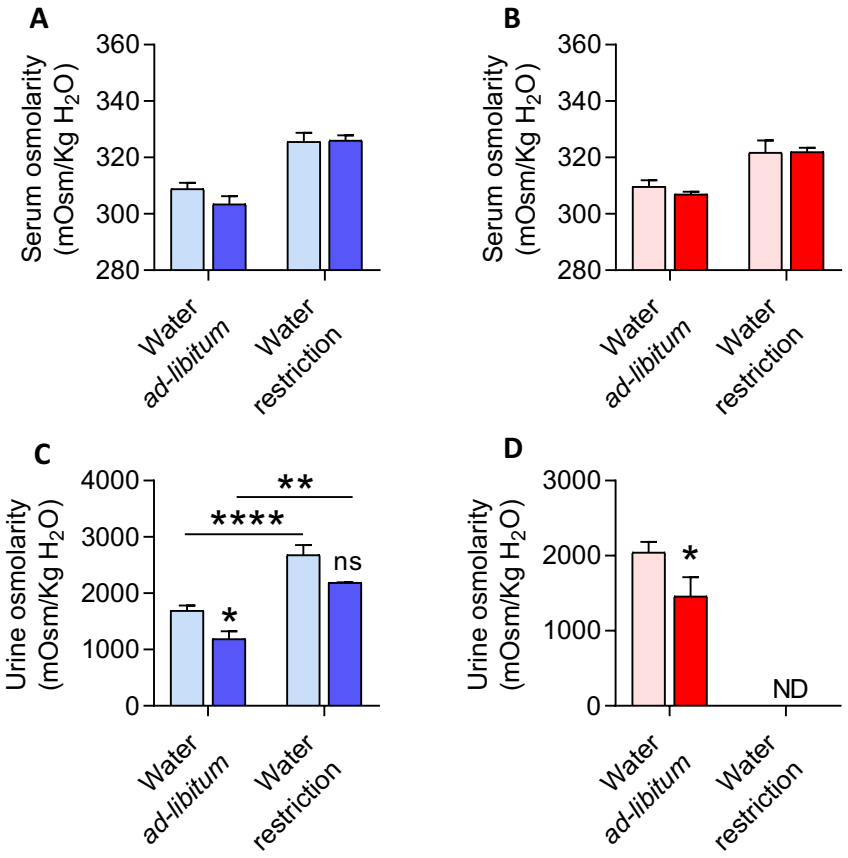

Figure 28. Effect of *cpt1a* deletion in AgRP neurons on serum and urinary osmolality.
(A) Analysis of the serum osmolality of male and (B) female mice under 24 hours of water restriction and *ad libitum* access to water. (C) Analysis of the urine osmolarity from male (D) and female mice under 24 hours of water restriction and *ad libitum* access to water. ns, no significant, ND: non-detected. Data are expressed as mean ± SEM; n = 6-10; Student's T, * $p < 0.05$, ** $p < 0.01$, **** $p < 0.0001$.

4.9. Effect of *Cpt1a* deletion in AgRP neurons on thirst induced-SFO activation

To gain greater depth in fluid homeostasis we next focus on neuronal control of fluid balance. SFO is one of the CVOs implicated in the regulation of body fluid (Figure 29A). It exhibits a heterogeneous population of neurons that have been experimentally associated to the water consumption or water satiety. Then, we explore the SFO activation by the detection of cFos protein using immunofluorescence. Animals were challenged to 24 hours of water restriction and the cFos in SFO was evaluated. The experiment was done 1 month after tamoxifen induction in female mice. cFos positive cells were counted per nucleus in SFO area.

No cFos positive neurons were observed *ad libitum* access to water, neither in control or in $Cpt1a_{AgRP}^{(-/-)}$ mice (Figure 29B top panel). This is an interesting observation due to $Cpt1a_{AgRP}^{(-/-)}$ showed an increase of water consumption in this condition. When mice were challenged to 24 hours of water restriction, SFO from control mice exhibit an increase of SFO positive neurons. Surprisingly, no activation was observed in $Cpt1a_{AgRP}^{(-/-)}$ mice suggesting that *Cpt1a* in AgRP neurons could be involved in the regulation of SFO neurons (Figure 29B bottom panel, C).

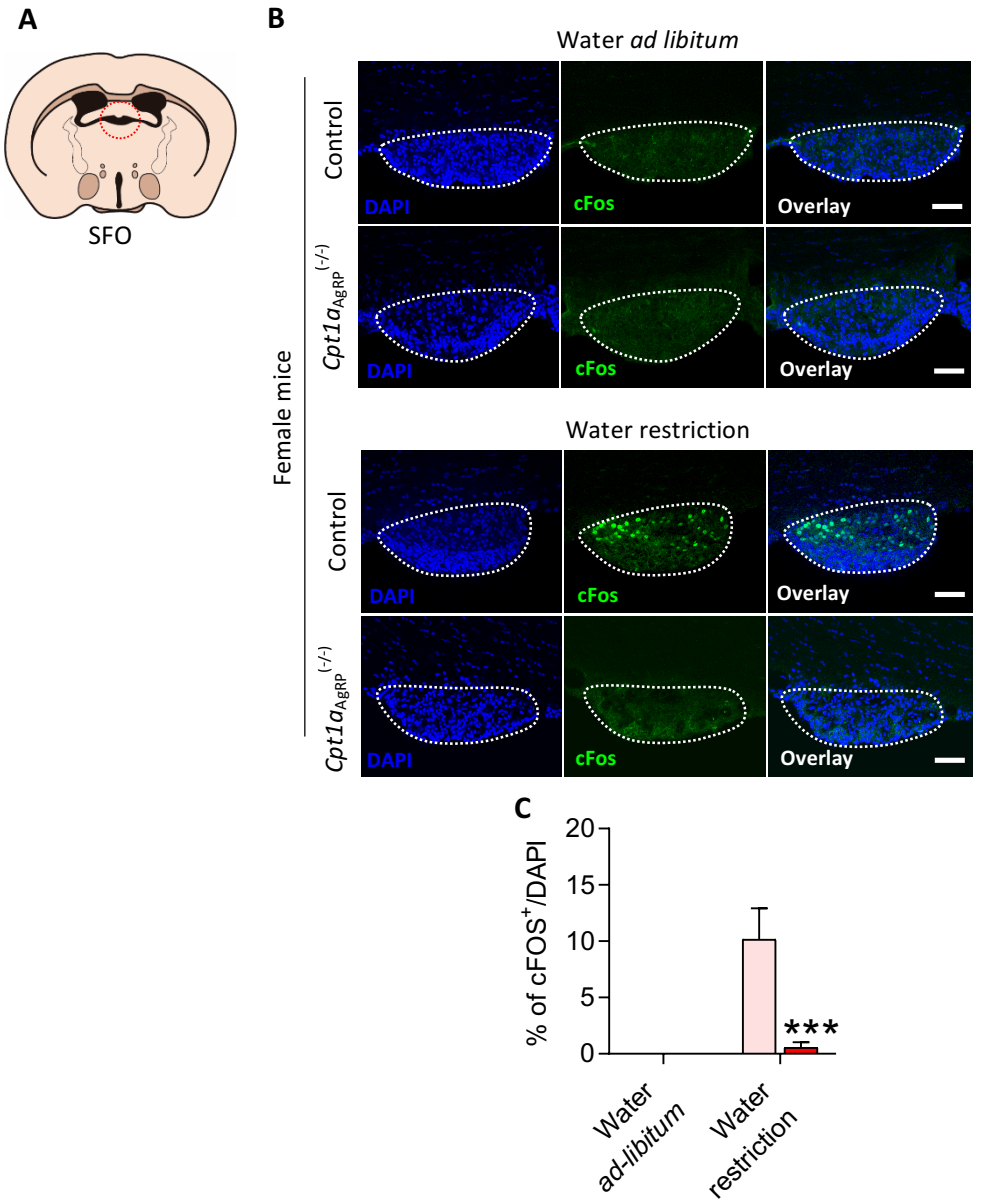

Figure 29. Analysis of cFos activation in mice lacking *Cpt1a* in AgRP neurons
(A) Scheme of SFO area analyzed. (B) Representative section of cFos activation in the SFO of mice with water *ad libitum* (Upper panel) and animals restricted for 24 hours (Lower panel). Dashed lines indicate the SFO area analyzed. (C) Quantification of cFos positive/DAPI nuclei in the SFO. Data are expressed as mean ± SEM; n = 3; Student's T, * $p < 0.05$, Scale bar 50 µm.

4.10. Effect of *Cpt1a* deletion in AgRP neurons on thirst induced-PVN activation

To further explore the neurological mechanisms that underlie the control of thirst behavior, cFos immunofluorescense was used to detect the pattern of brain activity under *ad libitum* access to water and 24 hours of water restriction. Brain sections from PVN were analyzed for cFos immunolabeling due to VP^{+} neurons are located in this hypothalamic nucleus. Water intake was monitored during the experiment (Figure 30A,D).

No statistical differences were observed in cFos activation of PVN section in *ad libitum* access to water both in male and female mice (Figure 30B, left panels). This is an interesting observation due to male and female $Cpt1a_{AgRP}^{(-/-)}$ mice showed a 3-fold increase of the water intake with no signs of cFos activation in PVN section under free access to water (Figure 30A,D). Furthermore, cFos activation was importantly decreased in male and female $Cpt1a_{AgRP}^{(-/-)}$ mice in water deprivation compared with their control littermates (265.5 ± 43.9 *vs.* 115.8 ± 53.20 cFos/PVN section, * $p < 0.05$ in male and 203 ± 43.14 *vs.* 81.33 ± 10.26 cFos/PVN section, ** $p < 0.01$ in female mice) (Figure 30C,E)

In short, this result suggests that AgRP lacking $Cpt1a_{AgRP}^{(-/-)}$ mice impair the PVN activation induced by thirst.

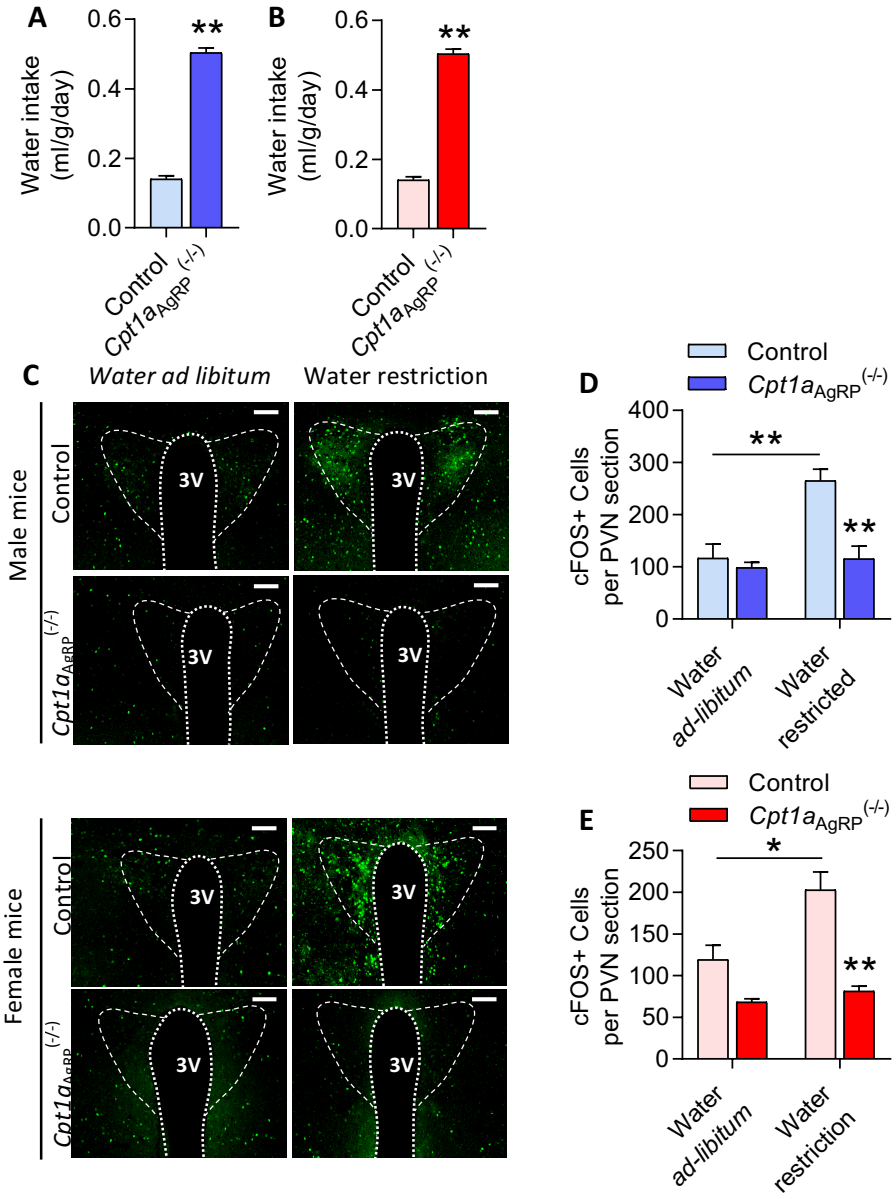

Figure 30. The deletion of *Cpt1a* in AgRP neurons impairs the PVN activation induced by water restriction

(A) Water consumption *ad libitum* in male and (B) female mice. (C) Representative cFos activation in the paraventricular nucleus (PVN) of mice with water *ad libitum* (left panel) and animals restricted for 24 hours (right panel). Dashed lines indicate the PVN area analyzed. (D) Quantification of cfos positive per PVN section in male and (E) female mice. Data are expressed as mean ± SEM; n = 3-4; Student's T, * $p < 0.05$, Scale bar 50 µm.

Next we wanted to elucidate whether an acute increase in the plasma osmolality could restore the activation of PVN nucleus in *Cpt1a*$_{AgRP}^{(-/-)}$ mice. Salt induced-PVN activation was performed in female mice by an ip injection of NaCl and mannitol. After 2 hours of water restriction animals were perfused and the IF was performed. Female *Cpt1a*$_{AgRP}^{(-/-)}$ mice respond to this acute change of the plasma osmolality by increasing the cFos signal in PVN section (Figure 31A,B).

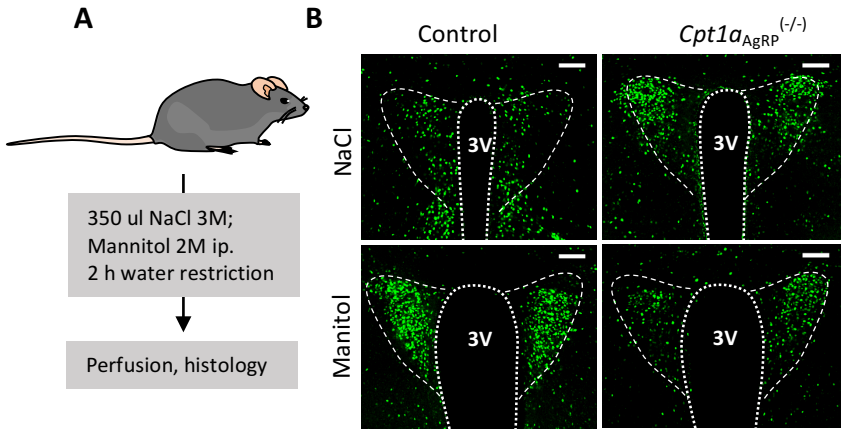

Figure 31. Effect of hyperosmolar solution injection in female mice lacking *Cpt1a* in AgRP neurons
(A) Experimental setting of hyperosmolar sodium chloride (NaCl) and mannitol injection. Animals get either 3 M NaCl or 2 M mannitol by intraperitoneally injection (350 µl/20 g mouse). (B) cFos analysis 2 hours after NaCl and mannitol injection. Dashed lines indicate PVN section analyzed. n=2

4.11. CPT1A is necessary to maintain AgRP neuronal homeostasis

It is has been demonstrated that CPT1A is necessary to maintain the cell viability. While deletion of *Cpt1a* in naive T cells reduced their ability to oxidize and had a negative effect on T cell viability and proliferation [187] other studies have demonstrated that lack of *Cpt1a* in tumoral cells reduces their survival.

Although no evidence has been reported showing the effect of *Cpt1a* deletion in neuronal cell we first evaluate whether the lack of CPT1A affects the number of AgRP neurons. Thus, we first measured the number of AgRP neurons along the anterior-posterior axis of the ARC nucleus. To accomplish this, we injected AAVs that

conditionally expresses mCherry in the presence Cre-recombinase (FLEX switch) by stereotaxis into the arcuate nucleus of control mice (AgRP-CreER^{T2} mice) or mice that lack *Cpt1a* in AgRP neurons (*Cpt1a*$_{AgRP}^{(-/-)}$ mice). Female mice were analyzed 1 month after tamoxifen induction.

Importantly, no differences in the number of AgRP neurons was observed in the section selected from anterior, medial and posterior ARC (Figure 32A,B). When we analyzed the morphology of AgRP neurons by confocal microscopy we observed an alteration of dendritic morphology in AgRP-*Cpt1a* deleted neurons (Figure 32C). The dendritic spine examination revealed that AgRP control neurons have abundant dendritic spines whereas AgRP neurons lacking *Cpt1a* exert a reduction in the number of dendritic spines per 50 µm of dendrons (Figure 32D,E).

Finally, due to PVN is an important brain area controlling food and water consumption and sympathetic outflow we studied the projection AgRP → PVN. To study this, we administrated into the ARC nucleus adeno-associated virus that conditionally expresses synapthphysin-GFP in order to label the pre-synaptic area of AgRP neurons (Figure 32F). We observed a 50% less intensity of synapthosphyisin in the PVN section analyzed (13.5 *vs.* 5.5, U.A., * $p < 0.05$) (Figure 32G,H) indicating that *Cpt1a* deletion in AgRP neurons alters the synapsis and reduces the projections to the PVN nucleus.

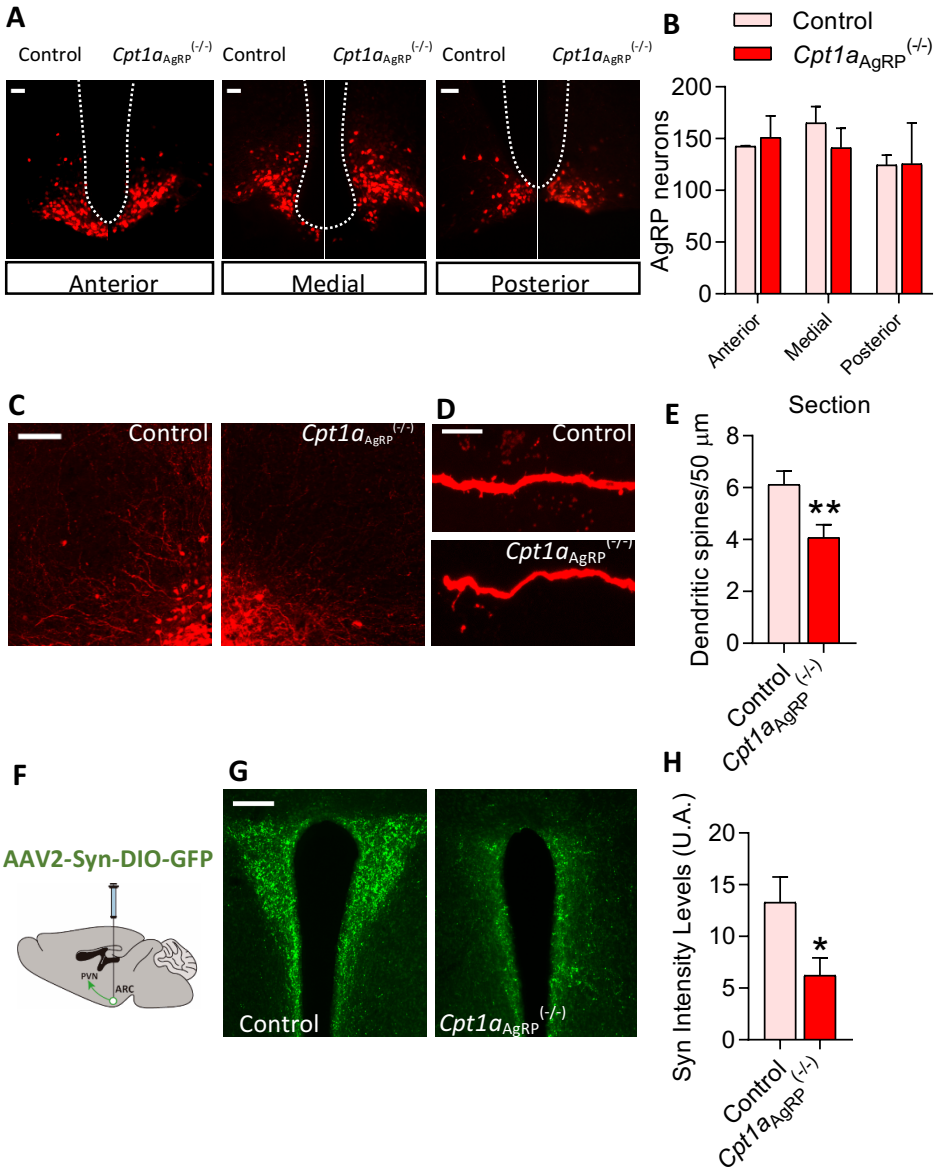

Figure 32. AgRP neurons lacking *Cpt1a* have impaired dendritic morphology and the projection to PVN.

(A) Representative images of AgRP neurons along the anterior-posterior axis of the ARC. (B) Quantification of AgRP neurons in anterior, medial and posterior section of ARC nucleus. (C) Representative microphotography of anterior ARC section. (D) Representative fluorescence microphotograph of dendrites of AgRP neurons. (E) Quantification of dendritic spines number per 50 µm of dendrites of AgRP neurons. (F) Scheme of Syn-GFP administration in ARC and the projection to the paraventricular nucleus (PVN). (G) Representative fluorescence microphotography of AgRP-syn projection to the PVN nucleus. (H) Syn-GFP intensity level quantification by imageJ. Data are expressed as mean ± SEM; n = 3; Student's T, * $p < 0.05$, ** $p < 0.01$. Scale bar 25 µm (A), 100 µm (C,G), 10 µm (D).

4.12. Enrichment of transcripts from specific AgRP Populations.

In order to isolate the specific transcript of AgRP neurons, the RiboTag mouse was crossed with *Cpt1a*$_{AgRP}^{(-/-)}$ mice (Section 3.3.1). mRNAs associated with tagged polysomes were immunoprecipitated from RPL22^{HA}-expressing cells of ARC nucleus.

We determined the enrichment of AgRP mRNAs from AgRP neurons in the immunoprecipitate of *Cpt1*a$_{AgRP}^{(+/+)}$:RiboTag mice according to the section 3.3.21. A 23-fold enrichment of AgRP mRNAs expressed in AgRP neurons of the ARC was observed compared to the input of isolated RNA. Conversely, no increase of *Pomc* and *Adh1* mRNAs, as a marker of POMC neurons and astrocytes respectively, were observed (Figure 33A). In line with this result, we observed a robust expression of RPL22^{HA} protein limited to the ARC nucleus, where AgRP neurons are located (Figure 33B). No other signal was detected in the neighborhood nuclei of the hypothalamus.

Once the *Cpt1*a$_{AgRP}^{(-/-)}$:RiboTag mice model was validated we compared the level of *Vgat* mRNA in control mice (*Cpt1*a$_{AgRP}^{(+/+)}$:RiboTag) *vs.* mice lacking *Cpt1a* in AgRP neurons (*Cpt1*a$_{AgRP}^{(-/-)}$:RiboTag). We observed that *Cpt1*a$_{AgRP}^{(-/-)}$:RiboTag mice tended to reduce the level of *Vgat* mRNAs from specific-AgRP neurons (Figure 33C). The involvement of CPT1A in the GABA metabolism will be studied in the future with the differential transcriptome sequencing analysis between *Cpt1*a$_{AgRP}^{(-/-)}$:RiboTag mice and control mice.

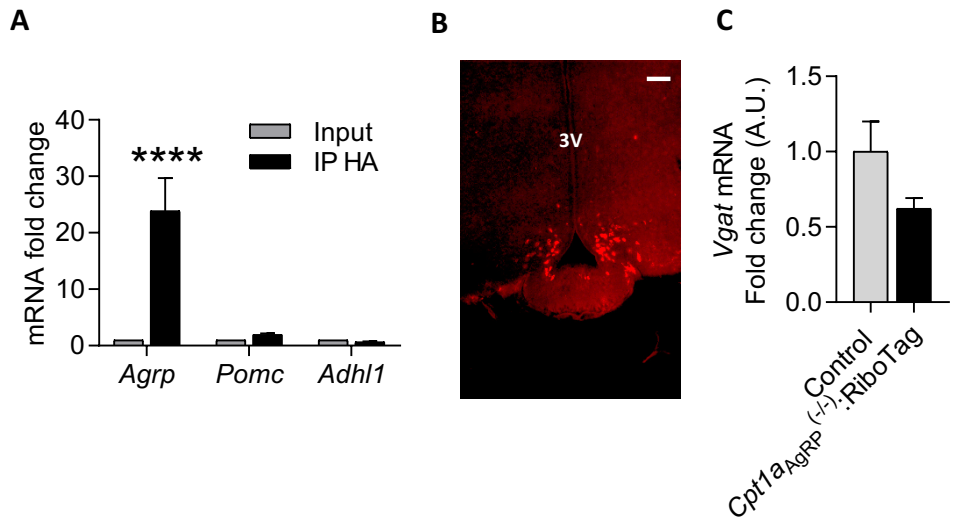

Figure 33. Validation of the *Cpt1a*$_{AgRP}^{(-/-)}$:RiboTag mice model.
(A) qRT-PCR analysis of transcripts expressed in AgRP neurons after immunoprecipitation (IP) of polysomes from ARC lysates. Total RNA was isolated from input and anti-HA pellets. All cell-specific marker genes and control genes not expressed in the target cells were normalized by *Gapdh* mRNA levels using the ΔΔCt method. The immunoprecipitated RNA samples were compared to the input sample in each case. 0.27 ng of cDNA were used to analyze the mRNA levels by qRT PCR. The specific mRNA levels analyzed were: *Agrp, Pomc* and *Adh1*. (B) Representative image of AgRP neurons tagged with anti-HA antibody. (C) *Vgat* mRNA levels in control and *Cpt1a*$_{AgRP}^{(-/-)}$:RiboTag mice analyzed by qRT-PCR from IP samples. Data are expressed as mean ± SEM; n = 3-5; Student's T, **** $p < 0.001$. Scale bar 100 μm (B).

4.13. Analysis of mitochondrial morphology in AgRP neurons

To analyze whether the *Cpt1a* deletion in AgRP neurons affects the mitochondrial morphology, *Cpt1a*$_{AgRP}^{(-/-)}$ mice was crossed with ZsGreen mice (section 3.1.1). *Cpt1a*$_{AgRP}^{(-/-)}$:ZsGreen and control mice were recombined at 8-weeks old. One week later, animals were fixed and brains were obtained and processed according to the section 3.3.16.

No mitochondria-specific fluorescent signal was detected in both *Cpt1a*$_{AgRP}^{(-/-)}$:ZsGreen and control mice (Figure 34A,B). The mitochondrial detection will probably require the amplification of ZsGreen protein by using specific antibodies.

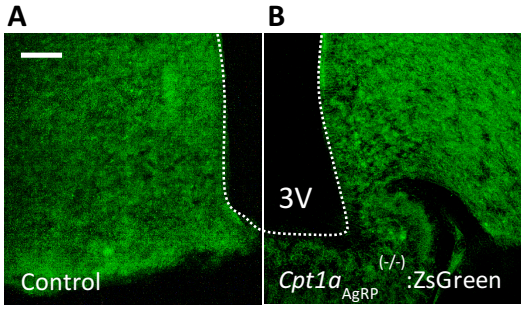

Figure 34. Detection of ZsGreen mitochondrial protein.
(A) Representative images of ARC sections of control and (B) Cpt1a$_{AgRP}^{(-/-)}$:ZsGreen mice. (Magnification 40x). Scale bar 40 µm. n = 2

5. DISCUSSION

Lipid metabolism has recently been postulated to have a key role in neuronal physiology. In this context, increasing evidence indicates that the modulation of lipid metabolism in the hypothalamus plays a critical role in feeding control [188]. In fact, the pharmacologic and genetic targeting of key enzymes from these pathways has a profound effect on food intake and body weight [115,188,189].

In this project, we focus on understanding the physiologic role of lipid metabolism in hypothalamic AgRP neurons. We assess whether CPT1A has a metabolic role in the control of energy homeostasis through AgRP neurons. Given that these neurons have a potent-appetite induction, it is important to identify the regulatory mechanisms and determine their role in food intake and the development of human obesity.

The main results of this project reveal that *Cpt1a* deletion in AgRP neurons has an impact on feeding behaviors differently in male and female. In addition, CPT1A in AgRP neurons regulate the lipid content in adipose tissues and BAT activity. Interestingly and surprisingly despite the well-described association between AgRP and food intake, CPT1A in AgRP neurons could be involved in fluid balance.

5.1 *Cpt1a* deletion in AgRP neurons affects differentially body weight in male and female

Considering the key role of AgRP neurons in the regulation of appetite, it has been postulated as an important druggable/modifiable target to treat some diseases related with overfeeding. In addition, it has been suggested that lipid metabolism plays a key role in the hypothalamic control of energy balance. Some enzymes and intermediates of fatty acid metabolism contribute to the hypothalamus' ability to serve as a monitor of energy status. In 2002, Rossetti and colleagues were the first to demonstrate that the central administration of LCFAs triggered a hypothalamic

response to regulate energy [83]. Importantly, AMPK, ACC, CPT1A, CPT1C, FAS, and malonyl-CoA decarboxylase mRNAs and proteins are highly expressed in hypothalamic nuclei involved in energy homeostasis, such as ARC, DMH, PVN and VMH [188]. Given the enormous heterogeneity of neurons in the hypothalamus, few studies have reported the effects of lipid metabolism on a single population of neurons. Previous results from our group demonstrated that the MBH overexpression of a mutated form of CPT1A insensible to malonyl-CoA (its physiological inhibitor) increased the hyperphagia concomitantly to the body weight suggesting the predominant role of lipid metabolism in the control of feeding behavior [190].

In this project, we delete *Cpt1a* gene encoding CPT1A enzyme in AgRP neurons. We took advantage of knock-out mouse technology to generate a mouse line lacking *Cpt1a* gene specifically in hypothalamic AgRP neurons in adult mice. Our results reveal a clear reduction of the body weight gain, which is most pronounced in male than female. After the *Cpt1a* recombination it is possible to observe that $Cpt1a_{AgRP}^{(-/-)}$ mice have a lower slope compared with their control littermates. The phenotype obtained following deletion of *Cpt1a* in AgRP neurons was difficult to predict since acute genetic ablation of AgRP in adult animals leads to anorexia. The depletion of >80% NPY/AgRP neurons causes a reduction of around 20% of the body weight within 2 days post AgRP neurons ablation reaching a maximal weight lost 7 days post ablation of around 70% body weight [40]. Although the deletion of *Cpt1a* affect the body weight gain no signs of body weigh lost were observed in our model. Interestingly, it has been demonstrated that the neonatal ablation of AgRP neurons did not induces body weigh changes suggesting a compensatory mechanism that control the feeding behavior, for that reason we decided to induce the recombination in adult stages [40].

In agreement with our results, the deletion of NMDA receptor subunit GluN2B, a glutamate-gated cation channels expressed in hypothalamic AgRP neurons, reduces the body weight gain in both male and female in KO mice [191]. At 16 weeks, they reported that male mice lacking GluN2B reduces around 5 g of body weight gain and

Cpt1a$_{AgRP}^{(-/-)}$ mice showed a reduction of around 7 g of body weight gain compared with their control littermates. Female AgRP-GluN2B KO mice had a weigh difference of around 2 g compared with their control littermates, exactly the same differences that we observed in female Cpt1a$_{AgRP}^{(-/-)}$ mice at 16 weeks old. Since NMDA receptor deletion exerts the same impact on body weight compared with *Cpt1a* KO, we could speculate that CPT1A could be involved in the regulation of some components of glutamate metabolism in AgRP neurons. In addition, previous studies from our group revealed that overexpression of the permanently active form of CPT1A in VHM of the hypothalamus affect the mRNA profile of vesicular glutamate transporters [115].

Interestingly, some studies that delete other important proteins for AgRP-mediated metabolic control such as *p53* [192] and *Vgat* [31], trigger a reduction of the body weight gain only in animals exposed to a challenge of HFD. However, no changes were observed in animals fed with a standard show diet in disagreement with what we observed in our model, suggesting that CPT1A enzyme is involved in the body weight control under physiological conditions.

More recently, two reports highlighted the involvement of AgRP-carnitine acetyltransferase (Crat) in energy balance. As we extensively describe in section 1.5.2.1, Crat belongs to the family of transferases in close association to CPT. Mice lacking for Crat selectively in Agrp neurons had impaired metabolic flexibility -the capacity to shift between energy substrates-. However, no differences on body weight gain was observed in animals fed with normal chow or HFD [95]. Even under 9 days of caloric restriction, no differences on the percentage of body weight increase were observed between genotypes [193]. Due to the different effect that CPT1A and Crat enzymes exerts on body weight, suggest that both enzymes assume a specific role in neuronal physiology although they are closely associated in lipid metabolism.

5.2 *Cpt1a* deletion in AgRP neurons induces a sex-based differential effect on food intake behaviour

To further understand why mice lacking *Cpt1a* reduces the body weight gain, food intake was measured. Intriguingly $Cpt1a_{AgRP}^{(-/-)}$ mice showed a sexual dimorphism in caloric intake. While $Cpt1a_{AgRP}^{(-/-)}$ male reduces food intake no changes were observed in $Cpt1a_{AgRP}^{(-/-)}$ female mice fed with normal show diet in *ad libitum* condition. This result measured by weekly food intake agrees with those measured by TSE system confirming and reinforcing the difference between male and female $Cpt1a_{AgRP}^{(-/-)}$ mice.

Most of the food intake studies are done on male mice and little is known about caloric intake in female mice. Despite this, it's pretty logical to assume a sex-based differences in food consumption and dietary intake as here we unravel. Males and females have distinct patterns of metabolic regulation, including the control of food consumption, which contributes to sex differences in the development of metabolic disease. Sex-based differences of feeding behavior in mammals have been attributed exclusively to the effects of gonadal hormones, especially estrogens and androgens, which regulate food intake and energy metabolism by acting on the brain and diverse peripheral tissues [194,195].

It has been shown that in gonadal-intact mice, the total food intake measured by BioDAQ cages, is higher in male than in female during dark phases and conversely female mice ate more than male during light phase. Interestingly this differences were blunted in gonadectomized animals, since no differences were observed between gender [196]. This study suggests a complex interaction between gonadal hormones on daily feeding rhythms and reveals gender differences depending on gonadal hormones.

In our model, the deletion of *Cpt1a* in AgRP neurons affect the dark phase of male $Cpt1a_{AgRP}^{(-/-)}$ mice, since food intake in this phase drooped by half. However, no differences in food intake were observed in $Cpt1a_{AgRP}^{(-/-)}$ female mice [196], suggesting that the influence of androgen hormone on food intake requires *Cpt1a* in AgRP neurons.

The expression of estrogen receptors (ERs) in AgRP neurons has been completely excluded and no androgen receptor (ARs) expression has been elucidated [197,198]. This fact suggest that gonadal hormones do not influence directly AgRP neurons. Interestingly, ARC nucleus also content an important population of neurons implicated in the control of reproduction. They are the Kisspeptin (Kiss) expressing neurons. Kiss neurons express the ERs and the ARs, and these cells are direct targets for the action of gonadal steroids in both male and female animals [199]. The connection between kiss neurons and AgRP neurons have been established and this would explain why changes in sexual hormones are also reflected on food intake [200,201]. Taking into account this information, if the sex-based differences that we observed in our model are the consequence of sexual hormones, this may not impact directly in AgRP neurons. It seems that *Cpt1a* in AgRP neurons has a key role in sexual hormone regulation of energy balance which is altered in male mice but do not interfere in female mice.

5.3 *Cpt1a* deletion in AgRP neurons produces sex differences in energy expenditure

Although the reduction of food intake in male could explain the drop in the body weight gain, the lack of reduction of food intake in female mice motivate us to evaluate for energy expenditure using TSE system. Total energy expenditure (TEE) is composed of the energy costs of the processes essential for life (also called basal metabolic rate (BMR), 60–80% of TEE), of the energy expended in order to processing of ingested food or diet-induced energy expenditure (DEE) (diet-induced thermogenesis, ~10%), and the energy expended during physical activities (activity energy expenditure, ~15–30%) [202,203].

The main determinants of energy expenditure are body size and body composition, food intake, and physical activity. The disturbances in these components cause changes in body mass due to the imbalance in energy balance. A positive energy

balance, in which energy intake exceeds expenditure causes weight gain, with 60–80 % of the resulting weight gain being attributable to body fat. In negative energy balance, the energy expenditure exceeds intake resulting in a loss of body mass [15]. Energy input and expenditure are interdependent and regulated at several levels. This involves a complex physiologic control system, including afferent neural and hormonal signals reaching the hypothalamus, with resultant efferent projections of the autonomic nervous system innervating the muscles, viscera, and adipose tissue [204].

Our results obtained from indirect calorimetry revealed that mice lacking CPT1A in AgRP neurons exert a negative energy balance. While in female *Cpt1a*$_{AgRP}^{(-/-)}$ mice the energy expenditure would exceed the energy ingested, in male *Cpt1a*$_{AgRP}^{(-/-)}$ mice energy ingested is substantially reduced. In both cases, the result is reflected in less body weight gain.

It is well stablished that food intake affects all three components of TEE. Thus, changing energy intake changes TEE accordingly. Although the drop-in food intake in male mice do not reduce statistically the EE measured with TSE, intriguingly the values in Cpt1a$_{AgRP}^{(-/-)}$ male mice tend to be less than the control littermates being this reduction significant during refeeding. These results suggest that in order to maintain the energy balance and body weight, the decrease in food consumption due to the deletion of CPT1A in AgRP neurons was compensated by a reduction in energy expenditure.

As we mentioned before, the direct function of AgRP neurons is to increase food intake and reduce EE resulting in a body weight increase. Interestingly, our results demonstrate that AgRP neurons lacking CPT1A from female mice has a greatest impact on EE than the food intake. Similar results have also been described for the KO mice for the glucocorticoid receptor in AgRP neurons [183]. Although the neurons which mediate glucocorticoid action have not been clarified yet. It has been described that glucocorticoid, which is an important modulator for EE, markedly stimulates de mRNA expression of NPY and AgRP in the hypothalamus. In 2015, Miyuki Shibata and

colleagues demonstrate that AgRP neurons-specific deletion of glucocorticoid receptor leads to increased EE and decreased body weight [183]. Although there is no evidence for CPT1A as a component downstream of glucocorticoid pathway in AgRP neurons, our results suggest that CPT1A can be involved in this pathway in the control of energy balance.

Physical activity is another important determinant for the TEE. It can have a major impact on total 24 hours energy expenditure and energy balance. Physical activity may increase BMR as well as have an effect on the thermal effect of food. The BMR is higher in trained individuals than in sedentary individuals of the same weight, but the difference may be predominantly attributed to changes in body composition, such as lower fat mass [204]. Our findings did not reveal any change in locomotion activities in both genders. This suggests that in our model food intake could be the most important determinant for the EE in male mice which is consistent with the main function of the AgRP neurons. However, a differential mechanism operate in female mice, since the deletion of *Cpt1a* in AgRP neurons impact directly on EE.

Although the reduction of body weight gain triggered by the *Cpt1a* deletion in AgRP neurons was independent of gender, our findings provide evidence that males and females are hardwired differently in their regulation of energy balance. Gender differences in body compositions are well stablished, many mammals show differences in fat-free mass (FFM) and fat mass (FM) between sexes. Female tend to have higher percentages of FM than males throughout life [205]. Not only is there a difference in percentage of FM between the sexes but there is also a well-recognized difference in body fat distribution. Consistent with our results obtained from EE, we suggest that specific *Cpt1a* deletion in AgRP neurons triggers in $Cpt1a_{AgRP}^{(-/-)}$ female mice through an increase of the EE to reduce their body weight gain. On the contrary, males contain less stores of FM and they are less efficient conserving energy. Thus, at physiological levels $Cpt1a_{AgRP}^{(-/-)}$ male reduce their body weight gain with a dietary restriction more efficiently than females.

These data may have translational relevance by providing a potential molecular explanation for the global sex differences in obesity prevalence. These data may have also broad implications for future sex-specific strategies in treating overweight and obesity.

5.4 *Cpt1a* deletion in AgRP neurons impairs the food intake response in fasting condition

It has extensively reported that the fasting-mediated activation of AgRP neurons serves to promote food-seeking behavior and conservation of energy [181]. According to our results the changes on the feeding behavior induced by the CPT1A deletion in AgRP neurons strongly suggest that AgRP neurons in *Cpt1a*$_{AgRP}^{(-/-)}$ mice are less active. Our results showed that *Cpt1a*$_{AgRP}^{(-/-)}$ mice reveal a statistical reduction of food intake during 4 hours of refeeding after an ON fasting. These results agree with those of Lowell and collegues in 2012 [206]. They studied the role of glutamateric input for activation of AgRP neurons under fasting condition. They strikingly demonstrated that deletion of NMDARs from AgRP neurons caused marked reductions in body weight and fasted-induced refeeding [35]. In agreement with that, our results suggest that CPT1A may be involved in the activation of AgRP neurons. In order to confirm that we also evaluate the physiological response after ghrelin i.p administration.

Ghrelin, the only known circulating hormone that stimulates appetite, is produced predominantly by a population of enteroendocrine “ghrelin” cells distributed sparsely throughout the gastric oxyntic mucosa. Circulating ghrelin levels rise before meal initiation, following food restriction and after acute or chronic stress [49]. Food intake in response to ghrelin has been demonstrated by both acute and chronic administration using protocols in which ghrelin is given by one of several peripheral routes, icv or by direct microinjection into the brain parenchyma. The effects of ghrelin on both homeostatic and hedonic eating behaviors are well-established in rodents and

humans and occur via GHSR, the only known ghrelin receptor [17]. On the one hand, patch clam studies on $Ghsr^{+/+}$mice, ghrelin significantly increased the firing activity of AgRP neurons. On the other hand, $Ghsr^{-/-}$ mice, the excitatory effect of ghrelin on AgRP neurons was abolished [49]. These results are also concordant with those obtained from GHS-R deletion in AgRP neurons, since these mice abolished ghrelin-induced food intake [120]. Although the ghrelin effect on AgRP neurons is well stablished, little is known about molecular pathway in the AgRP activation. It has been suggested that ghrelin activates AMPK-CPT1A-UCP1 axis in hypothalamic neurons. Our finding reinforces the importance of CPT1A downstream for AgRP neurons induction of food seeking, since mice lacking CPT1A in AgRP neurons reduce the food intake in both male and female mice after ghrelin administration. Despite this, the drop-in food intake in mice lacking ghrelin receptor is more pronounced than the decrease that we observed in our model, probably due to alternatives pathways that ghrelin may activate independent of CPT1A.

Taking all this information together, our results reveal that specific CPT1A deletion in AgRP neurons impact on body weight independent of gender. However, the homeostasis of energy balance exerts a sex based differences. While male reduces food intake in female increase the energy expenditure. No sex differences were observed in AgRP neurons under fasting condition or physiological targets as ghrelin, due to CPT1A deletion in AgRP blunted the response of food intake in response to the hormone or O/N fasting and suggests that CPT1A may be an imperative element for AgRP neurophysiology.

5.5 AgRP neurons requires *Cpt1a* enzyme to regulate peripheral tissue metabolism

One important property of hypothalamic AgRP neurons is to continuously monitor signals reflecting energy status and promoting appropriate behavioral and metabolic responses to changes in nutritional availability and demand. There is

increasing evidence that the regulation of energy balance by AgRP-neurons involves melanocortin-independent signaling outside of the hypothalamus. Interestingly, AgRP neurons send dense projections to preganglionic structures such as the PVN, which directly regulate autonomic nervous system (ANS) outflow to peripheral tissues. Thus, the action of AgRP neurons on energy balance might extend beyond the acute control of food intake.

It has been demonstrated that the ablation of AgRP neurons alters inter-organ communication and redirects peripheral nutrient utilization towards increased fat, versus carbohydrate, oxidation [207]. Furthermore, very recently it has been reported that acute activation of AgRP neurons rapidly shift whole-body metabolism towards lipid storage, an important mechanism for fat accumulation during positive energy balance (*i.e.,* a metabolic state coupled to weight gain) [94]. In our model we observed that after 3 months post recombination the lean phenotype in *Cpt1a*$_{\text{AgRP}}^{(-/-)}$ mice was profoundly correlated with a decrease of gWAT and iWAT. The WATs analysis reveals a decrease of the adipocyte size which is concordant with the reduction of the gWAT and iWAT weight in both males and females. The reduction of the WAT cell volume in *Cpt1a*$_{\text{AgRP}}^{(-/-)}$ mice, indicates increased lipolysis and altered nutrient partitioning that may contribute to the maintenance of the energy balance. We observed a tendency to increase *Atgl* expression in gWAT and iWAT of *Cpt1a*$_{\text{AgRP}}^{(-/-)}$ male mice whereas in females mice this increase is significant in iWAT. Although both genders exert a reduction of the total WAT content, the differential expression of *Atgl* in WAT depending on gender suggests that male and female have a differential regulation of the lipolytic activity.

Numerous findings provide evidence that there is great heterogeneity in lipolysis between adipose tissue depots of men and women. On average, adipose tissue lipolysis is substantially greater (~40%) in women than in men [208]. This fact is concordant with the results observed in gWAT. Whereas in *Cpt1a*$_{\text{AgRP}}^{(-/-)}$ males the adipocyte area is reduced by half, female Cpt1a$_{\text{AgRP}}^{(-/-)}$ mice showed a 3-fold reduction

compared with their control littermates. This is presumably due, in part, to increased fat oxidation and more efficient utilization and disposal of FFA in female.

It has been reported that the deletion of ATF4 in AgRP neurons (a transcriptional factor belonging to the CREBP families) promotes a decrease of the weights of sWAT and eWAT. Histological analysis of eWAT showed that the loss of ATF4 expression in AgRP neurons resulted in a 40% reduction in adipocyte volume [74], almost the same reduction that we observe in our model.

The altered nutrient partitioning in $Cpt1a_{AgRP}^{(-/-)}$ mice could be due to the insufficient energy intake, which is needed to mobilize more fat to be used as an energy source or due to an increase of the sympathetic outflow to the WAT. It has been reported that the *in vivo* NE released from sympathetic nerve terminals stimulates the G-protein coupled β3 ARs in rodents and β1 and β2 receptors in humans, respectively, leading to the canonical intracellular signaling sequence that ultimately results in lipolysis [209]. In humans, stimulation of the lateral femoral cutaneous nerve elicits lipolysis in the innervation area reducing the adipose tissue content similar that we observed in our model [210]. In addition, AgRP regulate preganglionic SNS neurons located in PVN for that reason it is logical to assume that any intervention of AgRP neuron will be reflected in WATs. Our results suggest an activation of sympathetic nervous system in both genders of mice lacking CPT1A in AgRP neurons.

Another important tissue that contributes to the energy balance is BAT. BAT is a unique tissue that is able to convert chemical energy directly into heat when activated by the SNS. In short, the unique thermogenic capacity of the tissue is due to its high content of mitochondria and the expression of UCP1. UCP1 is a proton channel within the inner mitochondrial membrane that, upon activation, short circuits the respiratory chain, thereby dissipating chemical energy as heat [211].

The connection between AgRP neurons and BAT it has also been stablished. Chronic CNS administration of AgRP neuropeptide decreases oxygen consumption and decreases the capacity of BAT to expend energy [212]. More recent studies have also

used viral tracing techniques, which allow for more detailed mapping of neuronal connections. In particular, the presence of anatomical connections between ARC, PVN and BAT were observed using retrograde transsynaptic studies with PRV [213], highlighting the existence of PVN-to-BAT pathways. Shi and colleagues have found that tyrosine hydroxylase expressing neurons in the PVN mediate ARC NPY-induced decrease in BAT thermogenesis [214]. This result was also confirmed by Brüning and colleagues, 2016. They demonstrated that optogenetic activation of AgRP neuron decreases BAT sympathetic nerve activity [185]. The results observed in our model seem that CPT1A deletion in AgRP neurons triggers an increase of the sympathetic outflow to the BAT. *Cpt1a*$_{\text{AgRP}}^{(-/-)}$ mice revealed a reduction of the BAT weigh independent of gender. This reduction was correlated with a reduction of lipid droplet content suggesting an increase of the thermogenic capacity. We measured the BAT activity by infrared imaging, registering an increase of the temperature of BAT interscapular skin area. This result was confirmed by measuring UCP1 protein in BAT tissue and the gene expression of lipolytic enzymes providing evidences of an enhanced FFA mobilization and heat production.

At a physiological level, it is coherent that BAT is an important target of AgRP neurons due to its involvement in the energy balance. However, here we provide new evidences that CPT1A may serve as a modulator of the BAT activity elicit for AgRP neurons. The icv infusion of AGRP (1 nmol) gradually suppressed BAT sympathetic nerve activity and was accompanied by a significant reduction in BAT temperature [120]. On the contrary, the lack of CPT1A may increase the sympathetic nerve activity increasing the BAT activity and the concomitant temperature. This phenomenon is mainly reflected in the increase of the EE in Cpt1a$_{\text{AgRP}}^{(-/-)}$ female mice but lesser extend in male mice probably due to the important drop of the calorie intake.

Our current study demonstrated a novel function of CPT1A in hypothalamic AgRP neurons for systematic metabolic control. Our results also provided novel insights

into understanding the signals in specific neurons that are critical for the regulation of energy homeostasis.

Liver is also an essential AgRP-target for the maintenance of energy homeostasis. On the one hand, mice engineered for lacking the IR in AgRP neurons showed an impairment of hepatic glucose production suppression [68]. On the other hand, the deletion of Crat enzyme in AgRP neurons reduced the glycogen content and increased the level of TG in liver during fasted state. These results are in agreement with the gene expression analyzed in liver of *Cpt1a*$_{AgRP}^{(-/-)}$ mice. Both male and female *Cpt1a*$_{AgRP}^{(-/-)}$ shown a significant increase of *Cpt1a* gene expression in liver, this may suggest the increase of β- oxidation of FFA coming from adipose tissue or stored in the liver. We also reported a significant increase of *Pepck* and *G6p in* male and the same tendency in female *Cpt1a*$_{AgRP}^{(-/-)}$ mice under fasting state suggesting that the profoundly reduction of lipid content shift to activate the glucose synthesis as a resource of energy.

This phenotype is also observed during the stimulation of hepatic efferent nerves. Activation of the sympathetic efferent nerves increases glucose production and suppressed glycogenesis. Assuming that AgRP neurons modulate the activation of SNS, this could explain the changes that we reported in *Cpt1a*$_{AgRP}^{(-/-)}$ mice. Thus, our result in liver indicate, during fasting, that the deletion of *Cpt1a* in AgRP neurons forces the liver to generate glucose through gluconeogenesis probably due to the decrease of fat depots as energy resource.

Taking all these results together, the deletion of *Cpt1a* in AgRP neurons have a great impact on peripheral target tissue. We provide evidence that AgRP neurons lacking *Cp1a* would activate sympathetic outflow to the WAT, BAT and liver. This result provide evidence that AgRP neurons have the property to adapt to changing metabolic substrates and this is an important mechanism affecting the development of obesity-related diseases.

5.6 *Cpt1a* deletion in AgRP neurons is also involved in water intake

Most studies focusing on AgRP function are related with food intake, energy metabolism and body weigh changes, however no evidence have been reported about the implication of AgRP and water consumption.

Here we shown a robust increase of water intake in $Cpt1a_{AgRP}^{(-/-)}$ mice which was not associated with a diabetic state, since no changes were observed in the GTT assay and kidney morphology. Interestingly, this increase in water consumption is comparable to the results obtained from the activation of the neural centers that control the homeostasis of body fluids. It has been reported that optogenetic activation of SFO and MnPO, trigger a robust increase of around 4-fold the number of lick of water and surprisingly we observed a drinking increase of the double amount of water in $Cpt1a_{AgRP}^{(-/-)}$ mice respect to the control littermates [215]. Although little is known about the evidence of water consuming in response of AgRP activity, this result may suggest that hunger neurons could also be linked to the water intake.

Due to this surprising increase of water intake, we next move forward to study the phenotype associated to body fluid balance in mice lacking CPT1A in AgRP neurons. The increase of water intake observed in $Cpt1a_{AgRP}^{(-/-)}$ mice was accompanied with an increase of daily average urine output. While it is true that male mice excrete urine at a rate 1.5-2.0-fold than females [216] (same that we observed in our controls animals), $Cpt1a_{AgRP}^{(-/-)}$ mice excrete 3-fold more respect to the control littermates independently of gender. The increase of the diuresis is associated with a low urine osmolality suggesting a compensatory mechanism engaged to alleviate the acute increase of water intake. Even, there were not changes in plasma osmolality *ad libitum* access of water and in water restriction.

Since VP/ADH hormone is a key modulator of water balance we then measured the plasmatic level of VP/ADH. According to the phenotype, $Cpt1a_{AgRP}^{(-/-)}$ mice shown a statistical reduction of the circulating level of VP/ADH. This result

suggests the impairment of the kidneys to reabsorb solute-free water and return it to the circulation from the tubules of the nephron.

VP/ADH is synthesized as a peptide prohormone in neurons in the hypothalamus, specifically SO and PVN nucleus and is converted to AVP [151]. It then travels down the axon of that cell, which terminates in the posterior pituitary, and is released from vesicles into the circulation in response to extracellular fluid hypertonicity (hyperosmolality). Considering that PVN is an important nucleus for VP/ADH production and moreover establishes neuronal network with ARC nucleus, we then evaluate the cFos activation of PVN *ad libitum* access to water and water restricted state. No cFos positive cells were observed in *Cpt1a*$_{AgRP}^{(-/-)}$ mice *ad libitum* access to water which is an interesting observation considering the increase of water intake in this this state. Intriguingly, water restriction increase the PVN cFos positive cells activation. However, no increase was observed in *Cpt1a*$_{AgRP}^{(-/-)}$ mice. This result may suggest a missed signal to activate this nucleus and probably release VP/ADH hormone.

Low levels of VP/ADH hormone would explain the water lost by urine and the increase of thirst in *Cpt1a*$_{AgRP}^{(-/-)}$ mice, however surprisingly the cFos analysis of SFO – as an important center involved in the thirst generation- was not activated in *Cpt1a*$_{AgRP}^{(-/-)}$ mice. In 2015 Charles S. Zuker and collegues demonstrate that approximately 30% of cells in SFO of a water-restricted animal (48 hours) are cFos positive and no significant cFos labelling was detected under the water satiated condition [152]. Here we reported that 24 hours of water restriction induce approximately a 10% of cFos activation in control animals and no signal was detected in water-satiated state. Unexpectedly *Cpt1a*$_{AgRP}^{(-/-)}$ mice did not reveal any cFos signal in *ad libitum* condition considering that in this state are consuming higher amount of water compared with the control littermates. This could be explained with the anticipatory response of SFO neurons [155]. It has been reported that ON water restriction strongly activated SFO neurons. When water was available, mice drank avidly and, surprisingly, SFO neurons were inhibited within 1 min. This inhibition was time-locked to the act of drinking, with

activity beginning to decline the moment of the first lick. This result suggest that although *Cpt1a*$_{AgRP}^{(-/-)}$ mice are consuming more water in *ad libitum* condition, the free access to water rapidly would inhibit SFO neurons making it difficult to visualize by labeling cFos. On the other hand, the miss-SFO activation under water restriction may suggest that AgRP neuron lacking *Cpt1a* impair the activity of SFO neurons, however no neuronal connection have been reported between AgRP and SFO neurons, suggesting that this regulatory response would be in an indirect manner.

5.7 *Cpt1a* is involved in neuronal morphology and physiology

In order to explain all the phenotype changes that we described in *Cpt1a*$_{AgRP}^{(-/-)}$ mice we examined specifically AgRP neurons at central level. In 2005, Richard D. Palmiter and colleagues demonstrate that the completely ablation (>80%) of AgRP expressing neurons in adult mice by using the diphtheria toxin method, trigger a loss of 20% of their body weight and induce a complete starvation 3day post ablation, suggesting that the energy homeostasis depending directly of the AgRP integrity. For that reason, we decided to examine whether the deletion of *Cpt1a* in AgRP neurons would affect the neuronal viability. We first measured the number of AgRP neurons along the anterior-posterior axis of the ARC nucleus 1 month post recombination. Although it was reported that the ARC contains 9,965 ± 66 AGRP neurons (mean ± SD, n = 2 mice), which are evenly distributed along the anterior to posterior ARC axis [179], we select one representative slice from the anterior medial an posterior section in order to examine a possible decrease in the AgRP number. We did not find differences in the section analyzed suggesting that the phenotype observed in *Cpt1a*$_{AgRP}^{(-/-)}$ is not associated with a decrease of the neuronal viability.

To gain depth in the morphological analysis of AgRP neurons we examined the dendritic spine, since they are important structures involved in the synapsis. Our result suggests that CPT1A is necessary to maintain a normal number of dendritic spines, since *Cpt1a*$_{AgRP}^{(-/-)}$ mice reveal a reduction of the number of spines per dendritic section

compared with the control littermates. Same results were obtained by Bradford B. Lowell and colleagues in 2012. They demonstrate that AgRP lacking *Grin1* gene, which encodes a subunit of NMDARs, reduces a 50% the number of dendritic spines [35]. In concordance with these results Bjørbæk C. and colleagues demonstrate that the deletion of f GluN2B (other subunit of NMDARs) in AgRP neurons reduced the spines length [217]. This allow us to conclude that NMDARs is important for the synaptogenesis in AgRP neurons.

The reduction of the dendritic spines is associated with an impair in the synapsis. In order to elucidate whether the *Cpt1a* deletion in AgRP neurons affect the synapse, we took advantage of the synaptophysin labeling to explore the presynaptic target of AgRP neurons. We observe a reduction of the PVN synaptophysin signal in $Cpt1a_{AgRP}^{(-/-)}$ mice suggesting that the deletion of *Cpt1a* modify the neuronal network between ARC and PVN.

In summary, our results support the notion that lipid metabolism is important for the hypothalamic control of energy balance. The deletion of *Cpt1a* in AgRP neurons does not affect the neuronal viability of AgRP neurons however interferes in the normal morphology of the synapse. The reduction of presynaptic signals to the PVN section would affect the control of neurons involved in the control of SNS. According to our results the reduction of the activity of AgRP neurons lead to activate the sympathetic outflow to the peripheral organs, increasing the BAT activity, reducing the WAT content and shifting the hepatic metabolism. The phenotype effect of the intervention in AgRP neurons reduces the body weight gain in male and female, by reducing the food intake and increase the EE respectively. Finally, we also report that AgRP neurons could be involved in the water homeostasis since mice lacking AgRP neurons reduces the level of AV/ADH hormone, increasing the thirst (water consumption) and the urine output.

6. CONCLUSIONS

1.- The deletion of *Cpt1a* in AgRP neurons induces a reduction of body weight gain in both male and female mice.

2.- Mice lacking CPT1A in AgRP neurons develop a sex-based differences on feeding behaviors. While male *Cpt1a*$_{AgRP}^{(-/-)}$ mice show a reduction in the cumulative food intake, no changes are observed in female *Cpt1a*$_{AgRP}^{(-/-)}$ mice.

3.- The *Cpt1a* ablation in AgRP neurons differentially influences the EE profile in male and female mice. While female *Cpt1a*$_{AgRP}^{(-/-)}$ mice show an increase of EE, no differences are observed in male mice.

4.- Both male and female *Cpt1a*$_{AgRP}^{(-/-)}$ mice show a reduction in food intake in response to a stimulus such as an exogenous dose of ghrelin and an overnight fasting.

5.- The lack of CPT1A in AgRP neurons induces an enhancement of BAT activity through an increase in UCP1 protein levels.

6.- CPT1A is required in AgRP neurons to regulate WAT lipid content. Both male and female *Cpt1a*$_{AgRP}^{(-/-)}$ mice show a reduction of fat mass and adipocyte cell surface area specially in gWAT and iWAT. Moreover, the lack of CPT1A in AgRP neurons stimulates iWAT browning.

7.- The deletion of *Cpt1a* in AgRP neurons does not alter the morphology of extra-target tissues such as pancreas, gonads and liver.

8.- The lack of CPT1A in AgRP neurons exerts an important increase of water intake that is not associated with the development of diabetes.

10.- *Cpt1a*$_{AgRP}^{(-/-)}$ mice have reduced levels of AV/ADH which is correlated with an increase in the urine output.

11.- The lack of CPT1A in AgRP neurons affects the activation of SFO and PVN centers induced by a 24 h water restriction.

12.- The deletion of CPT1A in AgRP neurons does not affect the number of AgRP neurons but alters their morphology by reducing the number of dendritic spines and modifying the neuronal network specially between ARC and PVN.

7. REFERENCES

[1] Health Effects of Overweight and Obesity in 195 Countries, N. Engl. J. Med. 377 (2017) 1495–1497. doi:10.1056/NEJMc1710026.

[2] M. Ezzati, J. Bentham, M. Di Cesare, V. Bilano, H. Bixby, B. Zhou, G. Stevens, L. Riley, C. Taddei, K. Hajifathalian, Y. Lu, S. Savin, M. Cowan, C. Paciore, A. Chirita-Emandi, A. Hayes, J. Katz, R. Kelishadi, A. Kengne, Worldwide trends in body-mass index, underweight, overweight, and obesity from 1975 to 2016: a pooled analysis of 2416 population-based measurement studies in 128.9 million children, adolescents, and adults, Lancet (London, England). 390 (2017) 2627–2642. doi:10.1016/S0140-6736(17)32129-3.

[3] G. Whitlock, S. Lewington, P. Sherliker, R. Clarke, J. Emberson, J. Halsey, N. Qizilbash, R. Collins, R. Peto, Body-mass index and cause-specific mortality in 900 000 adults: collaborative analyses of 57 prospective studies., Lancet (London, England). 373 (2009) 1083–1096. doi:10.1016/S0140-6736(09)60318-4.

[4] K.M. Gadde, C.K. Martin, H.-R. Berthoud, S.B. Heymsfield, Obesity: Pathophysiology and Management, J. Am. Coll. Cardiol. 71 (2018) 69–84. doi:https://doi.org/10.1016/j.jacc.2017.11.011.

[5] D. Sellayah, F.R. Cagampang, R.D. Cox, On the Evolutionary Origins of Obesity: A New Hypothesis, Endocrinology. 155 (2014) 1573–1588. doi:10.1210/en.2013-2103.

[6] J.A. Yanovski, Trends in underweight and obesity — scale of the problem, Nat. Rev. Endocrinol. 14 (2018) 5–6. doi:10.1038/nrendo.2017.157.

[7] J.D. Mackenbach, H. Rutter, S. Compernolle, K. Glonti, J.-M. Oppert, H. Charreire, I. De Bourdeaudhuij, J. Brug, G. Nijpels, J. Lakerveld, Obesogenic environments: a systematic review of the association between the physical environment and adult weight status, the SPOTLIGHT project., BMC Public

Health. 14 (2014) 233. doi:10.1186/1471-2458-14-233.

[8] S.M. Fruh, Obesity: Risk factors, complications, and strategies for sustainable long-term weight management., J. Am. Assoc. Nurse Pract. 29 (2017) S3–S14. doi:10.1002/2327-6924.12510.

[9] I.R. Back, R.R. Oliveira, E.S. Silva, S.S. Marcon, Risk Factors Associated with Overweight and Obesity in Japanese-Brazilians, J. Nutr. Metab. 2018 (2018) 5756726. doi:10.1155/2018/5756726.

[10] A. Biener, J. Cawley, C. Meyerhoefer, The High and Rising Costs of Obesity to the US Health Care System., J. Gen. Intern. Med. 32 (2017) 6–8. doi:10.1007/s11606-016-3968-8.

[11] B.E. Schneider, E.C. Mun, Surgical Management of Morbid Obesity, Diabetes Care. 28 (2005) 475 LP-480. doi:10.2337/diacare.28.2.475.

[12] M.B. Mumphrey, L.M. Patterson, H. Zheng, H.-R. Berthoud, Roux-en-Y gastric bypass surgery increases number but not density of CCK-, GLP-1-, 5-HT-, and neurotensin-expressing enteroendocrine cells in rats, Neurogastroenterol. Motil. 25 (2013) e70–e79. doi:10.1111/nmo.12034.

[13] J.J. Holst, S. Madsbad, K.N. Bojsen-Møller, M.S. Svane, N.B. Jørgensen, C. Dirksen, C. Martinussen, Mechanisms in bariatric surgery: Gut hormones, diabetes resolution, and weight loss, Surg. Obes. Relat. Dis. 14 (2018) 708–714. doi:https://doi.org/10.1016/j.soard.2018.03.003.

[14] P. BAILLIE, S.D. MORRISON, The nature of the suppression of food intake by lateral hypothalamic lesions in rats., J. Physiol. 165 (1963) 227–245. doi:10.1113/jphysiol.1963.sp007054.

[15] J.O. Hill, H.R. Wyatt, J.C. Peters, The Importance of Energy Balance., Eur. Endocrinol. 9 (2013) 111–115. doi:10.17925/EE.2013.09.02.111.

[16] L.F. Faulconbridge, M.R. Hayes, Regulation of energy balance and body weight by the brain: a distributed system prone to disruption, Psychiatr. Clin. North Am. 34 (2011) 733—745. doi:10.1016/j.psc.2011.08.008.

[17] Y. Sun, P. Wang, H. Zheng, R.G. Smith, Ghrelin stimulation of growth hormone release and appetite is mediated through the growth hormone secretagogue receptor., Proc. Natl. Acad. Sci. U. S. A. 101 (2004) 4679–84. doi:10.1073/pnas.0305930101.

[18] A.W. Hetherington, S.W. Ranson, The relation of various hypothalamic lesions to adiposity in the rat, J. Comp. Neurol. 76 (1942) 475–499. doi:10.1002/cne.900760308.

[19] B.K. Anand, J.R. Brobeck, Hypothalamic control of food intake in rats and cats., Yale J. Biol. Med. 24 (1951) 123–40.

[20] J.K. Elmquist, C.F. Elias, C.B. Saper, From lesions to leptin: hypothalamic control of food intake and body weight., Neuron. 22 (1999) 221–32. doi:S0896-6273(00)81084-3 [pii].

[21] P.S. Singru, E. Sánchez, C. Fekete, R.M. Lechan, Importance of melanocortin signaling in refeeding-induced neuronal activation and satiety, Endocrinology. 148 (2007) 638–646. doi:10.1210/en.2006-1233.

[22] A.A. Van Der Klaauw, J.M. Keogh, E. Henning, C. Stephenson, S. Kelway, V.M. Trowse, N. Subramanian, S. O'Rahilly, P.C. Fletcher, I.S. Farooqi, Divergent effects of central melanocortin signalling on fat and sucrose preference in humans, Nat. Commun. 7 (2016) 1–5. doi:10.1038/ncomms13055.

[23] K.G. Mountjoy, Pro-Opiomelanocortin (POMC) Neurones, POMC-Derived Peptides, Melanocortin Receptors and Obesity: How Understanding of this System has Changed Over the Last Decade, J. Neuroendocrinol. 27 (2015) 406–418. doi:10.1111/jne.12285.

[24] E.J.P. Anderson, I. Cakir, S.J. Carrington, R.D. Cone, M. Ghamari-Langroudi, T. Gillyard, L.E. Gimenez, M.J. Litt, Regulation of feeding and energy homeostasis by α-MSH, J. Mol. Endocrinol. 56 (2016) T157–T174. doi:10.1530/JME-16-0014.

[25] G.S. Kelly J, GABA and hypothalamic feeding systems. II. A comparison of GABA, glycine and actylcholine agonists and their antagonists.Pharmacol Biochem

Behav, Pharmacol Biochem Behav. 11 (1979) 647–52.

[26] S.P.K. John T. Clark, Pushpa S. Kalra, William R. Crowley, Neuropeptide Y and human pancreatic polypeptide stimulate feeding behavior in rats, Endocrinology. 115 (1984) 427–429. doi:org/10.1210/endo-115-1-427.

[27] J. Douglass, a a McKinzie, P. Couceyro, PCR differential display identifies a rat brain mRNA that is transcriptionally regulated by cocaine and amphetamine., J. Neurosci. 15 (1995) 2471–2481.

[28] K. Yang, H. Guan, E. Arany, D.J. Hill, X. Cao, Neuropeptide Y is produced in visceral adipose tissue and promotes proliferation of adipocyte precursor cells via the Y1 receptor, FASEB J. 22 (2008) 2452–2464. doi:10.1096/fj.07-100735.

[29] C.W. Shaun P. Brothers, Therapeutic potential of neuropeptide Y (NPY) receptor ligands, EMBO Mol. Med. 2 (2010) 429–439. doi:10.1002/emmm.201000100.

[30] Y. Chen, Z.A. Knight, Making sense of the sensory regulation of hunger neurons, BioEssays. 38 (2016) 316–324. doi:10.1002/bies.201500167.

[31] Q. Tong, C.-P. Ye, J.E. Jones, J.K. Elmquist, B.B. Lowell, Synaptic release of GABA by AgRP neurons is required for normal regulation of energy balance, Nat. Neurosci. 11 (2008) 998. doi:org/10.1038/nn.2167.

[32] G.J. Morton, D.E. Cummings, D.G. Baskin, G.S. Barsh, M.W. Schwartz, Central nervous system control of food intake and body weight, Nature. 443 (2006) 289. doi:org/10.1038/nature05026.

[33] J.W. Sohn, Network of hypothalamic neurons that control appetite, BMB Rep. 48 (2015) 229–233. doi:10.5483/BMBRep.2015.48.4.272.

[34] S.M. Sternson, Let them eat fat, Nature. 477 (2011) 166. doi:org/10.1038/477166a.

[35] T. Liu, D. Kong, B.P. Shah, C. Ye, S. Koda, A. Saunders, J.B. Ding, Z. Yang, B.L. Sabatini, B.B. Lowell, Fasting activation of AgRP neurons requires NMDA receptors and involves spinogenesis and increased excitatory tone., Neuron. 73 (2012) 511–522. doi:10.1016/j.neuron.2011.11.027.

[36] Y. Aponte, D. Atasoy, S.M. Sternson, AGRP neurons are sufficient to orchestrate feeding behavior rapidly and without training, Nat. Neurosci. 14 (2011) 351. doi:org/10.1038/nn.2739.

[37] K. Tan, Z.A. Knight, J.M. Friedman, Ablation of AgRP neurons impairs adaption to restricted feeding, Mol. Metab. 3 (2014) 694–704. doi:10.1016/j.molmet.2014.07.002.

[38] Q. Wu, M.P. Howell, M.A. Cowley, R.D. Palmiter, Starvation after AgRP neuron ablation is independent of melanocortin signaling, Proc. Natl. Acad. Sci. 105 (2008) 2687–2692. doi:10.1073/pnas.0712062105.

[39] M. Saito, T. Iwawaki, C. Taya, H. Yonekawa, M. Noda, Y. Inui, E. Mekada, Y. Kimata, A. Tsuru, K. Kohno, Diphtheria toxin receptor–mediated conditional and targeted cell ablation in transgenic mice, Nat. Biotechnol. 19 (2001) 746. doi:org/10.1038/90795.

[40] R.D.P. Serge Luquet, Francisco A. Perez, Thomas S. Hnasko, NPY/AgRP Neurons Are Essential for Feeding in Adult Mice but Can Be Ablated in Neonates, Science (80-.). 310 (2005) 683–685. doi:10.1126/science.1115524.

[41] E. Gropp, M. Shanabrough, E. Borok, A.W. Xu, R. Janoschek, T. Buch, L. Plum, N. Balthasar, B. Hampel, A. Waisman, G.S. Barsh, T.L. Horvath, J.C. Brüning, Agouti-related peptide-expressing neurons are mandatory for feeding, Nat. Neurosci. 8 (2005) 1289–1291. doi:10.1038/nn1548.

[42] J.C. Erickson, K.E. Clegg, R.D. Palmiter, Sensitivity to leptin and susceptibility to seizures of mice lacking neuropeptide Y, Nature. 381 (1996) 415. doi:org/10.1038/381415a0.

[43] S. Qian, H. Chen, D. Weingarth, E. Myrna, D.E. Novi, X. Guan, H. Yu, Y. Feng, E. Frazier, A. Chen, E. Ramon, L.P. Shearman, S. Gopal-truter, D.J. Macneil, L.H.T. Van Der Ploeg, J. Donald, M.E. Trumbauer, Z. Shen, R.E. Camacho, D.J. Marsh, Neither Agouti-Related Protein nor Neuropeptide Y Is Critically Required for the Regulation of Energy Homeostasis in Mice, Society. 22 (2002) 5027–5035.

doi:10.1128/MCB.22.14.5027.

[44] Q. Wu, M.P. Boyle, R.D. Palmiter, Loss of GABAergic Signaling by AgRP Neurons to the Parabrachial Nucleus Leads to Starvation, Cell. 137 (2009) 1225–1234. doi:10.1016/j.cell.2009.04.022.

[45] Joel K. Elmquist Roberto Coppari Nina Balthasar Masumi Ichinose Bradford B. Lowell, Identifying hypothalamic pathways controlling food intake, body weight, and glucose homeostasis, J. Comp. Neurol. 493 (2005) 63–71. doi:org/10.1002/cne.20786.

[46] D. Atasoy, J.N. Betley, H.H. Su, S.M. Sternson, Deconstruction of a neural circuit for hunger, Nature. 488 (2012) 172. doi:org/10.1038/nature11270.

[47] S.M. Steculorum, J. Ruud, I. Karakasilioti, H. Backes, L.E. Ruud, K. Timper, M.E. Hess, E. Tsaousidou, J. Mauer, M.C. Vogt, L. Paeger, S. Bremser, A.C. Klein, D.A. Morgan, P. Frommolt, P.T. Brinkkötter, P. Hammerschmidt, T. Benzing, K. Rahmouni, F.T. Wunderlich, P. Kloppenburg, J.C. Brüning, HHS Public Access, 165 (2016) 125–138. doi:10.1016/j.cell.2016.02.044.AgRP.

[48] P. J. Verhulst A. Lintermans S. Janssen D. Loeckx U. Himmelreich J. Buyse J. Tack I. Depoortere, GPR39, a Receptor of the Ghrelin Receptor Family, Plays a Role in the Regulation of Glucose Homeostasis in a Mouse Model of Early Onset Diet-Induced Obesity, J. Neuroendocrinol. 23 (2011) 490–500. doi:10.1111/j.1365-28262011.02132.x.

[49] D. Chen, S., Chen, H., Zhou, J., Pradhan, G., Sun, Y., Pan, H. and Li, Ghrelin receptors mediate ghrelin-induced excitation of agouti-related protein/neuropeptide Y but not pro-opiomelanocortin neurons, J. Neurochem. 4 (2017). doi:org/10.1111/jnc.14080.

[50] M. Goto, H. Arima, M. Watanabe, M. Hayashi, R. Banno, I. Sato, H. Nagasaki, Y. Oiso, Ghrelin increases neuropeptide Y and agouti-related peptide gene expression in the arcuate nucleus in rat hypothalamic organotypic cultures, Endocrinology. 147 (2006) 5102–5109. doi:10.1210/en.2006-0104.

[51] R. Lage, C. Diéguez, A. Vidal-Puig, M. López, AMPK: a metabolic gauge regulating whole-body energy homeostasis, Trends Mol. Med. 14 (2008) 539–549. doi:10.1016/j.molmed.2008.09.007.

[52] Z.B. Andrews, Z.-W. Liu, N. Walllingford, D.M. Erion, E. Borok, J.M. Friedman, M.H. Tschöp, M. Shanabrough, G. Cline, G.I. Shulman, A. Coppola, X.-B. Gao, T.L. Horvath, S. Diano, UCP2 mediates ghrelin's action on NPY/AgRP neurons by lowering free radicals, Nature. 454 (2008) 846. doi:org/10.1038/nature07181.

[53] M.O. Dietrich, C. Antunes, G. Geliang, Z. Liu, Y. Nie, A.W. Xu, D.O. Souza, Q. Gao, S. Diano, B. Gao, T.L. Horvath, Agrp neurons mediate Sirt's action on the melanocortin system and energy balace: roles for Sirt1 in neuronal firing and synaptic plasticity, 30 (2011) 11815–11825. doi:10.1523/JNEUROSCI.2234-10.2010.Agrp.

[54] D.A. Velásquez, G. Martínez, A. Romero, M.J. Vázquez, K.D. Boit, I.G. Dopeso-Reyes, M. López, A. Vidal, R. Nogueiras, C. Diéguez, The Central Sirtuin 1/p53 Pathway Is Essential for the Orexigenic Action of Ghrelin, Diabetes. 60 (2011) 1177 LP-1185. doi:org/10.2337/db10-0802.

[55] R. Nogueiras, M. López, R. Lage, D. Perez-Tilve, P. Pfluger, H. Mendieta-Zerón, M. Sakkou, P. Wiedmer, S.C. Benoit, R. Datta, J.Z. Dong, M. Culler, M. Sleeman, A. Vidal-Puig, T. Horvath, M. Treier, C. Diéguez, M.H. Tschöp, Bsx, a novel hypothalamic factor linking feeding with locomotor activity, is regulated by energy availability, Endocrinology. 149 (2008) 3009–3015. doi:10.1210/en.2007-1684.

[56] A. Brunet, L.B. Sweeney, J.F. Sturgill, K.F. Chua, P.L. Greer, Y. Lin, H. Tran, S.E. Ross, R. Mostoslavsky, H.Y. Cohen, L.S. Hu, H.-L. Cheng, M.P. Jedrychowski, S.P. Gygi, D.A. Sinclair, F.W. Alt, M.E. Greenberg, Stress-Dependent Regulation of FOXO Transcription Factors by the SIRT1 Deacetylase, Science (80-.). 303 (2004) 2011 LP-2015. doi:10.1126/science.1094647.

[57] P.S. Pardo, J.S. Mohamed, M.A. Lopez, A.M. Boriek, Induction of Sirt1 by

mechanical stretch of skeletal muscle through the early response factor EGR1 triggers an antioxidative response, J. Biol. Chem. 286 (2011) 2559–2566. doi:10.1074/jbc.M110.149153.

[58] A.J. Physiol, R. Integr, C. Physiol, I.M. Chapman, E.A. Goble, G.A. Wittert, J.E. Morley, K. Beckoff, C.G. Macintosh, J.M. Wishart, A. Howard, M. Horowitz, K.L. Jones, G. Liver, I.A.N.M. Chapman, M. Ian, G.A. Wit-, Effect of intravenous glucose and euglycemic insulin infusions on short-term appetite and food intake appetite in the elderly, (1998) 596–603.

[59] D. Burdakov, S.M. Luckman, A. Verkhratsky, Glucose-sensing neurons of the hypothalamus, Philos. Trans. R. Soc. B Biol. Sci. 360 (2005) 2227–2235. doi:10.1098/rstb.2005.1763.

[60] B.F. Belgardt, T. Okamura, J.C. Brüning, Hormone and glucose signalling in POMC and AgRP neurons, J. Physiol. 587 (2009) 5305–5314. doi:10.1113/jphysiol.2009.179192.

[61] L.E. Parton, C.P. Ye, R. Coppari, P.J. Enriori, B. Choi, C.-Y. Zhang, C. Xu, C.R. Vianna, N. Balthasar, C.E. Lee, J.K. Elmquist, M.A. Cowley, B.B. Lowell, Glucose sensing by POMC neurons regulates glucose homeostasis and is impaired in obesity, Nature. 449 (2007) 228. doi:org/10.1038/nature06098.

[62] M. Claret, M.A. Smith, R.L. Batterham, C. Selman, A.I. Choudhury, L.G.D. Fryer, M. Clements, H. Al-qassab, H. Heffron, A.W. Xu, J.R. Speakman, G.S. Barsh, B. Viollet, S. Vaulont, M.L.J. Ashford, D. Carling, D.J. Withers, Jci0731516, 117 (2007). doi:10.1172/JCI31516.suming.

[63] N. Ibrahim, M.A. Bosch, J.L. Smart, J. Qiu, M. Rubinstein, O.K. Rønnekleiv, M.J. Low, M.J. Kelly, Hypothalamic proopiomelanocortin neurons are glucose responsive and express KATPchannels, Endocrinology. 144 (2003) 1331–1340. doi:10.1210/en.2002-221033.

[64] S.L. Padilla, J.S. Carmody, L.M. Zeltser, Pomc-expressing progenitors give rise to antagonistic neuronal populations in hypothalamic feeding circuits, Nat. Med.

16 (2010) 403. doi.org/10.1038/nm.2126.

[65] E. Sanz, A. Quintana, J.D. Deem, R.A. Steiner, R.D. Palmiter, G.S. McKnight, Fertility-regulating Kiss1 neurons arise from hypothalamic POMC-expressing progenitors, J. Neurosci. 35 (2015) 5549 LP-5556. doi:10.1523/JNEUROSCI.3614-14.2015.

[66] S. Muroya, T. Yada, S. Shioda, M. Takigawa, Glucose-sensitive neurons in the rat arcuate nucleus contain neuropeptide Y, Neurosci. Lett. 264 (1999) 113–116. doi:https://doi.org/10.1016/S0304-3940(99)00185-8.

[67] L. Hao, Z. Sheng, J. Potian, A. Deak, C. Rohowsky-Kochan, V.H. Routh, Lipopolysaccharide (LPS) and tumor necrosis factor alpha (TNFα) blunt the response of Neuropeptide Y/Agouti-related peptide (NPY/AgRP) glucose inhibited (GI) neurons to decreased glucose, Brain Res. 1648 (2016) 181–192. doi:https://doi.org/10.1016/j.brainres.2016.07.035.

[68] A.C. Könner, R. Janoschek, L. Plum, S.D. Jordan, E. Rother, X. Ma, C. Xu, P. Enriori, B. Hampel, G.S. Barsh, C.R. Kahn, M.A. Cowley, F.M. Ashcroft, J.C. Brüning, Insulin Action in AgRP-Expressing Neurons Is Required for Suppression of Hepatic Glucose Production, Cell Metab. 5 (2007) 438–449. doi:10.1016/j.cmet.2007.05.004.

[69] T. Kitamura, Y. Feng, Y. Ido Kitamura, S.C. Chua Jr, A.W. Xu, G.S. Barsh, L. Rossetti, D. Accili, Forkhead protein FoxO1 mediates Agrp-dependent effects of leptin on food intake, Nat. Med. 12 (2006) 534. doi:org/10.1038/nm1392.

[70] L. Varela, M.J. Vázquez, F. Cordido, R. Nogueiras, A. Vidal-Puig, C. Diéguez, M. López, Ghrelin and lipid metabolism: Key partners in energy balance, J. Mol. Endocrinol. 46 (2011) 43–63. doi:10.1677/JME-10-0068.

[71] W. Ma, G. Fuentes, X. Shi, C. Verma, G.K. Radda, W. Han, FoxO1 negatively regulates leptin-induced POMC transcription through its direct interaction with STAT3, Biochem. J. 466 (2015) 291 LP-298. doi:10.1042/BJ20141109.

[72] H. Inoue, W. Ogawa, A. Asakawa, Y. Okamoto, A. Nishizawa, M. Matsumoto, K.

Teshigawara, Y. Matsuki, E. Watanabe, R. Hiramatsu, K. Notohara, K. Katayose, H. Okamura, C.R. Kahn, T. Noda, K. Takeda, S. Akira, A. Inui, M. Kasuga, Role of hepatic STAT3 in brain-insulin action on hepatic glucose production, Cell Metab. 3 (2006) 267–275. doi:10.1016/j.cmet.2006.02.009.

[73] S.M. Steculorum, K. Timper, L. Engström Ruud, N. Evers, L. Paeger, S. Bremser, P. Kloppenburg, J.C. Brüning, Inhibition of P2Y6 Signaling in AgRP Neurons Reduces Food Intake and Improves Systemic Insulin Sensitivity in Obesity, Cell Rep. 18 (2017) 1587–1597. doi:10.1016/j.celrep.2017.01.047.

[74] J. Deng, F. Yuan, Y. Guo, Y. Xiao, Y. Niu, Y. Deng, X. Han, Y. Guan, S. Chen, F. Guo, Deletion of ATF4 in AgRP neurons promotes fat loss mainly via increasing energy expenditure, Diabetes. 66 (2017) 640–650. doi:10.2337/db16-0954.

[75] L. Rodríguez-Berdini, B.L. Caputto, Lipid Metabolism in Neurons: A Brief Story of a Novel c-Fos-Dependent Mechanism for the Regulation of Their Synthesis, Front. Cell. Neurosci. 13 (2019) 198. doi:10.3389/fncel.2019.00198.

[76] P. Mergenthaler, U. Lindauer, G.A. Dienel, A. Meisel, Sugar for the brain: the role of glucose in physiological and pathological brain function., Trends Neurosci. 36 (2013) 587–597. doi:10.1016/j.tins.2013.07.001.

[77] D. Ebert, R.G. Haller, M.E. Walton, Energy Contribution of Octanoate to Intact Rat Brain Metabolism Measured by ¹³C Nuclear Magnetic Resonance Spectroscopy, J. Neurosci. 23 (2003) 5928 LP-5935. doi:10.1523/JNEUROSCI.23-13-05928.2003.

[78] S.D. Jordan, A.C. Könner, J.C. Brüning, Sensing the fuels: glucose and lipid signaling in the CNS controlling energy homeostasis, Cell. Mol. Life Sci. 67 (2010) 3255–3273. doi:10.1007/s00018-010-0414-7.

[79] S.I. Rapoport, M.C.J. Chang, A.A. Spector, Delivery and turnover of plasma-derived essential PUFAs in mammalian brain., J. Lipid Res. 42 (2001) 678–685.

[80] N.H. Smith QR1, Fatty acid uptake and incorporation in brain: studies with the perfusion model., J Mol Neurosci. (2001). doi:10.1385/JMN:16:2-3:167.

[81] J.M. Inloes, K.-L. Hsu, M.M. Dix, A. Viader, K. Masuda, T. Takei, M.R. Wood, B.F. Cravatt, The hereditary spastic paraplegia-related enzyme DDHD2 is a principal brain triglyceride lipase, Proc. Natl. Acad. Sci. 111 (2014) 14924 LP-14929. doi:10.1073/pnas.1413706111.

[82] C. Yang, X. Wang, J. Wang, X. Wang, W. Chen, N. Lu, S. Siniossoglou, Z. Yao, K. Liu, Rewiring Neuronal Glycerolipid Metabolism Determines the Extent of Axon Regeneration, Neuron. 105 (2020) 276–292.e5. doi:https://doi.org/10.1016/j.neuron.2019.10.009.

[83] S. Obici, Z. Feng, K. Morgan, D. Stein, G. Karkanias, L. Rossetti, Central Administration of Oleic Acid Inhibits Glucose Production and Food Intake, Diabetes. 51 (2002) 271 LP-275. doi:org/10.2337/diabetes.51.2.2.271.

[84] N.R.V. Dragano, C. Solon, A.F. Ramalho, R.F. de Moura, D.S. Razolli, E. Christiansen, C. Azevedo, T. Ulven, L.A. Velloso, Polyunsaturated fatty acid receptors, GPR40 and GPR120, are expressed in the hypothalamus and control energy homeostasis and inflammation, J. Neuroinflammation. 14 (2017) 1–16. doi:10.1186/s12974-017-0869-7.

[85] C.F. Burant, Activation of GPR40 as a therapeutic target for the treatment of type 2 diabetes, Diabetes Care. 36 (2013) 175–179. doi:10.2337/dcS13-2037.

[86] M. López, R. Nogueiras, M. Tena-Sempere, C. Diéguez, Hypothalamic AMPK: a canonical regulator of whole-body energy balance, Nat. Rev. Endocrinol. 12 (2016) 421. doi:org/10.1038/nrendo.2016.67.

[87] M.K.Q. Huynh, A.W. Kinyua, D.J. Yang, K.W. Kim, Hypothalamic AMPK as a Regulator of Energy Homeostasis, Neural Plast. 2016 (2016). doi:10.1155/2016/2754078.

[88] Z.J. JulianSwierczynski, Elzbieta Goykea, Justyna Korczynska, Acetyl-CoA carboxylase and fatty acid synthase activities in human hypothalamus, Neurosci. Lett. 444 (2008) 209–211. doi:10.1016/jneulet.2008.08.046.

[89] M. López, R. Lage, A.K. Saha, D. Pérez-Tilve, M.J. Vázquez, L. Varela, S. Sangiao-

Alvarellos, S. Tovar, K. Raghay, S. Rodríguez-Cuenca, R.M. Deoliveira, T. Castañeda, R. Datta, J.Z. Dong, M. Culler, M.W. Sleeman, C. V Álvarez, R. Gallego, C.J. Lelliott, D. Carling, M.H. Tschöp, C. Diéguez, A. Vidal-Puig, Hypothalamic Fatty Acid Metabolism Mediates the Orexigenic Action of Ghrelin, Cell Metab. 7 (2008) 389–399. doi:10.1016/j.cmet.2008.03.006.

[90] Y. Minokoshi, T. Alquier, N. Furukawa, Y.-B. Kim, A. Lee, B. Xue, J. Mu, F. Foufelle, P. Ferré, M.J. Birnbaum, B.J. Stuck, B.B. Kahn, AMP-kinase regulates food intake by responding to hormonal and nutrient signals in the hypothalamus, Nature. 428 (2004) 569. doi:org/10.1038/nature02440.

[91] F.P.K. Thomas M. Loftus, Donna E. Jaworsky, Gojeb L. Frehywot, Craig A. Townsend, Gabriele V. Ronnett, M. Daniel Lane, Reduced Food Intake and Body Weight in Mice Treated with Fatty Acid Synthase Inhibitors, Science (80-.). 288 (2000) 2379–2382. doi:10.1126/science.288.5475.2379.

[92] R. Nogueiras, P. Wiedmer, D. Perez-Tilve, C. Veyrat-Durebex, J.M. Keogh, G.M. Sutton, P.T. Pfluger, T.R. Castaneda, S. Neschen, S.M. Hofmann, P.N. Howles, D.A. Morgan, S.C. Benoit, I. Szanto, B. Schrott, A. Schürmann, H.G. Joost, C. Hammond, D.Y. Hui, S.C. Woods, K. Rahmouni, A.A. Butler, I.S. Farooqi, S. O'Rahilly, F. Rohner-Jeanrenaud, M.H. Tschöp, The central melanocortin system directly controls peripheral lipid metabolism, J. Clin. Invest. 117 (2007) 3475–3488. doi:10.1172/JCI31743.

[93] P.D. Raposinho, R.B. White, M.L. Aubert, The melanocortin agonist Melanotan-II reduces the orexigenic and adipogenic effects of neuropeptide Y (NPY) but does not affect the NPY-driven suppressive effects on the gonadotropic and somatotropic axes in the male rat., J. Neuroendocrinol. 15 (2003) 173–81. doi:10.1046/j.1365-2826.2003.00962.x.

[94] J.P. Cavalcanti-de-Albuquerque, M.R. Zimmer, J. Bober, M.O. Dietrich, Rapid shift in substrate utilization driven by hypothalamic Agrp neurons, BioRxiv. (2016). doi:org/10.1101/086348.

[95] A. Reichenbach, R. Stark, M. Mequinion, R.R.G. Denis, J.F. Goularte, R.E. Clarke, S.H. Lockie, M.B. Lemus, G.M. Kowalski, C.R. Bruce, C. Huang, R.B. Schittenhelm, R.L. Mynatt, B.J. Oldfield, M.J. Watt, S. Luquet, Z.B. Andrews, AgRP Neurons Require Carnitine Acetyltransferase to Regulate Metabolic Flexibility and Peripheral Nutrient Partitioning, Cell Rep. 22 (2018) 1745–1759. doi:10.1016/j.celrep.2018.01.067.

[96] H. Bin Ruan, M.O. Dietrich, Z.W. Liu, M.R. Zimmer, M.D. Li, J.P. Singh, K. Zhang, R. Yin, J. Wu, T.L. Horvath, X. Yang, O-GlcNAc transferase enables AgRP neurons to suppress browning of white fat, Cell. 159 (2014) 306–317. doi:10.1016/j.cell.2014.09.010.

[97] C. Contreras, R. Nogueiras, C. Diéguez, K. Rahmouni, M. López, Traveling from the hypothalamus to the adipose tissue: The thermogenic pathway, Redox Biol. 12 (2017) 854–863. doi:10.1016/j.redox.2017.04.019.

[98] S. Eaton, K.B. Bartlett, M. Pourfarzam, Mammalian mitochondrial β-oxidation, Biochem. J. 320 (1996) 345–357. doi:10.1042/bj3200345.

[99] J.D. McGarry, N.F. Brown, The Mitochondrial Carnitine Palmitoyltransferase System — From Concept to Molecular Analysis, Eur. J. Biochem. 244 (1997) 1–14. doi:10.1111/j.1432-1033.1997.00001.x.

[100] A.G. Cordente, E. López-Viñas, M.I. Vázquez, J.H. Swiegers, I.S. Pretorius, P. Gómez-Puertas, F.G. Hegardt, G. Asins, D. Serra, Redesign of carnitine acetyltransferase specificity by protein engineering, J. Biol. Chem. 279 (2004) 33899–33908. doi:10.1074/jbc.M402685200.

[101] M. Schreurs, F. Kuipers, F.R. Van Der Leij, Regulatory enzymes of mitochondrial β-oxidation as targets for treatment of the metabolic syndrome, Obes. Rev. 11 (2010) 380–388. doi:10.1111/j.1467-789X.2009.00642.x.

[102] V. Esser, M. Kuwajima, C.H. Britton, K. Krishnan, D.W. Foster, J.D. McGarry, Inhibitors of mitochondrial carnitine palmitoyltransferase I limit the action of proteases on the enzyme. Isolation and partial amino acid analysis of a

truncated form of the rat liver isozyme, J. Biol. Chem. 268 (1993) 5810—5816. http://europepmc.org/abstract/MED/8449947.

[103] V. Esser, N.F. Brown, A.T. Cowan, D.W. Foster, J.D. McGarry, Expression of a cDNA isolated from rat brown adipose tissue and heart identifies the product as the muscle isoform of carnitine palmitoyltransferase I (M-CPT I): M-CPT I is the predominant CPT I isoform expressed in both white (epididymal) and brown adipo, J. Biol. Chem. 271 (1996) 6972–6977. doi:10.1074/jbc.271.12.6972.

[104] J.-P. Bonnefont, F. Djouadi, C. Prip-Buus, S. Gobin, A. Munnich, J. Bastin, Carnitine palmitoyltransferases 1 and 2: biochemical, molecular and medical aspects, Mol. Aspects Med. 25 (2004) 495–520. doi:https://doi.org/10.1016/j.mam.2004.06.004.

[105] M. Lopes-Marques, I.L.S. Delgado, R. Ruivo, Y. Torres, S.B. Sainath, E. Rocha, I. Cunha, M.M. Santos, L.F.C. Castro, The Origin and Diversity of Cpt1 Genes in Vertebrate Species, PLoS One. 10 (2015) 1–14. doi:10.1371/journal.pone.0138447.

[106] I.R. Schlaepfer, M. Joshi, CPT1A-mediated Fat Oxidation, Mechanisms, and Therapeutic Potential, Endocrinology. 161 (2020). doi:10.1210/endocr/bqz046.

[107] N.T. Price, F.R. Van Der Leij, V.N. Jackson, C.G. Corstorphine, R. Thomson, A. Sorensen, V.A. Zammit, A novel brain-expressed protein related to carnitine palmitoyltransferase I, Genomics. 80 (2002) 433–442. doi:10.1006/geno.2002.6845.

[108] A.Y. Sierra, E. Gratacós, P. Carrasco, J. Clotet, J. Ureña, D. Serra, G. Asins, F.G. Hegardt, N. Casals, CPT1c is localized in endoplasmic reticulum of neurons and has carnitine palmitoyltransferase activity, J. Biol. Chem. 283 (2008) 6878–6885. doi:10.1074/jbc.M707965200.

[109] J.A. Ontko, M.L. Johns, Evaluation of malonyl-CoA in the regulation of long-chain fatty acid oxidation in the liver. Evidence for an unidentified regulatory component of the system, Biochem. J. 192 (1980) 959–962.

doi:10.1042/bj1920959.

[110] G.A. Cook, D.A. Otto, N.W. Cornell, Differential inhibition of ketogenesis by malonyl-CoA in mitochondria from fed and starved rats, Biochem. J. 192 (1980) 955–958. doi:10.1042/bj1920955.

[111] E.D. Saggerson, C.A. Carpenter, Malonyl CoA inhibition of carnitine acyltransferase activities, FEBS Lett. 137 (1982) 124–128. doi:10.1016/0014-5793(82)80329-3.

[112] Z. Hu, S.H. Cha, S. Chohnan, M.D. Lane, Hypothalamic malonyl-CoA as a mediator of feeding behavior, Proc. Natl. Acad. Sci. 100 (2003) 12624 LP-12629. doi:10.1073/pnas.1834402100.

[113] S. Obici, Z. Feng, A. Arduini, R. Conti, L. Rossetti, Inhibition of hypothalamic carnitine palmitoyltransferase-1 decreases food intake and glucose production, Nat Med. 9 (2003) 756–761. doi:10.1038/nm873.

[114] M. Morillas, P. Gómez-Puertas, A. Bentebibel, E. Sellés, N. Casals, A. Valencia, F.G. Hegardt, G. Asins, D. Serra, Identification of conserved amino acid residues in rat liver carnitine palmitoyltransferase I critical for malonyl-CoA inhibition: Mutation of methionine 593 abolishes malonyl-CoA inhibition, J. Biol. Chem. 278 (2003) 9058–9063. doi:10.1074/jbc.M209999200.

[115] P. Mera, J.F. Mir, G. Fabriàs, J. Casas, A.S.H. Costa, M.I. Malandrino, J.-A. Fernández-López, X. Remesar, S. Gao, S. Chohnan, M.S. Rodríguez-Peña, H. Petry, G. Asins, F.G. Hegardt, L. Herrero, D. Serra, Long-Term Increased Carnitine Palmitoyltransferase 1A Expression in Ventromedial Hypotalamus Causes Hyperphagia and Alters the Hypothalamic Lipidomic Profile, PLoS One. 9 (2014) 1–13. doi:10.1371/journal.pone.0097195.

[116] S. Gao, W. Keung, D. Serra, W. Wang, P. Carrasco, N. Casals, F.G. Hegardt, T.H. Moran, G.D. Lopaschuk, Malonyl-CoA mediates leptin hypothalamic control of feeding independent of inhibition of CPT-1a, Am. J. Physiol. Integr. Comp. Physiol. 301 (2011) R209–R217. doi:10.1152/ajpregu.00092.2011.

[117] N.J. Rothwell, M.J. Stock, A role for brown adipose tissue in diet-induced thermogenesis, Nature. 281 (1979) 31. doi:org/10.1038/281031a0.

[118] M.D. Marian Apfelbaum, M.D. Jean Bostsarron, M.D. Dimitri Lacatis, Effect of caloric restriction and excessive caloric intake on energy expenditure, Am. J. Clin. Nutr. 24 (1971) 1405–1409.

[119] X. Yang, H.-B. Ruan, Neuronal Control of Adaptive Thermogenesis, Front. Endocrinol. (Lausanne). 6 (2015) 1–9. doi:10.3389/fendo.2015.00149.

[120] Y.H. Yasuda T, Masaki T, Kakuma T, Hypothalamic melanocortin system regulates sympathetic nerve activity in brown adipose tissue, Exp Biol Med. 229(3):235 (2004). doi:10.1177/153537020422900303.

[121] C.S. Wu, O.Y.N. Bongmba, J. Yue, J.H. Lee, L. Lin, K. Saito, G. Pradhan, D.P. Li, H.L. Pan, A. Xu, S. Guo, Y. Xu, Y. Sun, Suppression of GHS-R in AgRP neurons mitigates diet-induced obesity by activating thermogenesis, Int. J. Mol. Sci. 18 (2017). doi:10.3390/ijms18040832.

[122] W. Verplanck, J. Hayes, Eating and drinking as a function of maintenance schedule, J. Comp. Physiol. Psychol. 46 (1953) 327–333. doi:10.1037/h0055380.

[123] T. Vokes, Water Homeostasis, Annu. Rev. Nutr. 7 (1987) 383–406. doi:10.1146/annurev.nu.07.070187.002123.

[124] J. Gandy, Water intake: validity of population assessment and recommendations., Eur. J. Nutr. 54 Suppl 2 (2015) 11–16. doi:10.1007/s00394-015-0944-8.

[125] E. Jéquier, F. Constant, Water as an essential nutrient: the physiological basis of hydration, Eur. J. Clin. Nutr. 64 (2010) 115–123. doi:10.1038/ejcn.2009.111.

[126] M.N. Sawka, S.N. Cheuvront, I. Carter Robert, Human Water Needs, Nutr. Rev. 63 (2005) S30–S39. doi:10.1111/j.1753-4887.2005.tb00152.x.

[127] W.H. Streng, H.E. Huber, J.T. Carstensen, Relationship between Osmolality and Osmolarity, J. Pharm. Sci. 67 (1978) 384–386. doi:10.1002/jps.2600670330.

[128] M. Caon, Osmoles, osmolality and osmotic pressure: Clarifying the puzzle of

solution concentration, Contemp. Nurse. 29 (2008) 92–99. doi:10.5172/conu.673.29.1.92.

[129] W. V Dorwart, L. Chalmers, Comparison of Methods for Calculating Serum Osmolality from Chemical Concentrations, and the Prognostic Value of Such Calculations, Clin. Chem. 21 (1975) 190–194. doi:10.1093/clinchem/21.2.190.

[130] S.N. Cheuvront, R.W. Kenefick, Dehydration: Physiology, Assessment, and Performance Effects, in: Compr. Physiol., American Cancer Society, 2014: pp. 257–285. doi:10.1002/cphy.c130017.

[131] R. Joynt, Evidence in support of Verney's concept of the osmoreceptor, Trans. Am. Neurol. Assoc. 90 (1965) 199—202.

[132] E.B. Verney, Croonian Lecture - The antidiuretic hormone and the factors which determine its release, Proc. R. Soc. London. Ser. B - Biol. Sci. 135 (1947) 25–106. doi:10.1098/rspb.1947.0037.

[133] H.M. Stauss, Baroreceptor reflex function, Am. J. Physiol. Integr. Comp. Physiol. 283 (2002) R284–R286. doi:10.1152/ajpregu.00219.2002.

[134] N. Muñoz-Durango, C.A. Fuentes, A.E. Castillo, L.M. González-Gómez, A. Vecchiola, C.E. Fardella, A.M. Kalergis, Role of the Renin-Angiotensin-Aldosterone System beyond Blood Pressure Regulation: Molecular and Cellular Mechanisms Involved in End-Organ Damage during Arterial Hypertension., Int. J. Mol. Sci. 17 (2016). doi:10.3390/ijms17070797.

[135] N. Japundžić-Žigon, Vasopressin and oxytocin in control of the cardiovascular system., Curr. Neuropharmacol. 11 (2013) 218–230. doi:10.2174/1570159X11311020008.

[136] L. Bankir, Antidiuretic action of vasopressin: quantitative aspects and interaction between V1a and V2 receptor-mediated effects, Cardiovasc. Res. 51 (2001) 372–390. doi:10.1016/S0008-6363(01)00328-5.

[137] R.S. Wildin, D.E. Cogdell, V. Valadez, AVPR2 variants and V2 vasopressin receptor function in nephrogenic diabetes insipidus, Kidney Int. 54 (1998) 1909–

1922. doi:10.1046/j.1523-1755.1998.00214.x.

[138] D.G. Bichet, Vasopressin at Central Levels and Consequences of Dehydration, Ann. Nutr. Metab. 68(suppl 2 (2016) 19–23. doi:10.1159/000446200.

[139] B.M. Altura, B.T. Altura, Vascular smooth muscle and neurohypophyseal hormones, Fed. Proc. 36 (1977) 1853—1860.

[140] M.A. Sparks, S.D. Crowley, S.B. Gurley, M. Mirotsou, T.M. Coffman, Classical Renin-Angiotensin system in kidney physiology., Compr. Physiol. 4 (2014) 1201–1228. doi:10.1002/cphy.c130040.

[141] M.K. Ames, C.E. Atkins, B. Pitt, The renin-angiotensin-aldosterone system and its suppression., J. Vet. Intern. Med. 33 (2019) 363–382. doi:10.1111/jvim.15454.

[142] W. De Mello, E. Frohlich, Clinical Perspectives and Fundamental Aspects of Local Cardiovascular and Renal Renin-Angiotensin Systems, Front. Endocrinol. (Lausanne). 5 (2014) 16. doi:10.3389/fendo.2014.00016.

[143] H. Lu, L.A. Cassis, C.W. Vander Kooi, A. Daugherty, Structure and functions of angiotensinogen., Hypertens. Res. 39 (2016) 492–500. doi:10.1038/hr.2016.17.

[144] C. Dasgupta, L. Zhang, Angiotensin II receptors and drug discovery in cardiovascular disease., Drug Discov. Today. 16 (2011) 22–34. doi:10.1016/j.drudis.2010.11.016.

[145] B. Williams, Angiotensin II and the pathophysiology of cardiovascular remodeling, Am. J. Cardiol. 87 (2001) 10–17. doi:10.1016/S0002-9149(01)01507-7.

[146] A.M. Hilzendeger, M.D. Cassell, D.R. Davis, H.M. Stauss, A.L. Mark, J.L. Grobe, C.D. Sigmund, Angiotensin type 1a receptors in the subfornical organ are required for deoxycorticosterone acetate-salt hypertension, Hypertension. 61 (2013) 716–722. doi:10.1161/HYPERTENSIONAHA.111.00356.

[147] M.J. McKinley, M.J. Cairns, D.A. Denton, G. Egan, M.L. Mathai, A. Uschakov, J.D. Wade, R.S. Weisinger, B.J. Oldfield, Physiological and pathophysiological

influences on thirst, Physiol. Behav. 81 (2004) 795–803. doi:https://doi.org/10.1016/j.physbeh.2004.04.055.

[148] M. Millard-Stafford, D.M. Wendland, N.K. O'Dea, T.L. Norman, Thirst and hydration status in everyday life, Nutr. Rev. 70 (2012) S147–S151. doi:10.1111/j.1753-4887.2012.00527.x.

[149] P.J. Ryan, The Neurocircuitry of fluid satiation., Physiol. Rep. 6 (2018) e13744. doi:10.14814/phy2.13744.

[150] M.J. McKinley, D.A. Denton, P.J. Ryan, S.T. Yao, A. Stefanidis, B.J. Oldfield, From sensory circumventricular organs to cerebral cortex: Neural pathways controlling thirst and hunger, J. Neuroendocrinol. 31 (2019) e12689. doi:10.1111/jne.12689.

[151] M. Jurzak, H.A. Schmid, Vasopressin and sensory circumventricular organs, in: I.J.A. Urban, J.P.H. Burbach, D. [De Wed] (Eds.), Adv. Brain Vasopressin, Elsevier, 1999: pp. 221–245. doi:https://doi.org/10.1016/S0079-6123(08)61572-1.

[152] Y. Oka, M. Ye, C.S. Zuker, Thirst driving and suppressing signals encoded by distinct neural populations in the brain, Nature. 520 (2015) 349–352. doi:10.1038/nature14108.

[153] C.A. Zimmerman, D.E. Leib, Z.A. Knight, Neural circuits underlying thirst and fluid homeostasis., Nat. Rev. Neurosci. 18 (2017) 459–469. doi:10.1038/nrn.2017.71.

[154] D.E. Leib, C.A. Zimmerman, A. Poormoghaddam, E.L. Huey, J.S. Ahn, Y.-C. Lin, C.L. Tan, Y. Chen, Z.A. Knight, The Forebrain Thirst Circuit Drives Drinking through Negative Reinforcement., Neuron. 96 (2017) 1272–1281.e4. doi:10.1016/j.neuron.2017.11.041.

[155] C.A. Zimmerman, Y.-C. Lin, D.E. Leib, L. Guo, E.L. Huey, G.E. Daly, Y. Chen, Z.A. Knight, Thirst neurons anticipate the homeostatic consequences of eating and drinking, Nature. 537 (2016) 680. doi:10.1038/nature18950.

[156] T. Matsuda, T.Y. Hiyama, F. Niimura, T. Matsusaka, A. Fukamizu, K. Kobayashi, K. Kobayashi, M. Noda, Distinct neural mechanisms for the control of thirst and

salt appetite in the subfornical organ, Nat. Neurosci. 20 (2017) 230–241. doi:10.1038/nn.4463.

[157] S.J. Son, J.A. Filosa, E.S. Potapenko, V.C. Biancardi, H. Zheng, K.P. Patel, V.A. Tobin, M. Ludwig, J.E. Stern, Dendritic Peptide Release Mediates Interpopulation Crosstalk between Neurosecretory and Preautonomic Networks, Neuron. 78 (2013) 1036–1049. doi:10.1016/j.neuron.2013.04.025.

[158] M. Prager-Khoutorsky, C.W. Bourque, Mechanical Basis of Osmosensory Transduction in Magnocellular Neurosecretory Neurones of the Rat Supraoptic Nucleus, J. Neuroendocrinol. 27 (2015) 507–515. doi:10.1111/jne.12270.

[159] Y. Mandelblat-Cerf, A. Kim, C.R. Burgess, S. Subramanian, B.A. Tannous, B.B. Lowell, M.L. Andermann, Bidirectional Anticipation of Future Osmotic Challenges by Vasopressin Neurons., Neuron. 93 (2017) 57–65. doi:10.1016/j.neuron.2016.11.021.

[160] C.A. Zimmerman, E.L. Huey, J.S. Ahn, L.R. Beutler, C.L. Tan, S. Kosar, L. Bai, Y. Chen, T. V Corpuz, L. Madisen, H. Zeng, Z.A. Knight, A gut-to-brain signal of fluid osmolarity controls thirst satiation., Nature. 568 (2019) 98–102. doi:10.1038/s41586-019-1066-x.

[161] K.J. Pulman, W.M. Fry, G.T. Cottrell, A. V. Ferguson, The subfornical organ: A central target for circulating feeding signals, J. Neurosci. 26 (2006) 2022–2030. doi:10.1523/JNEUROSCI.3218-05.2006.

[162] C.N. Young, D.A. Morgan, S.D. Butler, A.L. Mark, R.L. Davisson, The brain subfornical organ mediates leptin-induced increases in renal sympathetic activity but not its metabolic effects., Hypertens. (Dallas, Tex. 1979). 61 (2013) 737–744. doi:10.1161/HYPERTENSIONAHA.111.00405.

[163] C.N. Young, D.A. Morgan, S.D. Butler, K. Rahmouni, S.B. Gurley, T.M. Coffman, A.L. Mark, R.L. Davisson, Angiotensin type 1a receptors in the forebrain subfornical organ facilitate leptin-induced weight loss through brown adipose tissue thermogenesis, Mol. Metab. 4 (2015) 337–343.

doi:10.1016/j.molmet.2015.01.007.

[164] K.E. Claflin, J.A. Sandgren, A.M. Lambertz, B.J. Weidemann, N.K. Littlejohn, C.M.L. Burnett, N.A. Pearson, D.A. Morgan, K.N. Gibson-corley, K. Rahmouni, J.L. Grobe, Angiotensin AT 1A receptors on leptin receptor – expressing cells control resting metabolism, 127 (2017) 1–11. doi:10.1172/JCI88641.

[165] L.R. Beutler, Y. Chen, J.S. Ahn, Y.-C. Lin, R.A. Essner, Z.A. Knight, Dynamics of Gut-Brain Communication Underlying Hunger., Neuron. 96 (2017) 461–475.e5. doi:10.1016/j.neuron.2017.09.043.

[166] M.P. Rosas-Arellano, L.P. Solano-Flores, J. Ciriello, Arcuate nucleus inputs onto subfornical organ neurons that respond to plasma hypernatremia and angiotensin II, Brain Res. 707 (1996) 308–313. doi:https://doi.org/10.1016/0006-8993(95)01368-7.

[167] E.P. Zorrilla, K. Inoue, É.M. Fekete, A. Tabarin, G.R. Valdez, G.F. Koob, Measuring meals: structure of prandial food and water intake of rats, Am. J. Physiol. Integr. Comp. Physiol. 288 (2005) R1450–R1467. doi:10.1152/ajpregu.00175.2004.

[168] D.E. Leib, C.A. Zimmerman, Z.A. Knight, Thirst., Curr. Biol. 26 (2016) R1260–R1265. doi:10.1016/j.cub.2016.11.019.

[169] J.F. Mir, S. Zagmutt, M.P. Lichtenstein, J. García-Villoria, M. Weber, A. Gracia, G. Fabriàs, J. Casas, M. López, N. Casals, A. Ribes, C. Suñol, L. Herrero, D. Serra, Ghrelin Causes a Decline in GABA Release by Reducing Fatty Acid Oxidation in Cortex., Mol. Neurobiol. 55 (2018) 7216–7228. doi:10.1007/s12035-018-0921-3.

[170] Q. Wang, C. Liu, A. Uchida, J.-C. Chuang, A. Walker, T. Liu, S. Osborne-Lawrence, B.L. Mason, C. Mosher, E.D. Berglund, J.K. Elmquist, J.M. Zigman, Arcuate AgRP neurons mediate orexigenic and glucoregulatory actions of ghrelin., Mol. Metab. 3 (2014) 64–72. doi:10.1016/j.molmet.2013.10.001.

[171] E. Sanz, L. Yang, T. Su, D.R. Morris, G.S. McKnight, P.S. Amieux, Cell-type-specific isolation of ribosome-associated mRNA from complex tissues, Proc. Natl. Acad.

Sci. 106 (2009) 13939 LP-13944. doi:10.1073/pnas.0907143106.

[172] Q. Wu, M. Lemus, R. Stark, J. Bayliss, A. Reichenbach, S. Lockie, Z. Andrews, The Temporal Pattern of cfos Activation in Hypothalamic, Cortical, and Brainstem Nuclei in Response to Fasting and Refeeding in Male Mice, Endocrinology. 155 (2014) en20131831. doi:10.1210/en.2013-1831.

[173] A.C. Teilmann, A. Nygaard Madsen, B. Holst, J. Hau, B. Rozell, K.S.P. Abelson, Physiological and Pathological Impact of Blood Sampling by Retro-Bulbar Sinus Puncture and Facial Vein Phlebotomy in Laboratory Mice, PLoS One. 9 (2014) 1–19. doi:10.1371/journal.pone.0113225.

[174] P.G. Watson C., Chemoarchitectonic Atlas of the Mouse Brain Title, Elsevier Acad. Press. (2010).

[175] F. Sanger, S. Nicklen, A.R. Coulson, DNA sequencing with chain-terminating inhibitors., Proc. Natl. Acad. Sci. U. S. A. 74 (1977) 5463–5467. doi:10.1073/pnas.74.12.5463.

[176] A. Fischer, K. Jacobson, J. Rose, R. Zeller, Hematoxylin and Eosin Staining of Tissue and Cell Sections, CSH Protoc. 2008 (2008) pdb.prot4986. doi:10.1101/pdb.prot4986.

[177] X. Lin, C.A. Itoga, S. Taha, M.H. Li, R. Chen, K. Sami, F. Berton, W. Francesconi, X. Xu, c-Fos mapping of brain regions activated by multi-modal and electric foot shock stress, Neurobiol. Stress. 8 (2018) 92–102. doi:https://doi.org/10.1016/j.ynstr.2018.02.001.

[178] M. Galarraga, J. Campión, A. Muñoz-Barrutia, N. Boqué, H. Moreno, J.A. Martínez, F. Milagro, C. Ortiz-de-Solórzano, Adiposoft: automated software for the analysis of white adipose tissue cellularity in histological sections., J. Lipid Res. 53 (2012) 2791–2796. doi:10.1194/jlr.D023788.

[179] J.N. Betley, Z.F.H. Cao, K.D. Ritola, S.M. Sternson, Parallel, redundant circuit organization for homeostatic control of feeding behavior., Cell. 155 (2013) 1337–1350. doi:10.1016/j.cell.2013.11.002.

[180] R. Gupta, Y. Ma, M. Wang, M.D. Whim, AgRP-Expressing Adrenal Chromaffin Cells Are Involved in the Sympathetic Response to Fasting, Endocrinology. 158 (2017) 2572–2584. doi:10.1210/en.2016-1268.

[181] Y. Yang, D. Atasoy, H.H. Su, S.M. Sternson, Hunger States Switch a Flip-Flop Memory Circuit via a Synaptic AMPK-Dependent Positive Feedback Loop, Cell. 146 (2011) 992–1003. doi:https://doi.org/10.1016/j.cell.2011.07.039.

[182] S.-R. Chen, H. Chen, J.-J. Zhou, G. Pradhan, Y. Sun, H.-L. Pan, D.-P. Li, Ghrelin receptors mediate ghrelin-induced excitation of agouti-related protein/neuropeptide Y but not pro-opiomelanocortin neurons., J. Neurochem. 142 (2017) 512–520. doi:10.1111/jnc.14080.

[183] A.H. Shibata M., Banno R., Sugiyama M., Tominaga T., Onoue T., Tsunekawa T., Azuma Y., Hagiwara D., Lu W., Ito Y., Goto M., Suga H., Sugimura Y., Oiso Y., AgRP Neuron-Specific Deletion of Glucocorticoid Receptor Leads to Increased Energy Expenditure and Decreased Body Weight in Female Mice on a High-Fat Diet, Endocrinology. 157 (2016) 1457–1466. doi:org/10.1210/en.2015-1430.

[184] H. Huang, S.H. Lee, C. Ye, I.S. Lima, B.-C. Oh, B.B. Lowell, J.M. Zabolotny, Y.-B. Kim, ROCK1 in AgRP neurons regulates energy expenditure and locomotor activity in male mice., Endocrinology. 154 (2013) 3660–3670. doi:10.1210/en.2013-1343.

[185] S.M. Steculorum, J. Ruud, I. Karakasilioti, H. Backes, L. Engström Ruud, K. Timper, M.E. Hess, E. Tsaousidou, J. Mauer, M.C. Vogt, L. Paeger, S. Bremser, A.C. Klein, D.A. Morgan, P. Frommolt, P.T. Brinkkötter, P. Hammerschmidt, T. Benzing, K. Rahmouni, F.T. Wunderlich, P. Kloppenburg, J.C. Brüning, AgRP Neurons Control Systemic Insulin Sensitivity via Myostatin Expression in Brown Adipose Tissue., Cell. 165 (2016) 125–138. doi:10.1016/j.cell.2016.02.044.

[186] C.D. Morrison, G.J. Morton, K.D. Niswender, R.W. Gelling, M.W. Schwartz, Leptin inhibits hypothalamic Npy and Agrp gene expression via a mechanism that requires phosphatidylinositol 3-OH-kinase signaling., Am. J. Physiol.

Endocrinol. Metab. 289 (2005) E1051-7. doi:10.1152/ajpendo.00094.2005.

[187] B. Raud, D.G. Roy, A.S. Divakaruni, T.N. Tarasenko, R. Franke, E.H. Ma, B. Samborska, W.Y. Hsieh, A.H. Wong, P. Stüve, C. Arnold-Schrauf, M. Guderian, M. Lochner, S. Rampertaap, K. Romito, J. Monsale, M. Brönstrup, S.J. Bensinger, A.N. Murphy, P.J. McGuire, R.G. Jones, T. Sparwasser, L. Berod, Etomoxir Actions on Regulatory and Memory T Cells Are Independent of Cpt1a-Mediated Fatty Acid Oxidation., Cell Metab. 28 (2018) 504–515.e7. doi:10.1016/j.cmet.2018.06.002.

[188] C. Diéguez, G. Fruhbeck, M. López, Hypothalamic lipids and the regulation of energy homeostasis., Obes. Facts. 2 (2009) 126–135. doi:10.1159/000209251.

[189] C. Cruciani-Guglielmacci, M. López, M. Campana, H. le Stunff, Brain Ceramide Metabolism in the Control of Energy Balance, Front. Physiol. 8 (2017) 787. doi:10.3389/fphys.2017.00787.

[190] D.S. Paula Mera , Joan Francesc Mir , Gemma Fabriàs, Josefina Casas, Ana S. H. Costa, Maria Ida Malandrino, José-Antonio Fernández-López, Xavier Remesar, Su Gao, Shigeru Chohnan, Maria Sol Rodríguez-Peña, Harald Petry, Guillermina Asins, Fausto G. Hegardt, Lau, Long-Term Increased Carnitine Palmitoyltransferase 1A Expression in Ventromedial Hypotalamus Causes Hyperphagia and Alters the Hypothalamic Lipidomic Profile, PLoS One. (2004). doi:10.1371/journal.pone.0097195.

[191] A. Üner, G.H.M. Gonçalves, W. Li, M. Porceban, N. Caron, M. Schönke, E. Delpire, K. Sakimura, C. Bjørbæk, The role of GluN2A and GluN2B NMDA receptor subunits in AgRP and POMC neurons on body weight and glucose homeostasis, Mol. Metab. 4 (2015) 678–691. doi:10.1016/j.molmet.2015.06.010.

[192] M. Quiñones, O. Al-Massadi, C. Folgueira, S. Bremser, R. Gallego, L. Torres-Leal, R. Haddad-Tóvolli, C. García-Caceres, R. Hernandez-Bautista, B.Y.H. Lam, D. Beiroa, E. Sanchez-Rebordelo, A. Senra, J.A. Malagon, P. Valerio, M.F. Fondevila, J. Fernø, M.M. Malagon, R. Contreras, P. Pfluger, J.C. Brüning, G. Yeo, M. Tschöp,

C. Diéguez, M. López, M. Claret, P. Kloppenburg, G. Sabio, R. Nogueiras, p53 in AgRP neurons is required for protection against diet-induced obesity via JNK1, Nat. Commun. 9 (2018) 3432. doi:10.1038/s41467-018-05711-6.

[193] A. Reichenbach, R. Stark, M. Mequinion, S.H. Lockie, M.B. Lemus, R.L. Mynatt, S. Luquet, Z.B. Andrews, Carnitine acetyltransferase (Crat) in hunger-sensing AgRP neurons permits adaptation to calorie restriction., FASEB J. Off. Publ. Fed. Am. Soc. Exp. Biol. 32 (2018) fj201800634R. doi:10.1096/fj.201800634R.

[194] M.M. Witte, D. Resuehr, A.R. Chandler, A.K. Mehle, J.M. Overton, Female mice and rats exhibit species-specific metabolic and behavioral responses to ovariectomy, Gen. Comp. Endocrinol. 166 (2010) 520–528. doi:https://doi.org/10.1016/j.ygcen.2010.01.006.

[195] L. Asarian, N. Geary, Modulation of appetite by gonadal steroid hormones, Philos. Trans. R. Soc. B Biol. Sci. 361 (2006) 1251–1263. doi:10.1098/rstb.2006.1860.

[196] X. Chen, L. Wang, D.H. Loh, C.S. Colwell, Y. Taché, K. Reue, A.P. Arnold, Sex differences in diurnal rhythms of food intake in mice caused by gonadal hormones and complement of sex chromosomes., Horm. Behav. 75 (2015) 55–63. doi:10.1016/j.yhbeh.2015.07.020.

[197] L.E. Olofsson, A.A. Pierce, A.W. Xu, Functional requirement of AgRP and NPY neurons in ovarian cycle-dependent regulation of food intake., Proc. Natl. Acad. Sci. U. S. A. 106 (2009) 15932–15937. doi:10.1073/pnas.0904747106.

[198] A. Kamitakahara, K. Bouyer, C.-H. Wang, R. Simerly, A critical period for the trophic actions of leptin on AgRP neurons in the arcuate nucleus of the hypothalamus., J. Comp. Neurol. 526 (2018) 133–145. doi:10.1002/cne.24327.

[199] A.E. Oakley, D.K. Clifton, R.A. Steiner, Kisspeptin signaling in the brain., Endocr. Rev. 30 (2009) 713–743. doi:10.1210/er.2009-0005.

[200] A. Stengel, L. Wang, M. Goebel-Stengel, Y. Taché, Centrally injected kisspeptin reduces food intake by increasing meal intervals in mice., Neuroreport. 22

(2011) 253–257. doi:10.1097/WNR.0b013e32834558df.

[201] C.C. Nestor, J. Qiu, S.L. Padilla, C. Zhang, M.A. Bosch, W. Fan, S.A. Aicher, R.D. Palmiter, O.K. Rønnekleiv, M.J. Kelly, Optogenetic Stimulation of Arcuate Nucleus Kiss1 Neurons Reveals a Steroid-Dependent Glutamatergic Input to POMC and AgRP Neurons in Male Mice, Mol. Endocrinol. 30 (2016) 630–644. doi:10.1210/me.2016-1026.

[202] K.R. Westerterp, Control of energy expenditure in humans, Eur. J. Clin. Nutr. 71 (2017) 340–344. doi:10.1038/ejcn.2016.237.

[203] J. Heydenreich, B. Kayser, Y. Schutz, K. Melzer, Total Energy Expenditure, Energy Intake, and Body Composition in Endurance Athletes Across the Training Season: A Systematic Review., Sport. Med. - Open. 3 (2017) 8. doi:10.1186/s40798-017-0076-1.

[204] D.C. Fonseca, P. Sala, B. de Azevedo Muner Ferreira, J. Reis, R.S. Torrinhas, I. Bendavid, D. Linetzky Waitzberg, Body weight control and energy expenditure, Clin. Nutr. Exp. 20 (2018) 55–59. doi:https://doi.org/10.1016/j.yclnex.2018.04.001.

[205] E. Fuente-Martín, P. Argente-Arizón, P. Ros, J. Argente, J.A. Chowen, Sex differences in adipose tissue: It is not only a question of quantity and distribution., Adipocyte. 2 (2013) 128–134. doi:10.4161/adip.24075.

[206] B. Liu, Tiemin & Kong, Dong & Shah, Bhavik & Ye, Chian & Koda, Shuichi & Saunders, Arpiar & Ding, Jun & Yang, Zongfang & L Sabatini, Bernardo & B Lowell, Fasting Activation of AgRP Neurons Requires NMDA Receptors and Involves Spinogenesis and Increased Excitatory Tone, Neuron. 73. 511-22 (2012). doi:10.1016/j.neuron.2011.11.027.

[207] A. Joly-Amado, R.G.P. Denis, J. Castel, A. Lacombe, C. Cansell, C. Rouch, N. Kassis, J. Dairou, P.D. Cani, R. Ventura-Clapier, A. Prola, M. Flamment, F. Foufelle, C. Magnan, S. Luquet, Hypothalamic AgRP-neurons control peripheral substrate utilization and nutrient partitioning, EMBO J. 31 (2012) 4276–4288.

doi:10.1038/emboj.2012.250.

[208] S. Nielsen, Z. Guo, J.B. Albu, S. Klein, P.C. O'Brien, M.D. Jensen, Energy expenditure, sex, and endogenous fuel availability in humans, J. Clin. Invest. 111 (2003) 981–988. doi:10.1172/JCI16253.

[209] T.J. Bartness, Y. Liu, Y.B. Shrestha, V. Ryu, Neural innervation of white adipose tissue and the control of lipolysis., Front. Neuroendocrinol. 35 (2014) 473–493. doi:10.1016/j.yfrne.2014.04.001.

[210] C. Dodt, P. Lönnroth, H.L. Fehm, M. Elam, Intraneural stimulation elicits an increase in subcutaneous interstitial glycerol levels in humans, J. Physiol. 521 (1999) 545–552. doi:10.1111/j.1469-7793.1999.00545.x.

[211] K.I. Stanford, R.J.W. Middelbeek, L.J. Goodyear, Exercise Effects on White Adipose Tissue: Beiging and Metabolic Adaptations, Diabetes. 64 (2015) 2361 LP-2368. doi:10.2337/db15-0227.

[212] C.J. Small, Y.L. Liu, S.A. Stanley, I.P. Connoley, A. Kennedy, M.J. Stock, S.R. Bloom, Chronic CNS administration of Agouti-related protein (Agrp) reduces energy expenditure., Int. J. Obes. Relat. Metab. Disord. J. Int. Assoc. Study Obes. 27 (2003) 530–533. doi:10.1038/sj.ijo.0802253.

[213] G. Cano, A.M. Passerin, J.C. Schiltz, J.P. Card, S.F. Morrison, A.F. Sved, Anatomical substrates for the central control of sympathetic outflow to interscapular adipose tissue during cold exposure, J. Comp. Neurol. 460 (2003) 303–326. doi:10.1002/cne.10643.

[214] Y.-C. Shi, J. Lau, Z. Lin, H. Zhang, L. Zhai, G. Sperk, R. Heilbronn, M. Mietzsch, S. Weger, X.-F. Huang, R.F. Enriquez, L. Castillo, P.A. Baldock, L. Zhang, A. Sainsbury, H. Herzog, S. Lin, Arcuate NPY Controls Sympathetic Output and BAT Function via a Relay of Tyrosine Hydroxylase Neurons in the PVN, Cell Metab. 17 (2013) 236–248. doi:https://doi.org/10.1016/j.cmet.2013.01.006.

[215] V. Augustine, S.K. Gokce, S. Lee, B. Wang, T.J. Davidson, F. Reimann, F. Gribble, K. Deisseroth, C. Lois, Y. Oka, Hierarchical neural architecture underlying thirst

regulation, Nature. 555 (2018) 204–209. doi:10.1038/nature25488.

[216] L.C. Drickamer, Rates of urine excretion by house mouse (Mus domesticus): Differences by age, sex, social status, and reproductive condition, J. Chem. Ecol. 21 (1995) 1481—1493. doi:10.1007/bf02035147.

[217] A. Üner, G.H.M. Gonçalves, W. Li, M. Porceban, N. Caron, M. Schönke, E. Delpire, K. Sakimura, C. Bjørbæk, The role of GluN2A and GluN2B NMDA receptor subunits in AgRP and POMC neurons on body weight and glucose homeostasis, Mol. Metab. 4 (2015) 678–691. doi:10.1016/j.molmet.2015.06.010.

8. ANNEXES

Supplementary table 1

STAR METHODS

KEY RESOURCES TABLE

REAGENT or RESOURCE	SOURCE	IDENTIFIER
Other		
Fisherbrand Animal Ear Punch	Thermo Fisher Scientific	Cat# 13-820-063
MicroAmp Optical 384-Well Reaction Plate	Thermo Fisher Scientific	Cat# 4309849
Greiner Bio-One 96-Well Non Binding Microplates	Thermo Fisher Scientific	Cat# 07-000-340
Mini-PROTEAN Spacer Plates	Bio-Rad	Cat# 1653312
Criterion empty cassettes	Bio-Rad	Cat# 345-9901 Cat# 3459902
Mini-PROTEAN tetra Verical Electrophoresis Cell	Bio-Rad	Cat# 1658004
Criterion Blotter	Bio-Rad	Cat# 1704071
Nitrocellulose Membrane, Roll, 0.45 µm, 30 cm x 3.5 m	Bio-Rad	Cat# 1620115
Model 900LS Small Animal Stereotaxic Instrument	KOPF	900LS
5 µL, Neuros Model 75 RN, point style 3, SYR	Hamilton	Cat# 65460-02
Microtome	Leica Biosystem	Modelo SM2000R
Superfrost Plus slides	Thermo Fisher Scientific	Cat# J7800AMNT
Fluorescent microscope	Leica Biosystem	
NanoDrop 1000 spectrophotometer	Thermo Fisher Scientific	Modelo ND-1000
Calorimetric System LabMaster	TSE Systems	N/A
LightCycler 480 Instrument II	Roche	Cat# 05015243001
Cryostat	Leica	CM3050S
Microvette 100 UL Serum	Sarstedt	Cat# 201.280
Hand Glucometer	Bayer	Cat# 83415194
Glucometer strips	Bayer	Cat# 84191389
Capillary tube	Deltalab	Cat#7301
Cantrifugue	Eppendorf	Cat# 5415 R
Tissue Adhesive	3M VetbondTM	Cat# 1469Sb
Combi-Vet	Rothacher Medical	NA
25G Needle	BD Microlance TM 3	Cat# 300600
Mouse Brain Matrices	Agnthos	Cat# 69-2175-1
Miniplus 3	Gilson	NA

Immersion Thermostat	Selecta	Digiterm-100
High performance infrarared camera	FLIR Commercial System	Cat# T420
Incubator Shaker	New Brunswick Scientific	Excella E25
Electroporator	Eppendorf	2510
Tissuelyser	QIAGEN	Cat# 85600
Beads	QIAGEN	Cat# 69989 Cat# 69997
Thermoblock	JP Selecta EN	Cat# 7462200
96-well microplate	Greiner bio-one	Cat# 655101
Orbital Shacker	Heidolph	Polymax 1040
ImageQuant LAS 4000 mini	GE Healthcare Life Sciences	N/A
Miroscope camera	Leica Biosystem	MC190
Leica DM IL LED Tissue Culture Microscope	Leica Biosystem	N/A
Osmometer	Advanced Instruments	3320
Thermo-shaker	Biosan	PST-100HL
Bacterial and Virus Strains		
SURE Competent Cells	Agilent	Cat# 200227
pAAV-EF1a-DIO-mCherry	Viral Vector Production Unit (VPU)	N/A
AAV2-Syn-DIO-GFP	Viral Vector Production Unit (VPU)	N/A
Experimental Models: Organisms/Strains		
Cpt1a(flox/flox)	Paper de Joan	N/A
AgRP-CreERT2	Paper Elquist	N/A
Cpt1aAgRP(+/+)	In this Paper	N/A
ZsGreen;Cpt1aAgRP(+/+)	In this Paper	N/A
RiboTag;Cpt1aAgRP(+/+)	In this Paper	N/A
Software and Algorithms		
FLIR-Tools-Software	FLIR	http://www.flir.com/instruments/display/?id=54865
ImageJ	NIH	https://imagej.nih.gov/ij/index.html; RRID: SCR_003070
Prism	Graph Pad	https://www.graphpad.com/scientific-software/prism/; RRID: SCR_002798
Bruker Albira Suite Software Version 5.0. Scatter	Bruker Biospin	https://www.bruker.com/
LAXZ	Leica	Versión 3.3

9. SCIENTIFIC PRODUCTION

Mir JF, Zagmutt S, Lichtenstein MP, García-Villoria J, Weber M, Gracia A, Fabriàs G, Casas J, López M, Casals N, Ribes A, Suñol C, Herrero L, Serra D. **Ghrelin Causes a Decline in GABA Release by Reducing Fatty Acid Oxidation in Cortex.** Mol Neurobiol. 2018 Sep;55(9):7216-7228. doi: 10.1007/s12035-018-0921-3. Epub 2018 Feb 2.

Zagmutt S, Mera P, Soler-Vázquez MC, Herrero L, Serra D. **Targeting AgRP neurons to maintain energy balance: Lessons from animal models.** Biochem Pharmacol. 2018 Sep;155:224-232. doi: 10.1016/j.bcp.2018.07.008. Epub 2018 Jul 18. Review.

Soler-Vázquez MC, Mera P, Zagmutt S, Serra D, Herrero L. **New approaches targeting brown adipose tissue transplantation as a therapy in obesity.** Biochem Pharmacol. 2018 Sep;155:346-355. doi: 10.1016/j.bcp.2018.07.022. Epub 2018 Jul 19. Review.

Bastías-Pérez M, Zagmutt S, Soler-Vázquez MC, Serra D, Mera P, Herrero L. **Impact of Adaptive Thermogenesis in Mice on the Treatment of Obesity.** Cells. 2020 Jan 28;9(2). pii: E316. doi: 10.3390/cells9020316. Review.